A VELOCITY-TRACKING FILTER FOR IMPROVED ESTIMATION OF SEISMIC SIGNALS

A THESIS

Presented to

The Faculty of the Graduate Division

by

Winsor Letton, III

In Partial Fulfillment

of the Requirements for the Degree

Doctor of Philosophy

in the School of Electrical Engineering

Georgia Institute of Technology

June, 1969

In presenting the dissertation as a partial fulfillment of the requirements for an advanced degree from the Georgia Institute of Technology, I agree that the Library of the Institute shall make it available for inspection and circulation in accordance with its regulations governing materials of this type. I agree that permission to copy from, or to publish from, this dissertation may be granted by the professor under whose direction it was written, or, in his absence, by the Dean of the Graduate Division when such copying or publication is solely for scholarly purposes and does not involve potential financial gain. It is understood that any copying from, or publication of, this dissertation which involves potential financial gain will not be allowed without written permission.

_____

_____

7/25/68

A VELOCITY-TRACKING FILTER FOR IMPROVED

ESTIMATION OF SEISMIC SIGNALS

Approved:

Chairman

Date approved by Chairman: June 26, 1965

ACKNOWLEDGMENTS

I sincerely wish to thank Dr. Aubrey M. Bush, my thesis advisor in this work; without his technical help and encouragement in several crucial instances, this research surely could not have been completed in the allotted time. Thanks also to Dr. R. H. Pettit and Dr. R. W. Larson, both of whom served on the proposal and reading committees.

Special thanks are due the people of the Atlantic Richfield Company for the services which they provided. Though too numerous to mention, these mainly involved access to their two IBM System 360 computers, with associated software, and a knowledge of exploration geophysics not available at Georgia Tech. I especially want to thank Dr. C. Floyd George, head of the Seismic Analysis Section of the Exploration Research Group, for his encouragement during the past 12 months, and Mr. Steve Hall, whose knowledge of geophysics and programming expertise were readily accessible by me.

Finally, I want to thank my dear wife Ann, who never thought I wouldn't make it.

TABLE OF CONTENTS

LIST OF ILLUSTRATIONS

Figure Page

Figure Page

Figure Page

SUMMARY

This research is an attempt to improve the estimation of signals received in the process known as seismic reflection prospecting. This process has been and still is the most popular and successful technique available for determining the structure of the near-surface part of the earth's crust. A mapping of the layered structure is obtained by exciting acoustic wavelets near the surface of the earth, then observing when the wavelets return to various receiver points on the surface after reflection from a layer.

Once these returning signals have been recorded, a number of means are available for improving the clarity of the records. Understanding these requires a knowledge of the characteristics of the signals received. One of these characteristics is the fact that both signal (primary reflection) and noise (multiple reflection) wavelets spread out on a spherical wavefront as they leave their source. Another is the multidimensional nature of signals and noise; they are functions of both time and space, and also have multidimensional frequency spectra. Velocity filtering is a means of improving record clarity when the spectra of signal and noise are separated; the records are filtered by a multidimensional linear filter which accepts the signal spectrum and rejects the noise spectrum. Other filtering techniques are available for making the records more intelligible, such as deconvolution filtering, a means of sharpening the events on the records, and least-squares linear filtering, which can be used for a

variety of purposes. However, the only means for rejecting multiple reflections which has been proved effective is a process known as common-depth-point (CDP) stacking, in which the records are shifted and summed (or shifted, filtered, and summed) in such a way that primary reflections reinforce one another and multiple reflections do not.

The reason CDP stacking is the only method effective against multiples is that it is the only processing method which adapts to the changing characteristics of primaries and multiples. These two look so very much alike on seismic records that only a very subtle difference permits separation by stacking. It is known that interval velocity increases with depth, therefore, at a given time, a multiple which is received at adjacent receiver points exhibits a greater difference in arrival time than does a primary which is received at about the same time. But this difference in *moveout per trace* means the apparent horizontal velocity of a primary is greater than that of a multiple, if both are present at the same time. Consequently, a velocity filter whose pass and reject regions change with changing apparent horizontal velocity is proposed to continually separate primaries and multiples.

Such a time-varying velocity filter has been designed and implemented on a digital computer. A synthetic seismogram has been processed to demonstrate the feasibility of the method and to observe how much rejection might be obtained. Actual data recorded at a location in West Texas has also been processed. Both sets of processed data exhibit multiple reduction, though the reduction is greater in the synthetic example, due to the high-velocity nature of the data from West Texas. It is felt that refinement of the filter transfer

function and faster temporal sampling might lead to even better reduction of multiples than that shown.

The new method presented is unique in two ways. First, it is the only technique for *filtering* multiple reflections which requires no knowledge of the locations or moveouts of the multiples. In addition, it is the only means of eliminating multiples which takes place on such an early processing level; the output of the time-varying filter is suited for any kind of common-depth-point stacking. For these reasons, it can be a valuable tool in seismic reflection analyses.

CHAPTER I

INTRODUCTION

The research reported in this thesis is an attempt to improve the estimation of seismic signals in the exploration for natural gas and oil. More specifically, it is the implementation of a linear time-varying system for the purpose of separating desired signal from noise in the process known as seismic reflection prospecting. The chapters which follow describe the process, discuss the data processing techniques currently used, explain proposed improvements, and discuss results obtained using the improved method.

In Chapter II the purpose of seismic reflection prospecting is explained and the way the process is carried out is discussed in detail. The principal objective of seismic reflection prospecting is to obtain an accurate "picture" of the earth's subsurface without actually drilling a hole. The chapter describes how this is accomplished. As in the classic radar problem, a signal source injects energy into a channel, and energy reflected from discontinuities in this channel is received at or near the source. Though the seismic and radar problems appear to be quite similar, they are, in fact, basically different in a number of respects.

The object of Chapter III is to place the problem in the proper theoretical framework, and to acquaint the reader with the point of view used by practicing exploration geophysicists. First, the physical

properties of the waves generated and the media through which they travel are considered. Later these signals are viewed in the context of communication theory; the concept of multidimensional signals and spectra is introduced.

In Chapter IV some of the processing techniques currently used in the exploration industry are examined. These include several suboptimum filtering and "stacking" operations, namely velocity filtering, deconvolution filtering, normal moveout corrections, and common depth point stacking. By "stacking" one means any process whereby the data are shifted and summed in such a way that desired signals are reinforced and noise is cancelled. Also discussed are some applications of optimum least-squares filtering and processing techniques.

In Chapter V a closer look is taken at some of the assumptions required to make the techniques discussed in Chapter IV work successfully. For instance, the assumption that seismic signal and noise are uncorrelated is considered more closely. This is one of the basic requirements for all optimum processing methods considered in Chapter IV.

After presenting shortcomings of methods currently used, a new processing system is proposed in Chapter VI. The new method would take advantage of the changing characteristics of signal and noise. Whereas most systems currently used remain fixed throughout the course of processing, the proposed system would change as it processed in order to meet the changing appearance of signal and noise.

Results of the research are presented in Chapter VII. Synthetic data as well as actual field data are used, and both unprocessed and

conventionally processed traces are compared to traces processed using the proposed method.

Conclusions and proposed further research are offered in Chapter VIII.

CHAPTER II

SEISMIC REFLECTION PROSPECTING

Seismic reflection prospecting is an attempt to determine the subsurface characteristics of the earth. The portion of the earth's crust located within a few miles of the surface exists in layers. Boundaries between layers generally are almost parallel to the surface and are very sharply defined. A mapping of this subsurface structure, that is, a knowledge of the locations of the boundaries between layers, is invaluable when trying to decide whether to drill for oil. It is the objective of seismic reflection prospecting to obtain such a map. Present methods for obtaining this map are described below; first an overall description is given in a very qualitative manner, after which each part of the seismic reflection process is described in detail.

Acoustic energy delivered by a source at or near the surface of the earth is transmitted into the ground. When the propagating energy is incident on a discontinuity in the composition of the earth, a portion of that energy must be reflected in order to satisfy certain fundamental boundary conditions imposed by the physics of the problem. The reflected energy returning to the surface is observed, with the time of arrival giving a relative indication of the depth of the discontinuity. Repeating the process over a large area hopefully yields sufficient data to map the subsurface, presuming the data is properly processed.

Consider Figure 1. The acoustic energy is generated by a source at the point shown. Two kinds of sources are used: explosive sources and vibratory sources. The explosive method requires drilling a "shot-hole" 25 to 250 feet deep, loading dynamite into the hole, and detonating the charge. In the vibratory methods, known by such trade names as Vibroseis,* Dinoseis,** and Thumper,*** a weight is dropped, beat, or rolled against the ground for several seconds by a truck-borne unit. The "signal" which is vibrated into the earth is usually carried on tape in the truck; a "chirp" (linearly frequency-modulated pulse) is widely used. Before the data are processed the received signals are correlated with the transmitted waveform. Such a waveform and its autocorrelation function are shown in Figure 2. The explosive method generally permits sounding to greater depths, while the vibratory techniques are safer, more convenient, and seem to offer greater promise for the future.

The acoustic energy which is directed into the earth is in the form of longitudinal waves. The signal excited by a dynamite explosion is a spike of a very large amplitude and short duration; hence it has a very large bandwidth initially. Due to the attenuating properties of the earth, however, most of the high frequency components are absorbed in a short distance, and the propagating signal looks very much like the correlation function in Figure 2. The absorption mechanism also

---

* Trademark of Continental Oil Company.

** Trademark of Sinclair Research.

*** Trademark of Mandrel Industries.

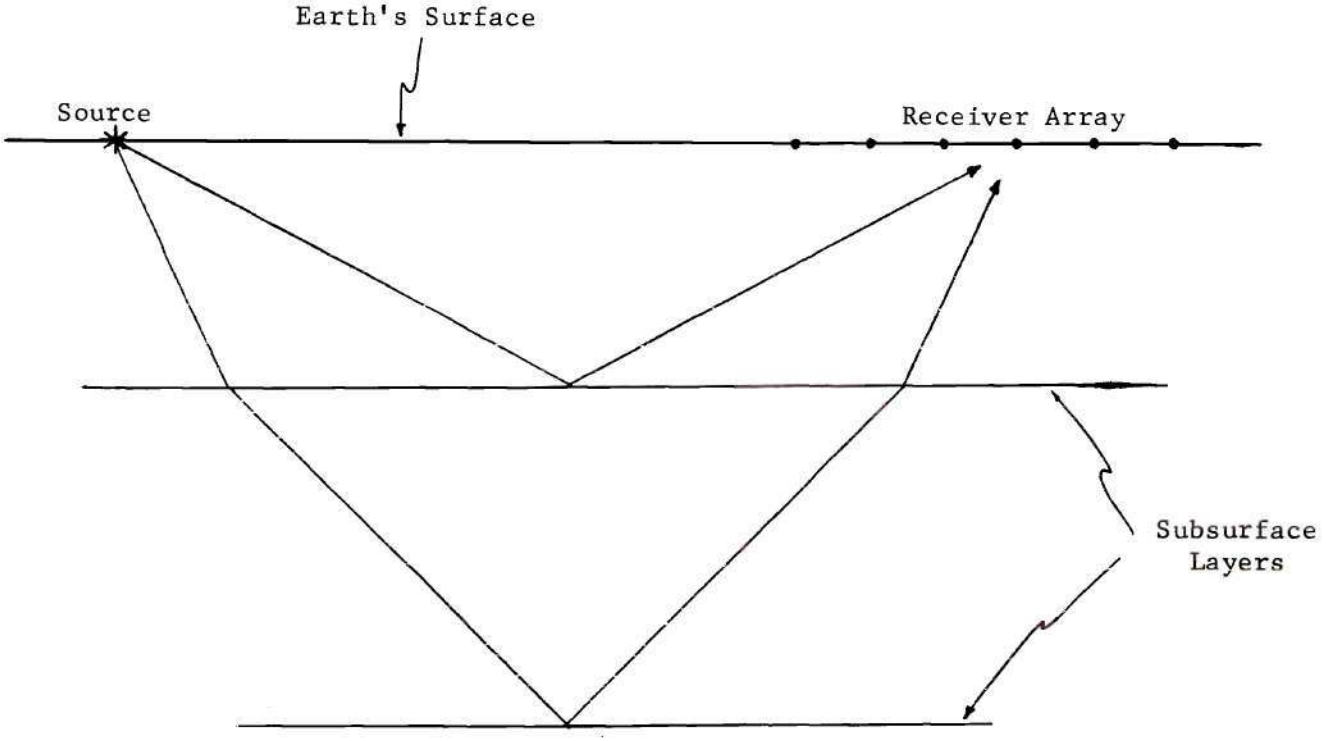

Figure 1. The Excitation, Reflection, and Detection of Seismic Waves

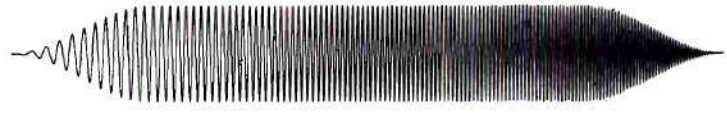

SWEEP (10-60) T=4.096 S. WITH COSINE TAPER

AUTOCORRELATION OF ABOVE TAPERED SWEEP

Figure 2. A "Chirp" Signal and its Autocorrelation Function

acts to damp the higher frequencies in the "chirp" signal sent out by a vibrator; the crosscorrelation function between the "chirp" and an attenuated "chirp," though, is still very much like that shown in Figure 2. This wave packet, in this case the result of correlating transmitted and received signals, is called a *wavelet*.

After reflection (possibly more than once) in the subsurface, wavelets which return to the earth's surface are detected by acoustic sensors called *geophones*. These geophones, which come in a variety of forms,[1] respond only to the vertical component of the earth's motion. They can detect earth movements as small as 10^{-8} inches. The individual geophones are part of a group; the groups are arranged in a one-dimensional array on the surface as shown in Figure 3. Figure 3 is a diagram of the source-receiver geometry of Figure 1 as seen from above. A typical array consists of from 12 to 24 groups, each group containing up to 100 geophones. Within a group the geophones fall into no particular framework, other than one from which it is easy to record. Generally, the outputs from the individual geophones are summed, and the resultant "trace" is recorded digitally on magnetic tape. Thus, for a single "shot" (explosive method) or "sweep" (vibratory method) there will be 24 individual records, or traces. The source and receiving array must be moved over a large area, and the process repeated at each location, in order to provide an adequate mapping of the near subsurface of the earth.

Once the data have been recorded in the field, it is taken to the laboratory where filtering and other processing methods are applied

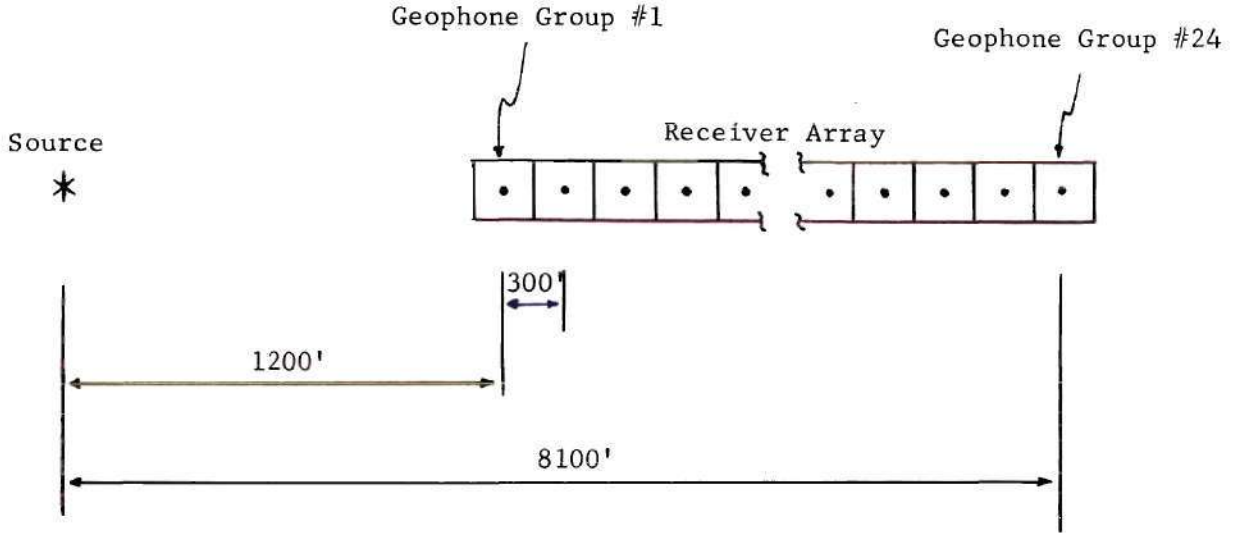

Figure 3. Seismic Transmitter-Receiver Geometry

to it. In addition, moveout corrections must be applied to the data at some stage. This may best be understood by considering Figure 4. In most cases the received signal has traveled a raypath to the receiver like that shown, i.e., a path other than the vertical. But it is the reflection from the point P which has been recorded, and it is essential for clarity's sake that the source point, receiver point, and reflection point all *appear* to lie on the same vertical line. Correcting for moveout is a process of "shrinking" the record so that this appearance is effected. It will be discussed in detail later.

Once the data have been recorded and then processed, some means must be used to extract the desired information from it. There is currently no automatic reflection-picking technique which is as effective at seismogram interpretation as a trained geophysicist. Hence, at this time the ultimate decision on whether or not to drill for oil is made by an individual who has subjectively interpreted a visual display. Three modes of display are used more than any other: the *wiggle trace*, *variable area*, and *variable density* displays. A wiggle trace is shown in Figure 5. It is simply a line plot of a number of traces, or records, as functions of time. Increasing record time is plotted down the paper, with distance from shotpoint plotted across the paper. The root of the name wiggle trace is obvious from the figure. The variable area presentation is formed by merely darkening the area under the wiggle trace when its amplitude exceeds a certain threshold. Figure 6 illustrates this method of display. Finally, a variable density display is prepared by generating a narrow strip of constant width down the plot; the strip is dark at times when signal amplitude is large, and light when the

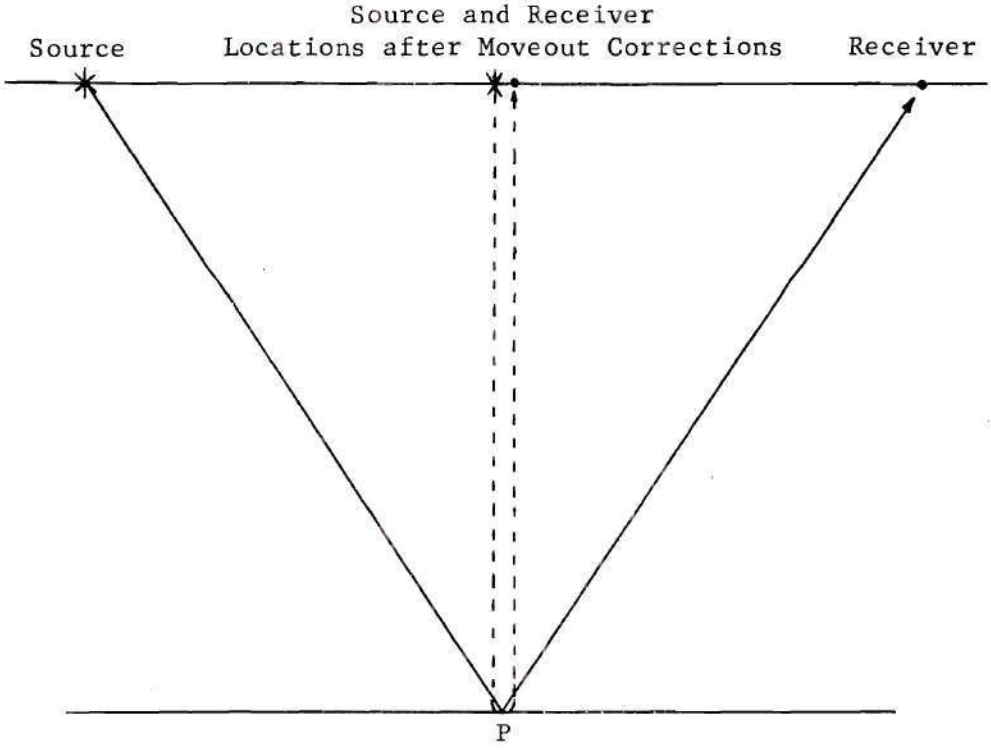

Figure 4. Correcting for Normal Moveout

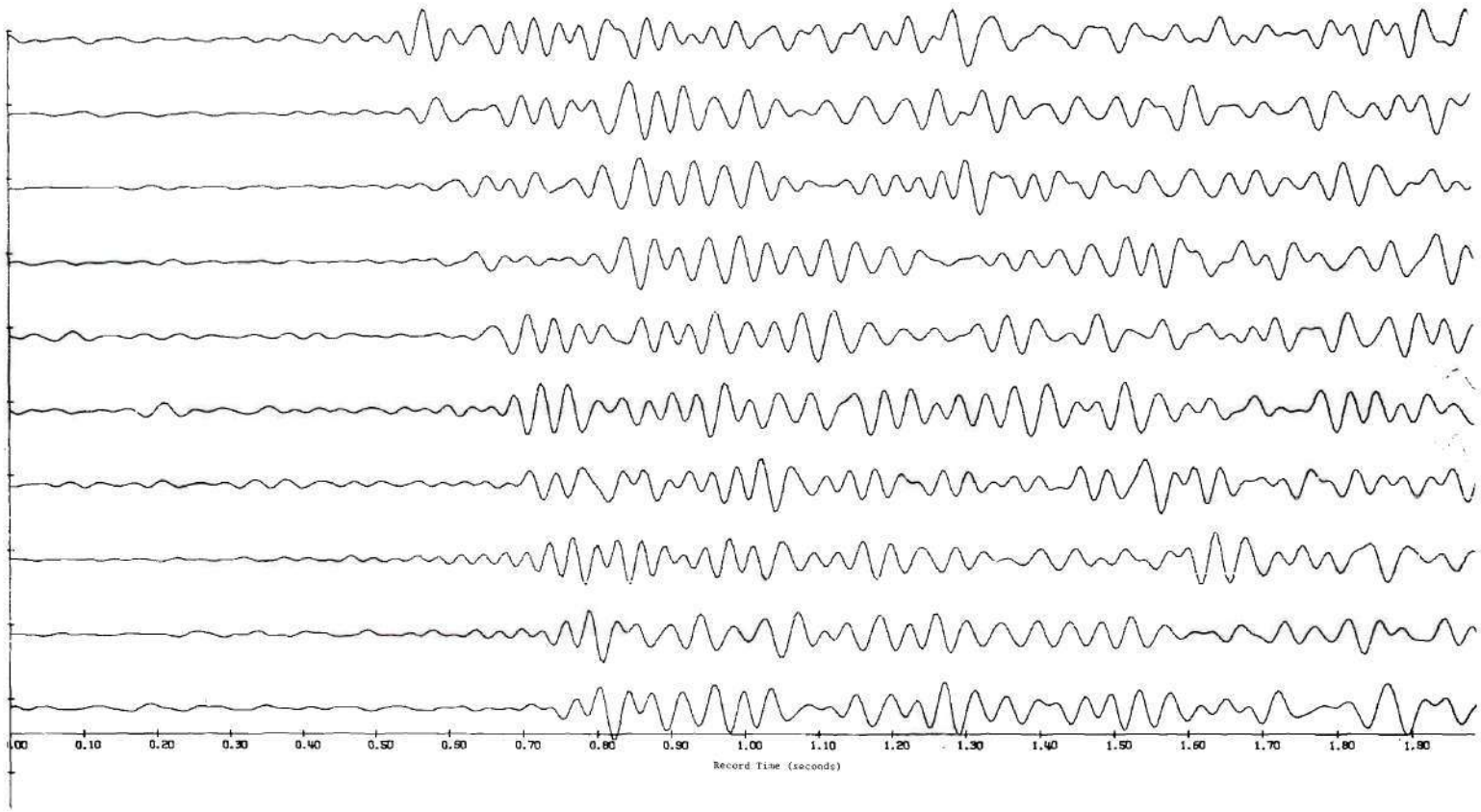

Figure 5. A Wiggle Trace Display

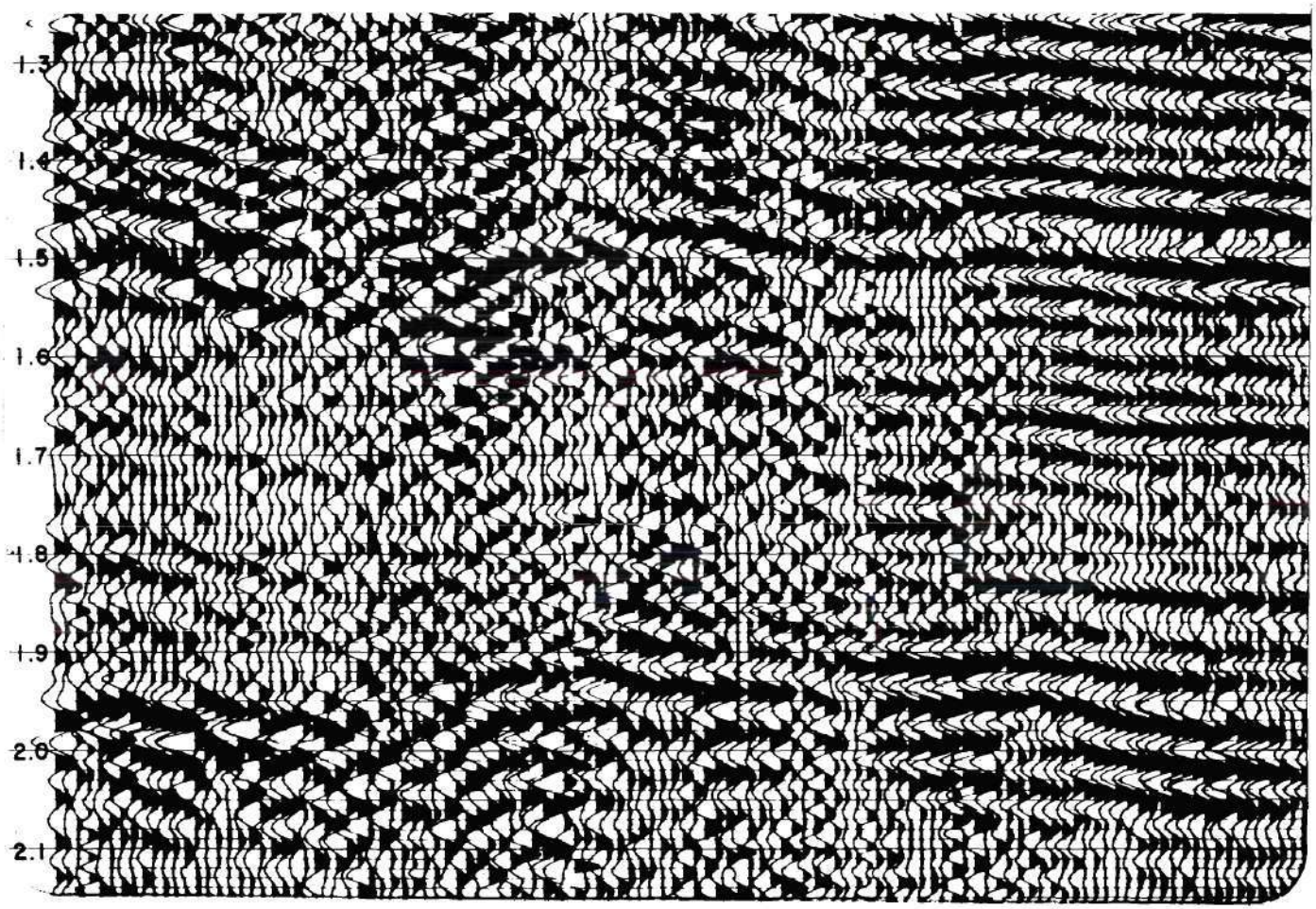

Figure 6. A Variable Area Display

amplitude is small. Of course, shades of gray in between are also generated. Such a presentation is shown in Figure 7. The variable area and variable density are the more commonly used displays in seismic analysis.

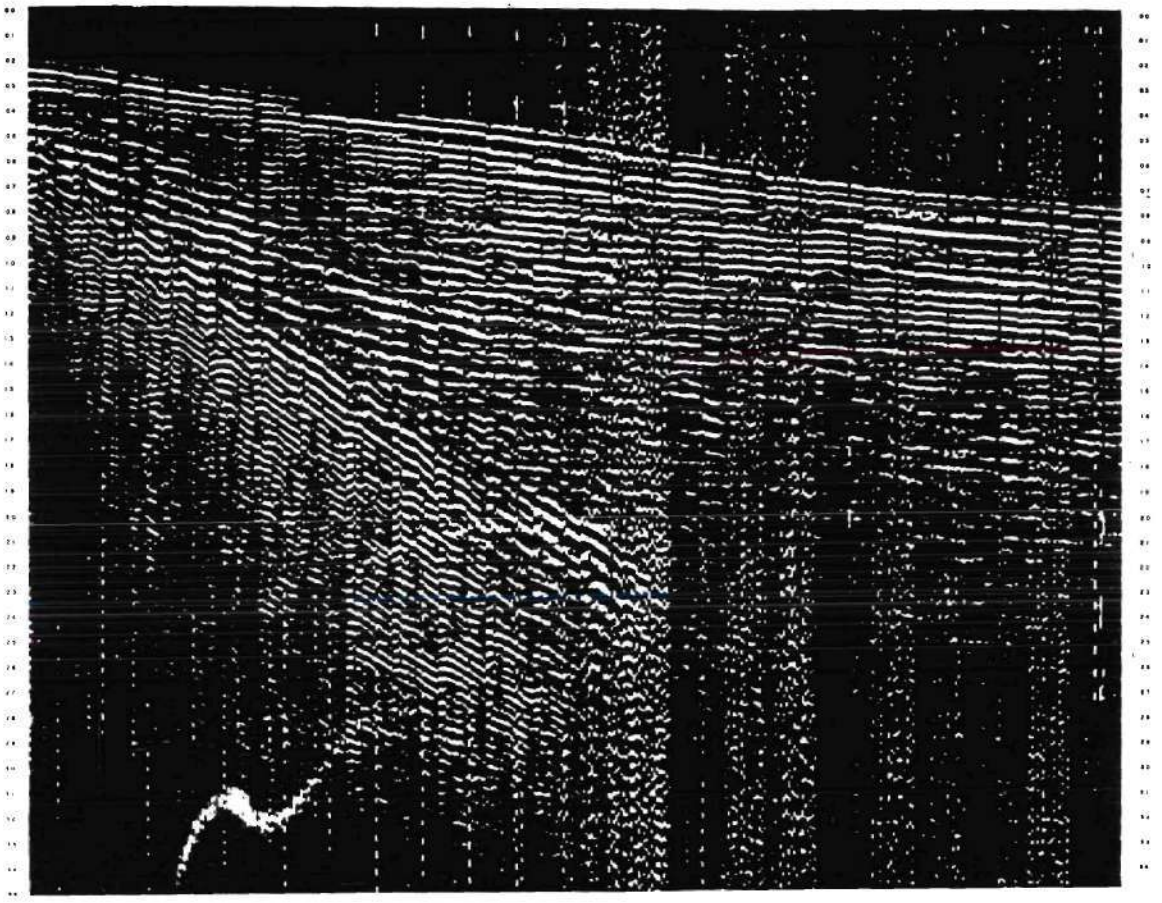

Figure 7. A Variable Density Display

CHAPTER III

CHARACTERISTICS OF SEISMIC SIGNALS

Although seismic reflection prospecting was begun about 1920, and though it immediately became the most powerful and popular exploration tool, many years passed before geophysicists began to understand the characteristics of the signals which they generated. However, a combination of (1) the increasing difficulty of finding oil in the traditionally abundant areas of Oklahoma and Texas, (2) an influx of young men with fresh points of view into the industry, and (3) a new technology which produced computers, digital recording, etc., has completely revamped reflection prospecting. The characteristics of seismic signals are now better understood, though there is still much to be learned.

In this chapter some of the characteristics of seismic signals and noise are presented, first from a wave propagation outlook, then from a communication theory point of view. The two viewpoints taken together lend insight into the problem.

Seismic Wave Propagation

There are many kinds of seismic waves which can be excited; those which one wants to detect, which travel to the subsurface layers, are *longitudinal*, or *compressional*, waves. Their velocity may range from as low as 2000 feet per second in clay near the surface, to as high as 20,000 feet per second in some kinds of limestone. This true

phase velocity of a medium, often called the *interval* velocity, usually increases with increasing depth. This increase, of course, is by no means a rule.

In both vibrator and explosive excitation methods, the source is approximately a point source. Hence the disturbance diverges as if on the surface of an expanding sphere. As these spherical wavelets spread out from their source, their energy is distributed over an area which increases as the square of the raypath distance from this source. Now consider the situation shown in Figure 8. A spherical wavelet is excited at the surface, travels to point P on a subsurface layer at depth d, and then returns to a detector location on the surface. A convenient and often illuminating way to represent this event is as a spherical wavelet, excited at a depth of 2d, which travels through the same medium as that traveled by the actual wavelet. This "image" wavelet is illustrated with dashed lines. Thus it would appear that the energy detected is directly proportional to the energy put into the earth and inversely proportional to the square of the distance from the image source to the detector location. However, this does not account for the energy absorption mechanism of the earth, in which acoustic energy is converted to heat through frictional dissipation. This loss can be included in the model by an exponential attenuation factor, $e^{-\alpha r}$, where α is an attenuation constant and r is the distance between the image source and the detector. Thus the energy received at a detector point might be given by

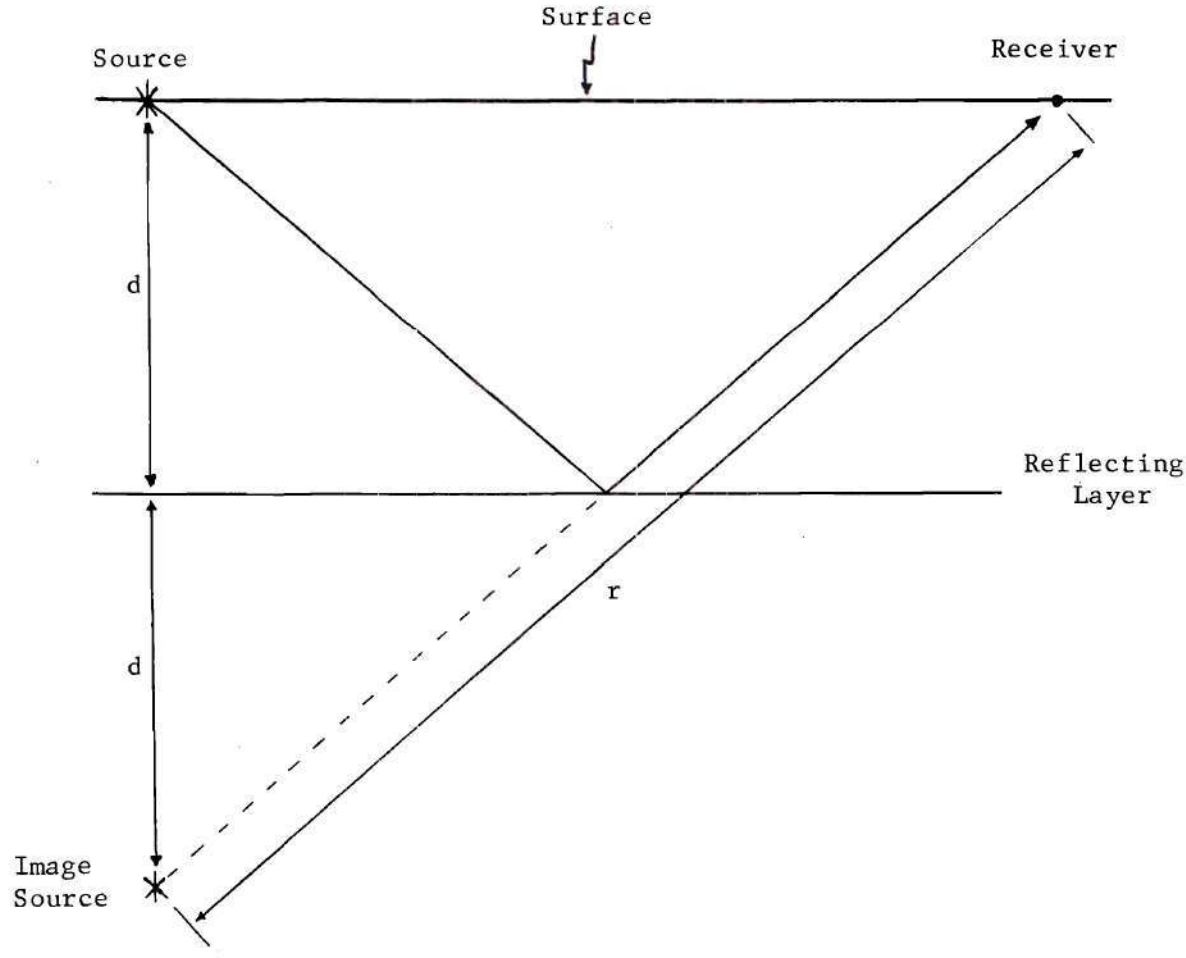

Figure 8. The Propagation of Spherical Wavelets

$$[\text{Energy at detector point}] = [\text{Energy from source}] \cdot \frac{e^{-\alpha r}}{r^2}$$

In addition to losses due to attenuation and spherical divergence, the traveling wavelet also loses energy through reflection. Each time the signal is transmitted through an interface, part of its total energy is reflected.

One can see that received signal strength decreases greatly as a function of record time. A reflection from a layer at a depth of 3000 feet may be more than 20 db weaker than a reflection from a layer at 1000 feet. In an attempt to offset this, one commonly applies a gain which increases with time to each recorded trace. However, when the signal strength has decreased to a point where it is comparable to or less than the background noise, further equalization is not practicable.

In discussing the propagation of spherical waves, the distance from the source to the observation point is often so great that in a localized area about the point the disturbance is approximately a plane wave. In the detection and propagation of electromagnetic spherical waves, this approximation is made quite often. To a lesser extent it is used in the seismic problem, though it certainly does not apply to reflections from shallow layers. It is more easily justified when the signals received are reflected from deep layers.

The straight-raypath approximation is a method of viewing wavelet reflection which is used almost universally by researchers in this field. Consider the situation depicted in Figure 9. Ray A shows the

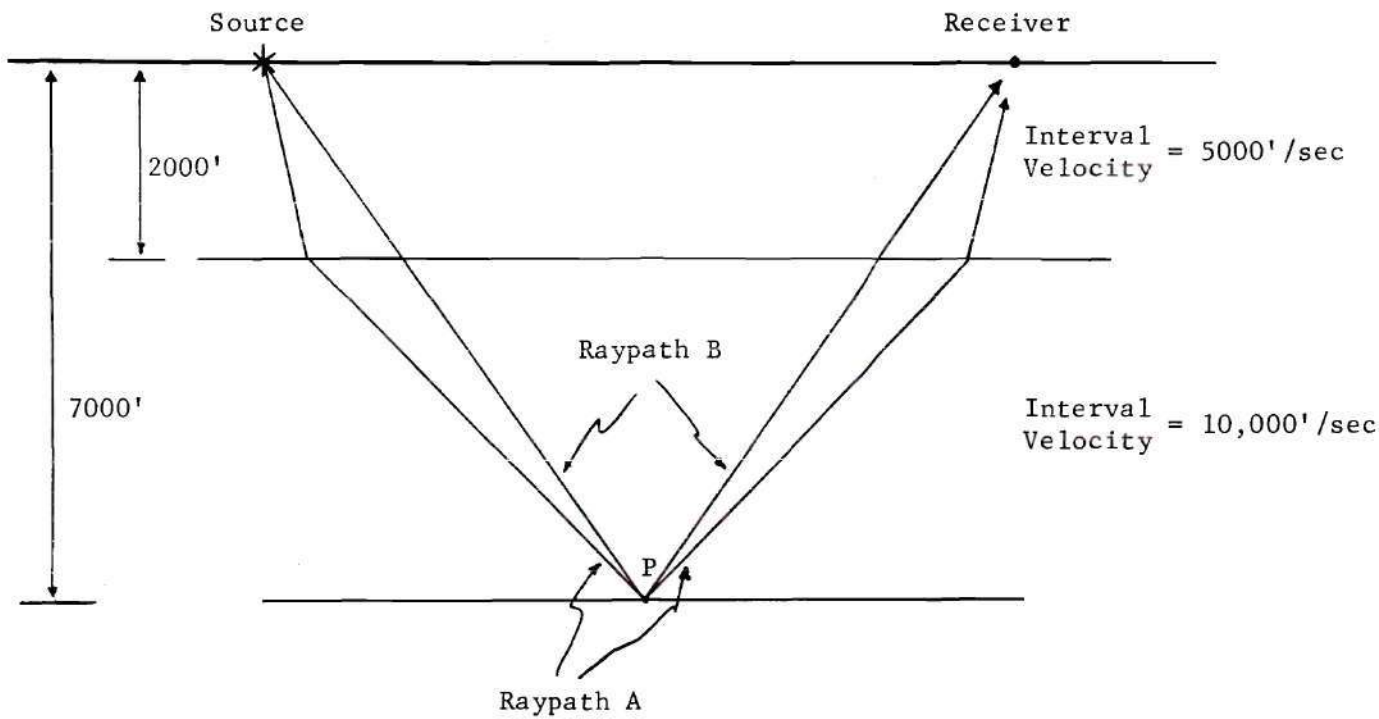

Figure 9. The Straight Raypath Approximation

path a wavelet would actually follow from the source to the second subsurface interface and up to the receiver. Since the interval velocity of the second layer is greater than that of the first, the ray is bent away from the normal to the interface.

The substitution of ray B for ray A is an attempt to make one "average" layer from the two actual layers. The average layer has the thickness of the two layers combined (7000 feet in this case), and an interval velocity which is a weighted average of the interval velocities of the two true layers. Since one now has a single layer, the ray B propagates straight to the point P, then straight up to the receiver. The interval velocity of the new "layer" is determined by simply dividing twice the depth to the second interface by the actual time it would take a wavelet to propagate vertically through the first two layers and back to the surface. For the example above, one calculates this average interval velocity (generally called just the *average velocity*) as follows:

$$V_{ave} = \frac{2z}{T_o}$$

$$= \frac{2 \cdot 7000 \text{ ft}}{2 \cdot \left(\frac{2000 \text{ ft}}{5000 \text{ ft/sec}} + \frac{5000 \text{ ft}}{10{,}000 \text{ ft/sec}}\right)}$$

$$= \frac{14{,}000 \text{ ft}}{1.8 \text{ sec}}$$

$$= 7778 \text{ ft/sec}$$

where

z = depth to reflection point.

T_o = two-way vertical travel time.

The one-layer simplification permits the derivation of a number of simple formulas; these are developed in Appendix A.

Average velocity as a function of depth or record time is an idea used most extensively throughout the petroleum exploration field. Knowledge of the average velocity profile is required in order to use some of the more successful processing techniques.

Another velocity parameter which is often of great interest is the *apparent horizontal velocity* of a wavelet impinging on a detector array. It should be emphasized that this parameter is a characteristic of a particular signal, as well as the structure of the earth. Consider the situation shown in Figure 10. The points 1 and 2 represent receiver points on the surface of the earth, separated by a distance d. The arrow pointing at 2 represents the direction of propagation of a plane wave. Also shown are planes of constant phase normal to the direction of propagation. The wave is incident at an angle θ with respect to the surface.

Assume that the wave impinges on detector point 1 at time t_1 and on 2 at time t_2. To receivers at these points, not knowing the direction from which the signal came, the wave appears to propagate at a velocity

$$v_{app} = \frac{d}{t_1 - t_2} = \frac{d}{\Delta t}$$

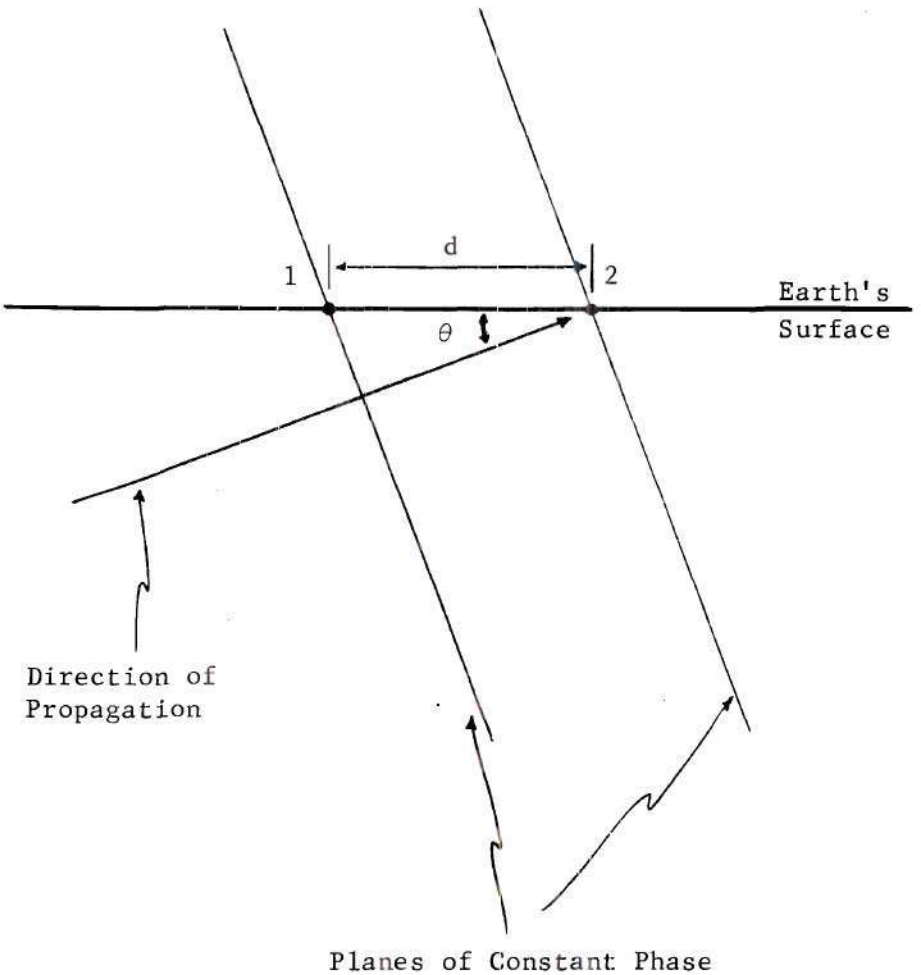

Figure 10. An Illustration of Apparent Horizontal Velocity

It is known, though, that the wave traveled a distance of only d cos θ; hence its actual phase velocity was

$$V_{pha} = \frac{d \cos \theta}{\Delta t} = V_{app} \cdot \cos \theta$$

Thus the apparent horizontal velocity along the axis of the array is

$$V_{app} = \frac{V_{pha}}{\cos \theta}$$

Observe that the apparent horizontal velocity is always greater than the actual phase velocity (interval velocity) of the medium, and that it becomes infinite as the direction of propagation approaches the vertical.

Thus there are three velocity parameters of interest in the seismic problem--interval velocity, average velocity, and apparent horizontal velocity. An average velocity profile of the subsurface can be obtained if one knows the interval velocities of the layers. Then from average velocity information one is able to determine apparent horizontal velocity as a function of record time. This last will be demonstrated in a later section.

Seismic Signal and Noise Characteristics

Before discussing detailed characteristics of seismic signals and noise, one is first concerned with defining which disturbances are to be called desired signals and which are to be classed as "noise."

Wavelets which have undergone a single subsurface reflection are called *primary* reflections, or just primaries. These are the signals one wishes to detect; once moveout corrections have been made, these primaries indicate the relative locations of the subsurface interfaces. Typical primaries are shown in Figure 11. Unfortunately, in addition to the desired primaries the geophone array receives noise of many kinds. This noise can be classified in two groups, ambient, or background, noise and source-generated noise. Ambient noise may be the result of wind, highway traffic, low-flying aircraft, faulty instruments, or anything else not a direct effect of the source. Source-generated noise is, however, a greater problem in seismic reflection prospecting. The most common examples of source-generated noise are "first breaks," low-velocity ground roll, and multiple reflections, or multiples. First breaks and ground roll are surface waves excited by the source, like those waves in the membrane of a drum that has been tapped. The phase velocity of first breaks is fairly high, and consequently, as its name implies, this disturbance is usually the first event on the record. In contrast, the phase velocity of ground roll is very low. In some instances, particularly when using vibratory methods, the magnitudes of these surface waves can be the limiting factor on receiver performance. However, in most cases multiple reflections are a greater problem. A multiple is any wavelet which has been reflected more than once. Figure 11 shows two possible multiples. Both are *surface multiples*, which are distinguished from *interbed multiples* in that the latter undergo no surface reflections. The problems caused by multiples are obvious; on a record section they look a great deal

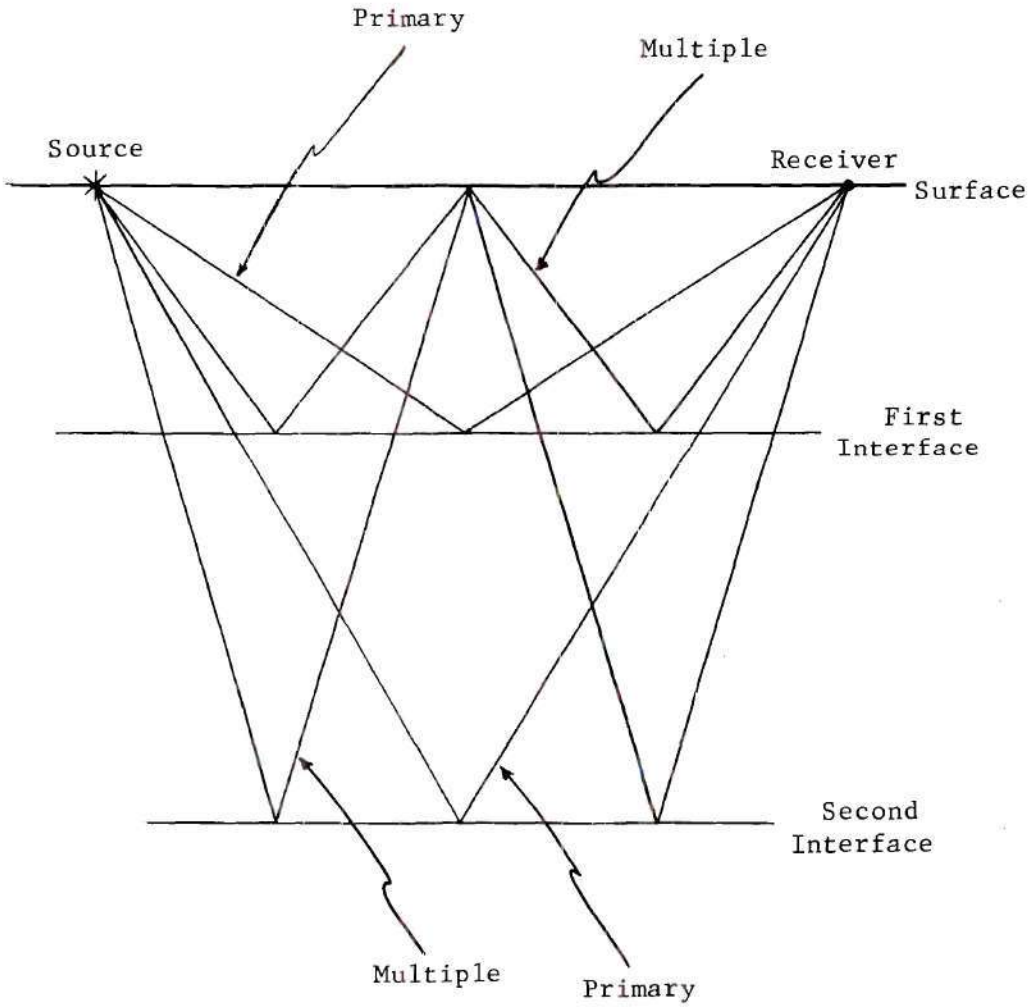

Figure 11. Primary Reflections and Three-Bounce Surface Multiple Reflections

like primaries, the two often being indistinguishable.

Figure 7 illustrates how first breaks and ground roll can literally "swamp" a set of records. The data were recorded at 15-foot intervals over a distance of about 7000 feet; what is shown are the output traces after correlation with the waveform which was sent into the earth. One can see that ground roll masks any event which might lie in the lower left part of the figure. In addition, first breaks cover any events which occur early in the record. Very little useful information can be derived from a set of traces in this condition.

Figure 12 shows how simple primary and multiple reflections might appear on a record section. These reflections were the result of exciting the structure of Figure 13. The first event on the record occurs at vertical two-way time T_o, and is just the primary reflection off the first subsurface interface. The second event, at time $2T_o$, is the multiple shown in Figure 13. Notice that the use of images, as was done earlier in this chapter, permits one to think of the multiple as a primary reflection from a layer at a depth of 2d. The interval velocity of the image layer is the same as that of the actual layer. Though the amplitude of the multiple is in reality equal to or less than that of the primary, the multiple looks so very much like a primary that only subtle differences in the two permit separation. Observe that, in contrast to the linear time-distance relationships shown in Figure 7 for the surface waves, the primary and multiple reflections lie on curved paths on the record. The linearity of the surface wave events is due to the fact that these waves, though diverging from a point source, are propagating along the axis of the

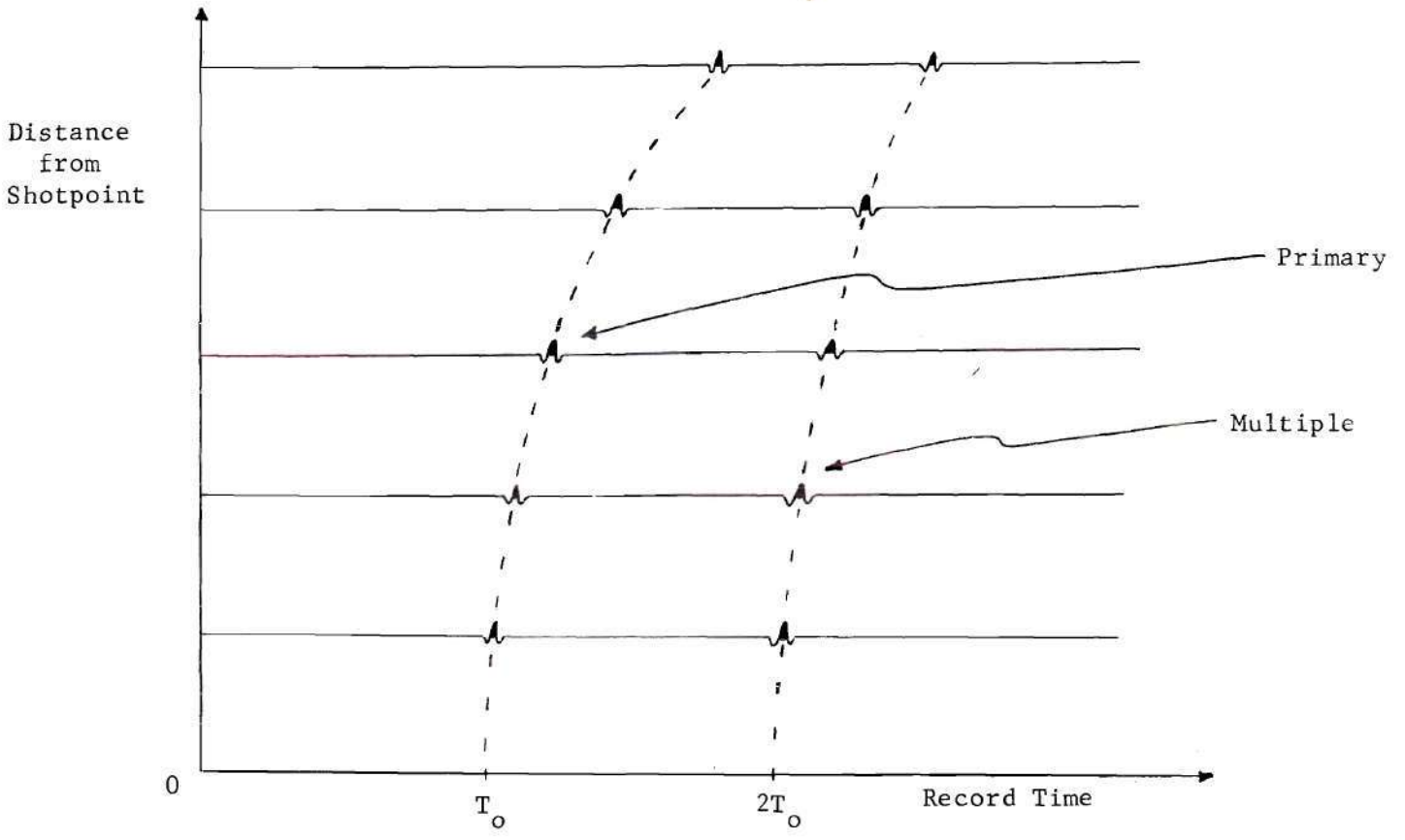

Figure 12. The Appearance of Primary and Multiple Reflections on a Seismogram

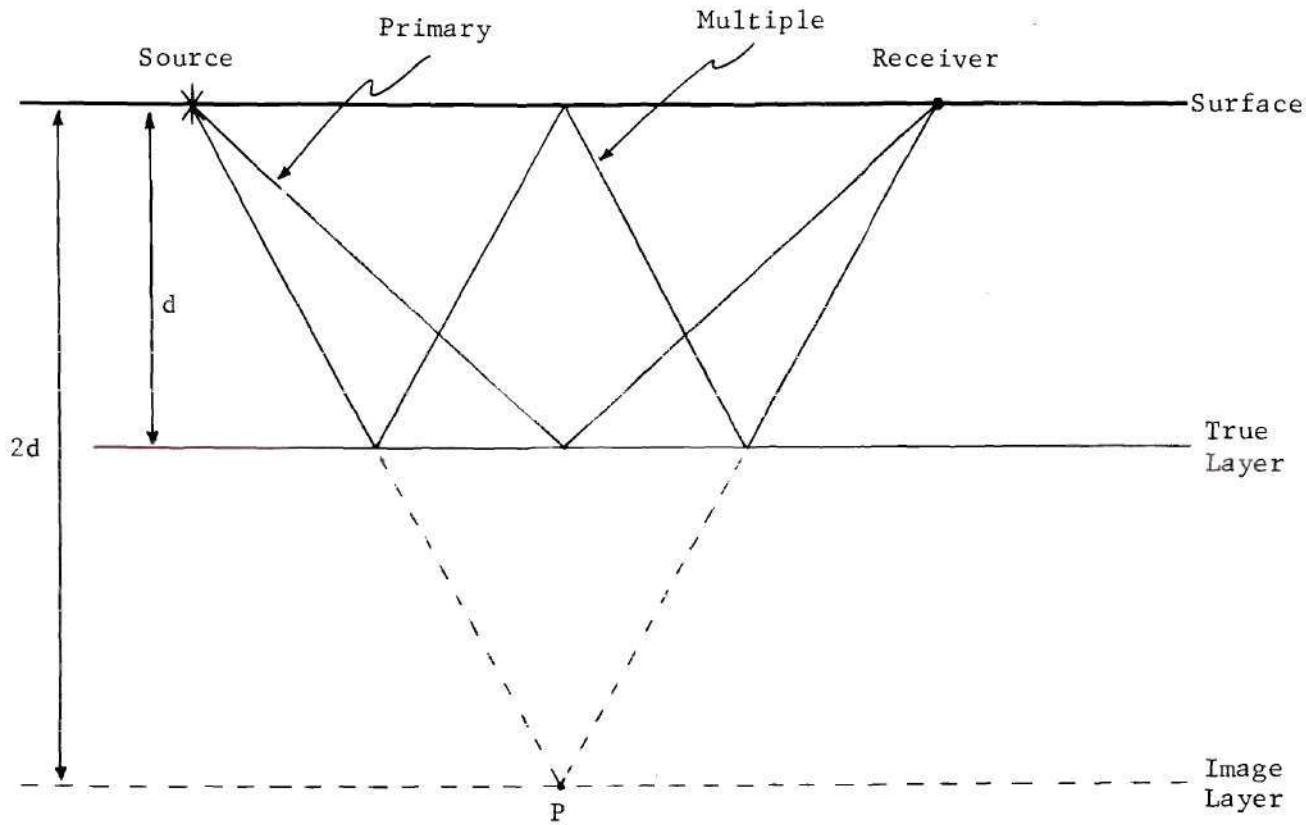

Figure 13. The Generation of the Primary and Multiple Reflections of Figure 12

array. Hence the time difference between events arriving at successive receiver points is constant. This is not the case with primaries and multiples since the diverging wavelets are obliquely incident on the axis of the array.

The main point to be noted here is that the multiple reflection on the record could, in the absence of contradictory information, have been generated by the image layer described. In this case, only the presence of the primary indicates that the second event is truly a multiple. In other situations, to effect separation one is still forced to exploit differences in the two which might never be noticed by a casual observer. For these reasons, multiple reflections represent the major problem in seismic reflection prospecting.

Since the signals and source-generated noise described above exist in the form of waves, they must satisfy some form of the wave equation. The general solution to this equation in three spatial dimensions is

$$s(t;x,y,z) = f\left(t - \frac{x}{V_x(x,y,z)} - \frac{y}{V_y(x,y,z)} - \frac{z}{V_z(x,y,z)}\right) \qquad (3\text{-}1)$$

The quantities V_x, V_y, and V_z are the apparent phase velocities in the x, y, and z directions. The signal of (3-1) is not a function of time only, but is a spatial function as well. Communications engineers have become quite comfortable using the standard time-frequency transform representation of signals. However, if one is able to record signals as functions of space as well as time, it is not illogical to

inquire about spatial frequencies present in the signal, just as one is often concerned with the temporal frequency content. Thus a four-dimensional signal spectrum of (3-1) would be

$$S(\omega;k_x,k_y,k_z) = F\{s(t;x,y,z)\} \tag{3-2}$$

$$= \int_{-\infty}^{\infty} \int \int \int s(t;x,y,z)e^{-j(\omega t-k_x x-k_y y-k_z z)}\, dx\, dy\, dz\, dt$$

In (3-2), k_x, k_y, and k_z are the spatial frequencies, or wavenumbers. Since the geophone group array in seismic reflection prospecting lies along a single spatial axis, one can actually sample signals in only two dimensions--x and t. Thus one is most interested in the spectrum $S(\omega;k_x)$.

Additional insight into the utility of a two-dimensional spectrum can be obtained from the following special case. Consider an impulsive "fence" in frequency-wavenumber (ω-k_x) space, as shown in Figure 14. Such a fence can be represented as

$$S(\omega;k_x) = A(\omega;k_x) \cdot \delta(\omega - uk_x) \tag{3-3}$$

where u is the slope of the fence, δ is the Dirac delta function, and $A(\omega;k_x)$ is any amplitude function. Taking the double inverse Fourier transform of (3-3) yields

$$s(t;x) = \int_{-\infty}^{\infty} \int S(\omega;k_x)e^{j(\omega t-k_x x)} \frac{d\omega}{2\pi} \frac{dk_x}{2\pi}$$

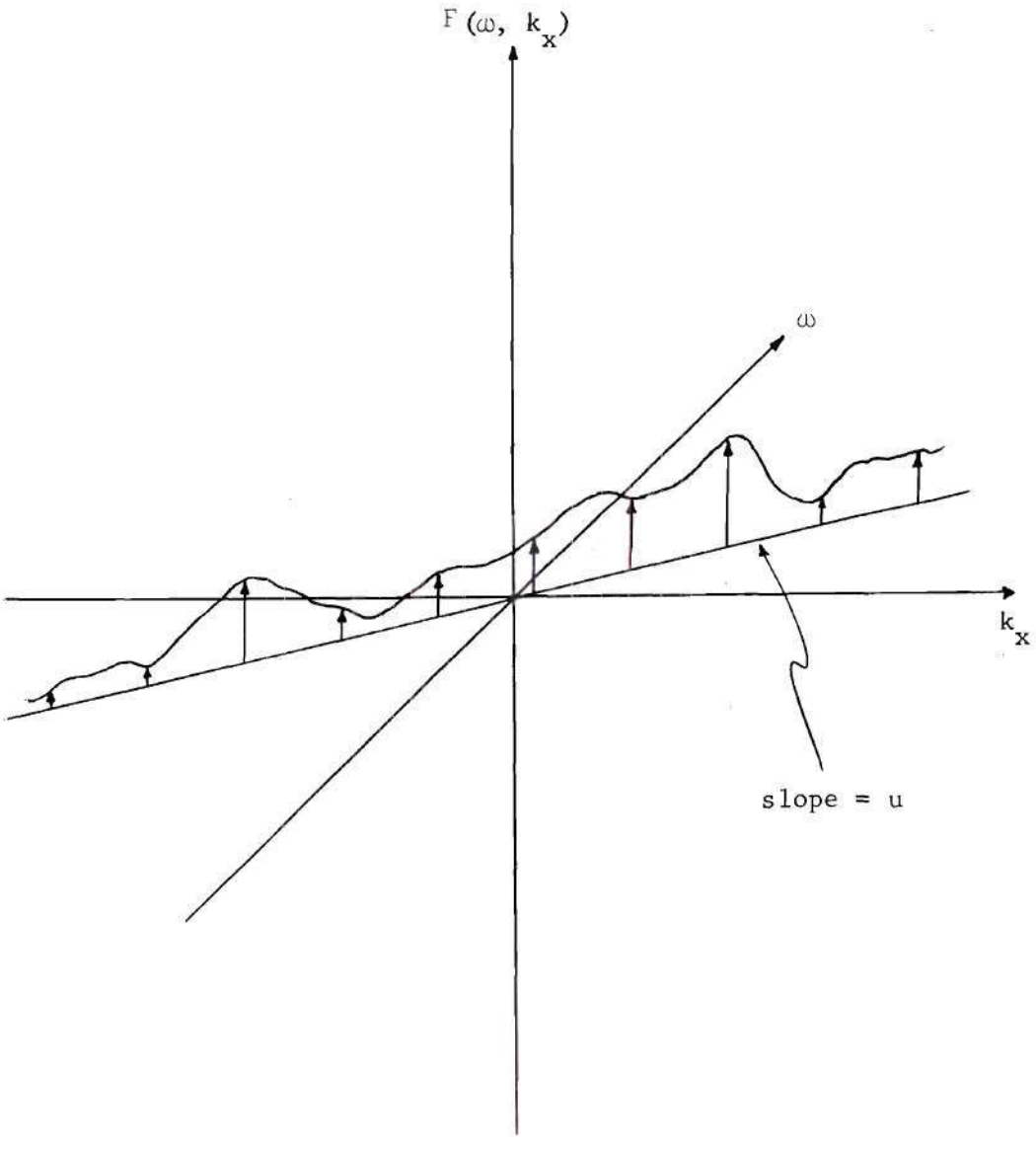

Figure 14. An Impulsive Fence in ω-k_x Space

$$= \int\int_{-\infty}^{\infty} A(\omega;k_x)\delta(\omega-uk_x)e^{j(\omega t-k_x x)}\,\frac{d\omega}{2\pi}\,\frac{dk_x}{2\pi}$$

$$= \int_{-\infty}^{\infty} A(\omega;\tfrac{\omega}{u})e^{j\omega(t-\frac{x}{u})}\,\frac{d\omega}{(2\pi)^2}$$

$$s(t;x) = s_1\left(t-\frac{x}{u}\right) \tag{3-4}$$

One can easily see that (3-4) is a special case of (3-1) in which the apparent phase velocity in the x-direction, $V_x(x,y,z)$, is a constant u. Thus signals of constant apparent horizontal velocity V_x map into points in the ω-k_x domain which lie on a line through the origin with slope V_x.

For a further illustration of the above ideas, consider Figure 15, which illustrates possible signal and noise spectra in ω-k_x space. Applying temporal frequency filters in an attempt to extract the desired signal from this input would have limited effect, since the signal and noise have approximately the same temporal frequency content. But after looking at the two-dimensional spectra one sees that separation can be achieved with an appropriately designed two-dimensional filter. This is, in fact, the basis for *velocity*, or *fan*, filtering,[2,3] a process described in detail in the next chapter.

Finally, the effect that sampling the time-space functions has on their spectral representation is considered. In the following, it is assumed that all sampling is the result of multiplying the function to be sampled by a train of equally-spaced ideal impulses. Though the

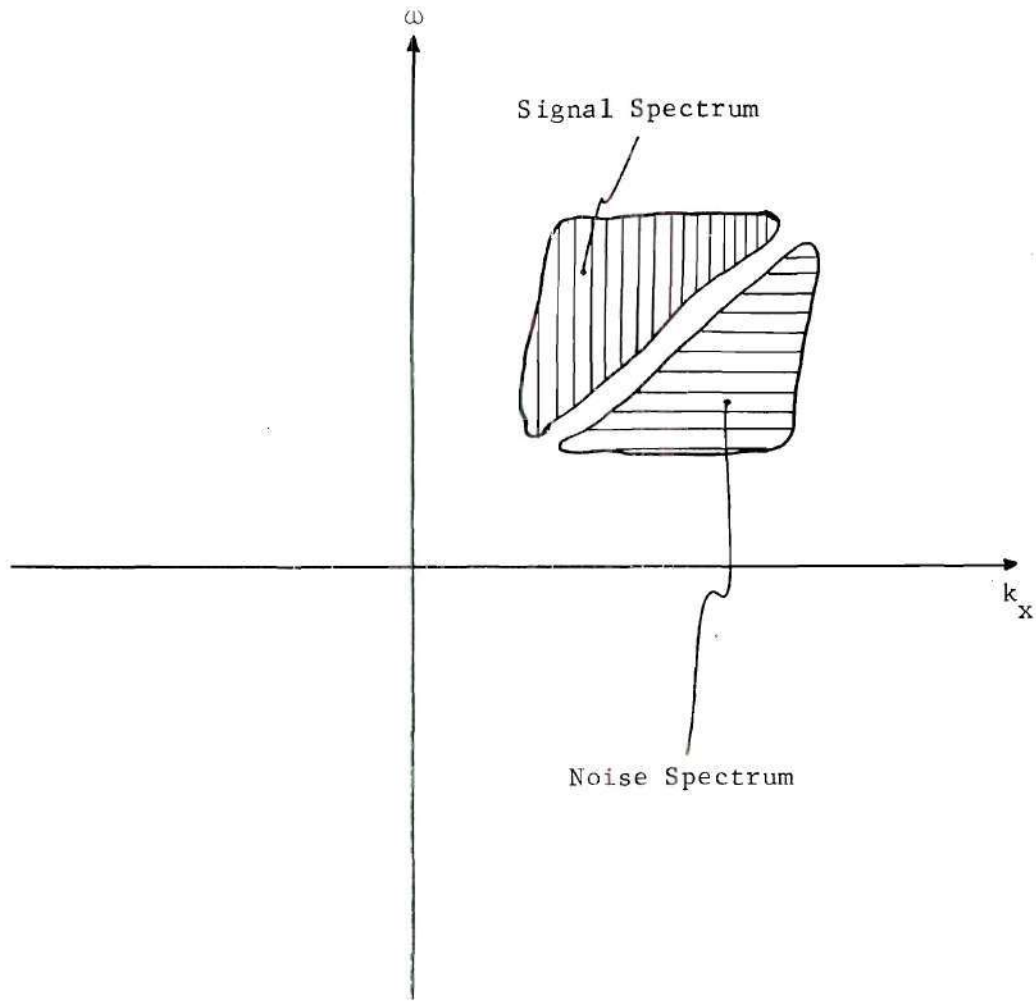

Figure 15. Possible Two-Dimensional Seismic Signal and Noise Spectra

result is developed only for one-dimensional functions and their transforms, the extension to two dimensions is obvious.

Consider an arbitrary function f(t) with Fourier transform F(ω). The sampled version of f(t) is f*(t), and is just

$$f^*(t) = f(t) \cdot \sum_{-\infty}^{\infty} \delta(t-nT)$$

where T is the distance between samples. Papoulis[4] demonstrates that multiplication of two functions, in either domain, is equivalent to convolution of their Fourier transforms. Thus, if F*(ω) is the Fourier transform of f*(t), then

$$F^*(\omega) = F(\omega) \circledast \mathcal{F}\{ \sum_{-\infty}^{\infty} \delta(t-nT)\}$$

where $\circledast$ denotes convolution of the two functions. Papoulis also shows that the Fourier transform of the function on the right is given by

$$\mathcal{F}\{ \sum_{-\infty}^{\infty} \delta(t-nT)\} = \frac{2\pi}{T} \sum_{-\infty}^{\infty} \delta\left(\omega - \frac{2\pi n}{T}\right)$$

Thus, the Fourier transform of an infinite uniform impulse train is another infinite uniform impulse train. The convolution of F(ω) with a shifted impulse $\delta(\omega-k\omega_o)$ is just the shifted version $F(\omega-k\omega_o)$ of F(ω). Thus

$$F^*(\omega) = \frac{2\pi}{T} \sum_{-\infty}^{\infty} F\left(\omega - \frac{2\pi n}{T}\right) \qquad (3\text{-}5)$$

This equation describes the *aliasing* phenomenon. It simply states that sampling of a function by impulses in one domain causes the Fourier transform to be periodic in the other domain, as described by (3-5). The effect of aliasing with regard to filter design is discussed in the next chapter.

CHAPTER IV

SEISMIC PROCESSING

Today nearly all techniques for processing seismic data employ large-memory, high-speed digital computers. In one sense it is logical to divide all processing techniques into two categories--those which filter the data and those which do not. Of the filtering methods, those which use linear filters are easily the most common. In the techniques which use no filtering, the traces are shifted, shrunk, multiplied, and added in various ways, but the convolution operation associated with linear filtering is not used.

Another way to classify the processing methods is according to whether or not optimum, or least-squares, techniques are used. Norbert Wiener devised and popularized optimum linear filtering at M.I.T. in the 1940's. In 1954 a geophysicist, E. A. Robinson, published a doctoral thesis, "Predictive Decomposition of Time Series with Applications to Seismic Exploration," at M.I.T. This was the first application of the theory of optimum linear filters to the seismic estimation problem.

In this chapter, several suboptimum filtering and processing schemes are discussed in some detail. Then a few optimum processing schemes are examined, with particular emphasis on assumptions which are made in deriving the system. It should be noted that all filters used in seismic exploration studies are computer realizations of digital

filters. As such one is not concerned with insuring the filters are causal, or with the problem of realizing the impulse response function by means of physical components like capacitors, resistors, etc.

Suboptimum Processing

Velocity Filtering

At the end of the last chapter it was observed that if seismic signal and noise lay in different parts of ω-k_x space, then an appropriately designed two-dimensional filter should be able to retain signal and reject noise, at least to some degree. This is precisely what one attempts when using velocity filtering. The method was devised and the work was published almost concurrently by two Frenchmen, Fail and Grau,[2] and by three Americans, Embree, Burg, and Backus.[3] It has recently been studied by others.[5,6]

Consider Figure 16. It is first presumed that both signal and noise spectra are bandlimited, both in temporal and spatial frequencies, and therefore both lie within the dashed rectangle in ω-k_x space which is shown. In velocity filtering, as in bandpass filtering, one assumes the signal lies in one part of the frequency domain and the noise in another; here the desired signal should lie in the shaded area, and the noise in any other part of the dashed rectangle. One therefore designs a filter in ω-k_x space which has unity response in the shaded area and zero response outside. This is a velocity (or fan, or pie-slice) filter. Fourier transformation of this frequency response $H(\omega;k_x)$ yields $h(t;x)$, the two-dimensional impulse response function. This derivation of $h(t;x)$ is performed in Appendix B; the sampled-data, or digital, impulse response is found to be

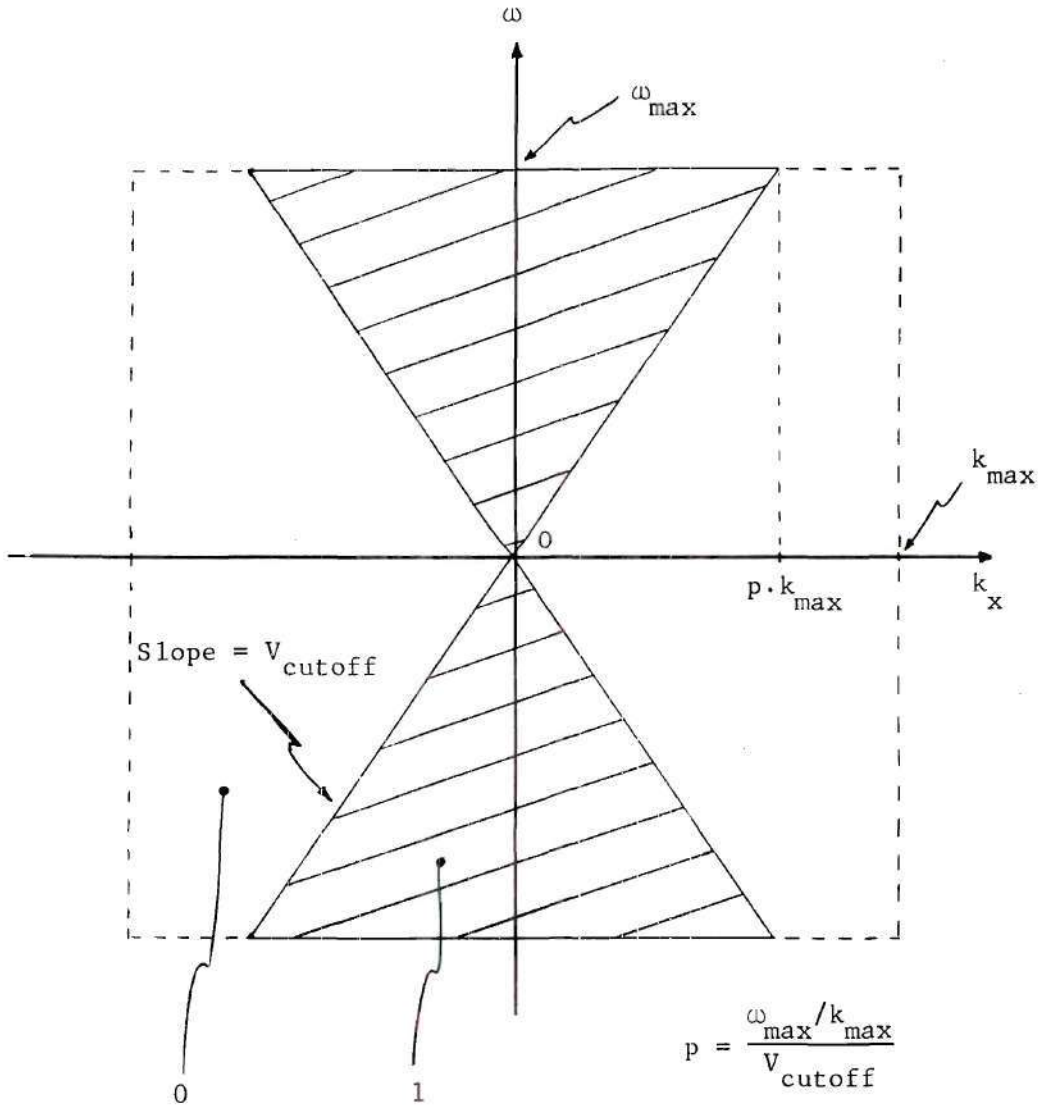

Figure 16. Desired Transfer Function of Velocity Filter

$$h(nT;mX) = \frac{p}{\pi^2 XT} \cdot \left[\frac{1}{n^2 - p^2 \cdot (|m|-0.5)^2}\right] \cdot \left[(-1)^n \cos\{p(|m|-0.5)\pi\}-1\right] \quad (4-1)$$

where p is the parameter defined on Figure 16, and T and X are the distances between time and space samples. The reason for assuming the signal and noise spectral distributions shown in Figure 16 is the fact that often the apparent horizontal velocities of all primary reflections are greater than the apparent horizontal velocity of some of the noise. For instance, the apparent horizontal velocity of ground roll is seldom more than 3000 feet/second, while that of primary reflections is always greater than the interval velocity of the first layer, say 6000 feet/second. The filter in Figure 16 would separate these two.

There are a number of observations which can be made about the implementation of the velocity filter. First, the idea that a spherical wavelet has a single apparent horizontal velocity is useful but not strictly valid. The direction of the phase velocity vector is a function of the position of the earth's surface, as shown by Figure 17. Consequently, at different locations along the receiver array the moveout per trace* will vary. The length of the array, the distance of the array from the shotpoint, and the depth of the reflection all influence how much it varies. The deeper the reflection and the shorter the array, the more nearly will the apparent horizontal velocity be constant.

---

*Moveout per trace--difference in wavelet arrival time at adjacent receiver points. For uniformly spaced arrays it is often used instead of apparent horizontal velocity, since moveout per trace is just the receiver spacing divided by apparent horizontal velocity.

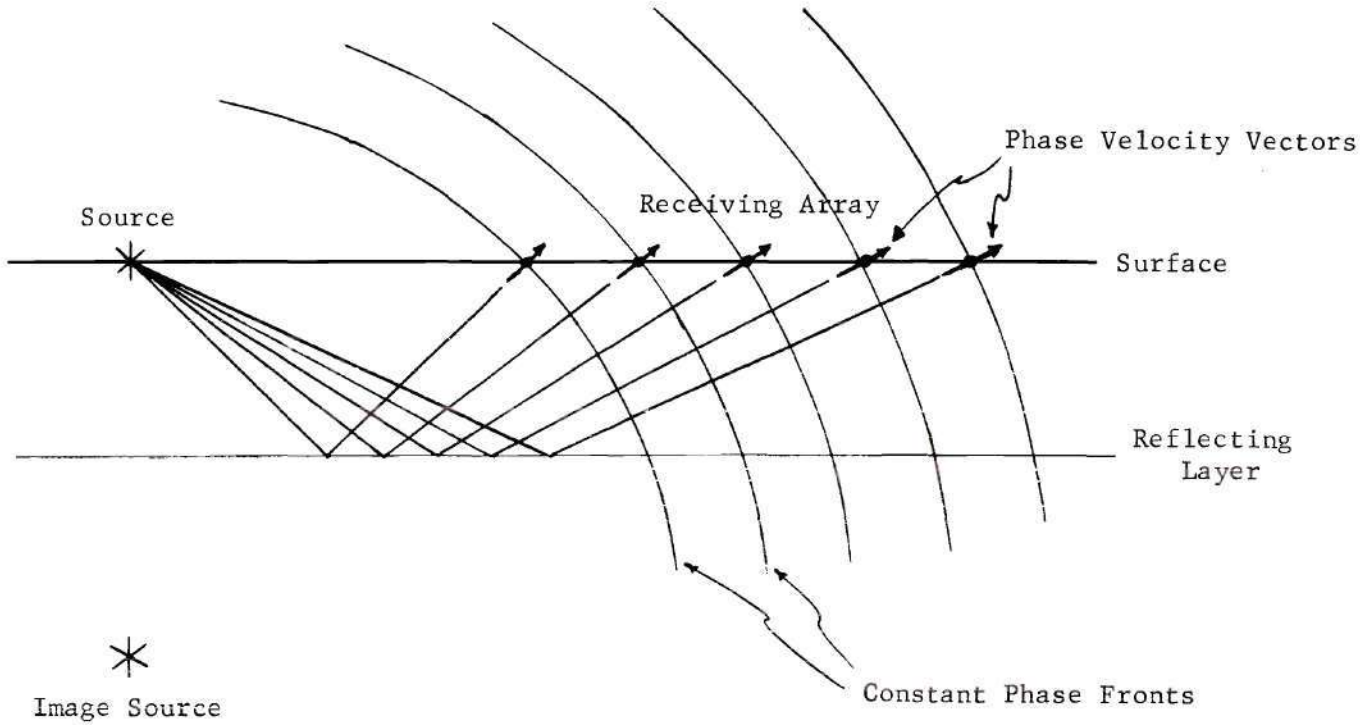

Figure 17. The Variation of the Direction of the Phase Velocity Vector of a Spherical Wavelet as a Function of Surface Location

The fact that the apparent horizontal velocity is not constant implies that the received spherical wavelet has a spectrum which is *not* an impulsive fence in ω-k_x space, but a surface which perhaps closely resembles such a fence. Hence even an ideal filter such as that of Figure 16 might not pass a desired wavelet undistorted, and might not be able to completely reject undesired wavelets.

Also to be noted is the aliasing of the transfer function of the velocity filter. If the signals are sampled every Δt seconds in time and Δx feet in space, the aliased transfer function is periodic in temporal frequency with period $2\pi/\Delta t$ and in spatial frequency with period $2\pi/\Delta x$. It is shown in Figure 18. Notice that the signals should be sampled at a rate greater than twice the highest frequency present in *signal or noise;* otherwise high-frequency noise might be passed by the first aliasing of the filter, when ordinarily it would be rejected.

A topic of considerable interest in both this and other kinds of filtering is the effect which truncation has on the ideal characteristic of Figure 16. Since this transfer function $H(\omega;k_x)$ is band-limited in both ω and k_x, its Fourier transform, the impulse response function $h(t;x)$, cannot be limited along either the time or space axis. One is limited practically to using a finite number of samples of $h(t;x)$, and consequently one might expect deterioration of the ideal characteristic in some way. The exact effect of using a finite number of samples point operators is best understood by recognizing that truncation is equivalent to multiplication by some kind of gate function, i.e., a function which is zero outside certain limits.

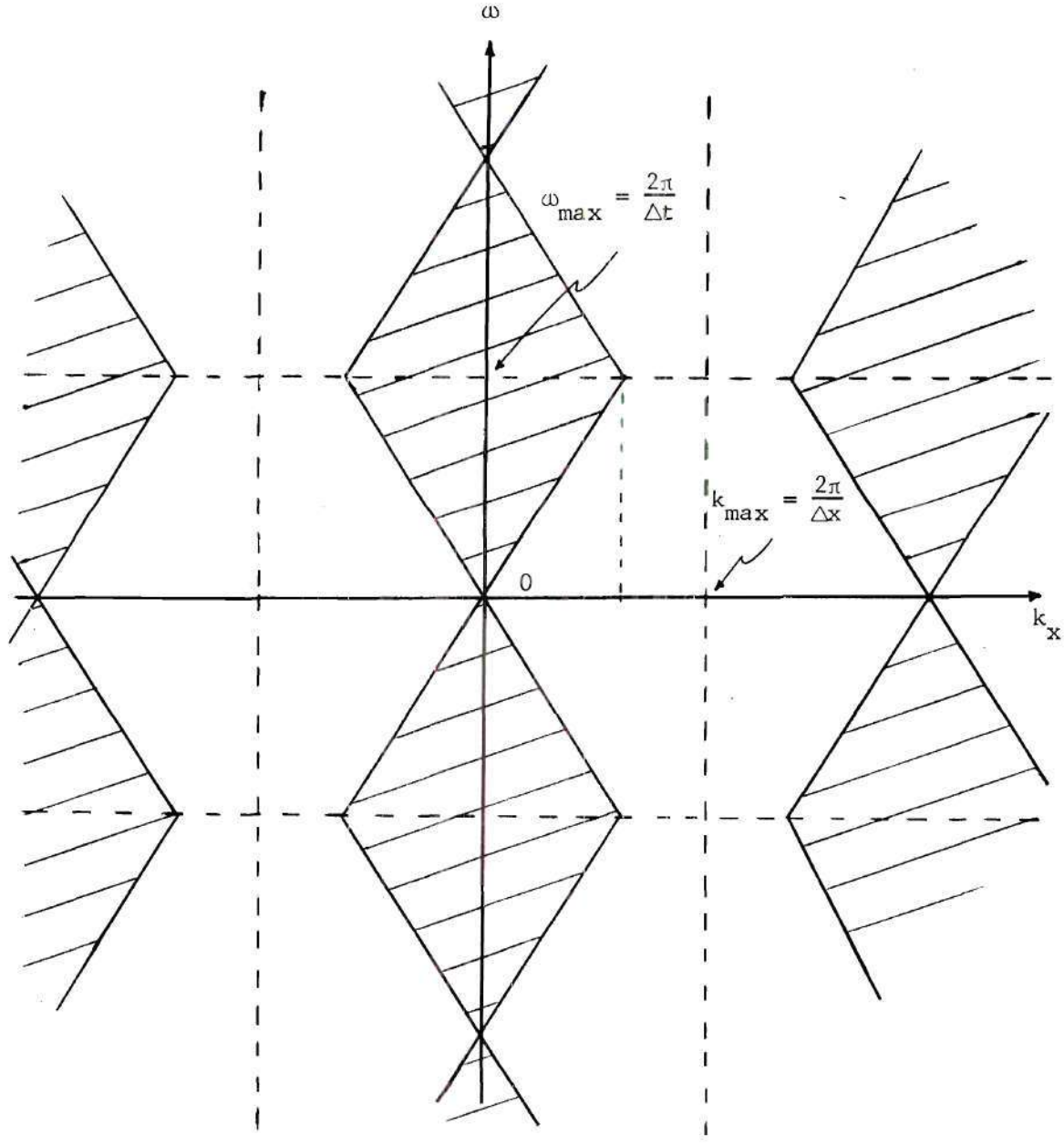

Figure 18. Aliased Velocity Filter Transfer Function

The most common type of gate function is a rectangular gate, which is unity inside the limits. As shown by Papoulis,[4] and as illustrated in Figure 19 by a rectangular gate, multiplication of two functions in one domain is equivalent to convolution of their Fourier transforms in the other. Consequently, the truncation problem can be reduced to the following question: What gate function has a Fourier transform which, when convolved with the desired filter transfer function, yields the best reproduction of the desired transfer function in some sense. The problem is discussed again in a later chapter.

Deconvolution Filtering

Another kind of suboptimum filtering which is quite popular among exploration geophysicists is *deconvolution*, or inverse, filtering. The basic idea of this processing scheme is illustrated by the block diagram of Figure 20. A signal x(t), possibly a sharp pulse, is put into the earth, which can be represented as a time-invariant linear filter with impulse response function b(t). Out of the earth filter comes the received signal y(t), which is just the convolution of x(t) and b(t). The object of the deconvolution filter is to "undo" the effect of the earth in such a way that the output signal is a wave form of some predetermined shape d(t). That is, the impulse response function a(t) of the inverse filter must be such that

$$d(t) = [x(t) \circledast b(t)] \circledast a(t)$$

Strictly speaking, the term inverse filtering should be applied only when d(t) = x(t). The term spiking filter is used when the desired

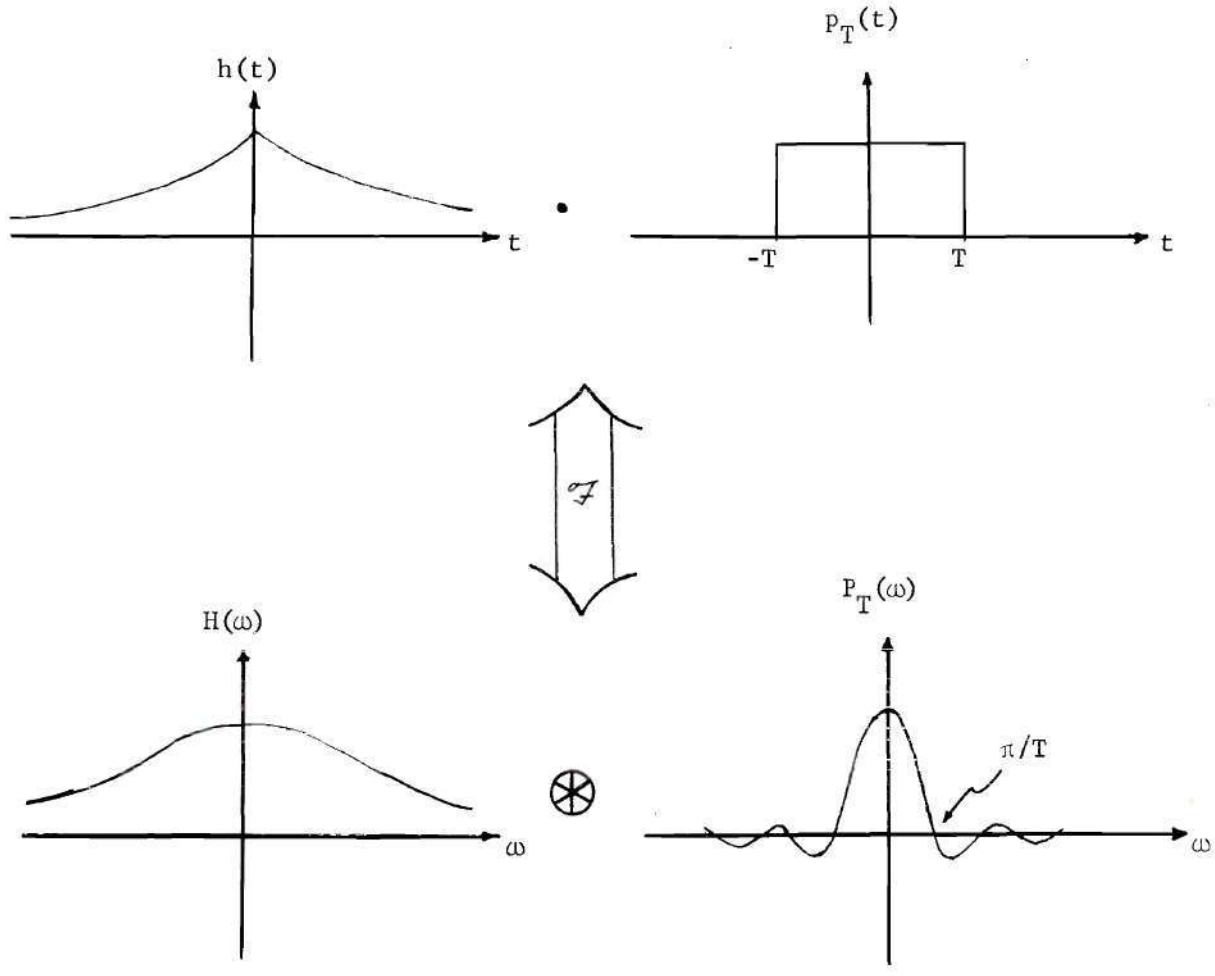

Figure 19. Equivalence of Multiplication and Convolution of Functions Under Fourier Transformation

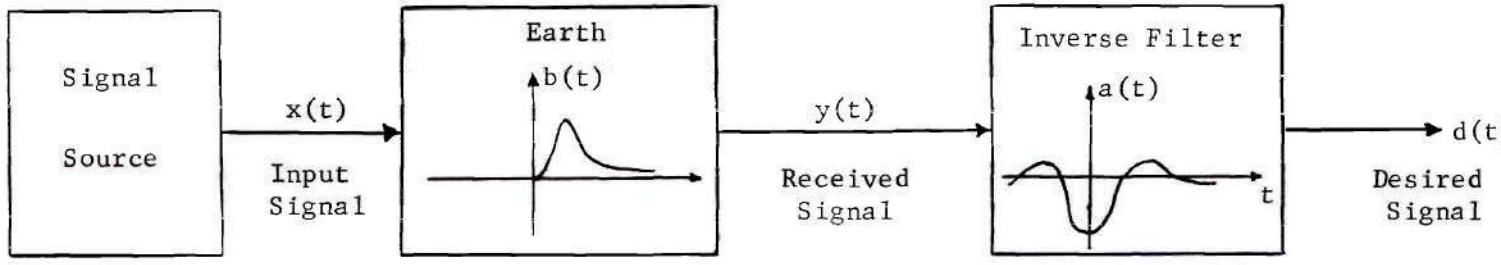

Figure 20. Deconvolution Filtering

signal d(t) is an impulse, and the term shaping filter may be used when d(t) is a wavelet of arbitrary shape. The filter a(t) may be unrealizable (two-sided) since it is a computer realization; however the filter b(t) is realizable since the earth cannot anticipate the presence of a signal. Since the digital computer is used for the processing, time functions like a(t) become series, which are represented as $(\ldots a_{-2},a_{-1},a_0,a_1,\ldots)$ where a_2 is the sample at time $t = 2T$, and so on. The following analysis of deconvolution is taken from Robinson.[7] For further study one should consult the literature.[8-13]

Consider the problem of deconvolving the received digital signal in such a way that the output series $\underline{d}$ is just a spike at $t = 0$, i.e.,

$$\underline{d} = (\ldots d_{-2},d_{-1},d_0,d_1,d_2,\ldots) = (\ldots 0,0,1,0,0,\ldots)$$

It is presumed that one knows *a priori* the signal which is put into the earth, and for simplicity let this also be an impulse. Hence the input to the deconvolution filter is just the impulse response function of the earth, $\underline{b} = (\ldots 0,0,b_0,b_1,b_2,\ldots)$. One further must know this impulse response, since it would hardly be practical to deconvolve without knowing the effect of convolution. Again for simplicity, assume that the series $\underline{b}$ is of length two and has been normalized, so that the input to the inverse filter is $(b_0,b_1) = (1,k)$. Thus

$$\underline{d} = \underline{a} \circledast \underline{b}$$

where the symbol ⊛ stands for convolution. Taking z-transforms[14] of both sides,

$$1 = A(z) \cdot (1+kz)$$

$$A(z) = \frac{1}{1 + kz}$$

$$= 1 - kz + (kz)^2 - (kz)^3 + \ldots$$

Thus, if $|k| < 1$, one has a stable filter of infinite length with operators

$$a_0 = 1$$

$$a_1 = -k$$

$$a_2 = k^2$$

and so on, with $a_i = 0$ if $i < 0$. If $|k| > 1$, one can expand A(z) as

$$A(z) = \frac{1}{1 + kz}$$

$$= (kz)^{-1} - (kz)^{-2} + (kz)^{-3} - \ldots$$

which represents a stable digital filter of infinite length, with operators

$$a_{-1} = k^{-1}$$

$$a_{-2} = -k^{-2}$$

$$a_{-3} = k^{-3}$$

and so on, with $a_i = 0$ for $i \geq 0$.

In most cases one would like the inverse filter to have a finite number of sample point operators, even if its output were not a duplicate of the desired series, $\underline{d}$. In a final look at deconvolution filters, a means of finding a filter of given length, which minimizes the mean-square difference between desired and actual outputs, will be shown. Let the inverse filter series be two operators long, and again let the input to the filter be (1,k) and the desired output be a unit spike at the origin. The difference between the desired output series $\underline{d}$ and the actual output series $\underline{c}$ is called the error series $\underline{e}$. The coefficients (a_0,a_1) are to be chosen in such a way that the energy (sum of the squares of the samples) of $\underline{e}$ is minimized. Following the details in Robinson,[7]

$$\underline{c} = \underline{a} \circledast \underline{b}$$

$$= (a_0,a_1) * (1,k)$$

$$= (a_0, a_0k+a_1, a_1k)$$

$$\underline{e} = \underline{d} - \underline{c}$$

$$= (1,0,0) - (a_0, a_0k+a_1, a_1k)$$

$$= (1-a_0, -a_0k-a_1, -a_1k)$$

The energy I in this error signal is

$$I = (1-a_0)^2 + (-a_0k-a_1)^2 + (-a_1k)^2$$

$$= 1 - 2a_0 + a_0^2(1+k^2) + 2a_0a_1k + a_1^2(1+k^2)$$

To minimize I with respect to a_0 and a_1, simply take derivatives with respect to each and set these to zero, solving the two resultant equations for a_0 and a_1.

$$\frac{\partial I}{\partial a_0} = -2 + 2a_0(1+k^2) + 2a_1k$$

$$\frac{\partial I}{\partial a_1} = 2a_0k + 2a_1(1+k^2)$$

and

$$a_0 = \frac{1 + k^2}{1 + k^2 + k^4} \qquad a_1 = \frac{-k}{1 + k^2 + k^4}$$

It can be shown that the minimum error energy is then

$$I_{min} = \frac{k^4}{1 + k^2 + k^4}$$

as compared to $I = k^4$ obtained by taking the first two terms ($a_0 = 1$ and $a_1 = -k$) of the infinite series obtained earlier. It is easy to see how approximate inverse filters of greater length might be obtained by this same procedure.

Common-Depth-Point Stacking

The final suboptimum technique to be considered is common-depth-point (CDP) stacking. The fact that it is considered last should not be interpreted as a commentary on its importance. It is the most widely used method in the industry today, and the only technique reported to date which has been proved effective in reducing multiple reflections.

Before explaining the CDP method, the subject of normal moveout (NMO) corrections should be examined in greater detail. As was pointed out in Chapter II, this correction causes each event on the record to occur at the time at which it would have occurred had the wavelet propagated along a vertical path to the reflection point and back to the surface. Consider Figure 21. The traces of Figure 22(a) are records from the receiver points 1, 2, and 3 shown in Figure 21, with no moveout corrections applied. Once the events have been moveout corrected using the following formula derived in Appendix A,

$$T_0^2 = \sqrt{T^2 - \left(\frac{X}{2V}\right)^2}$$

where

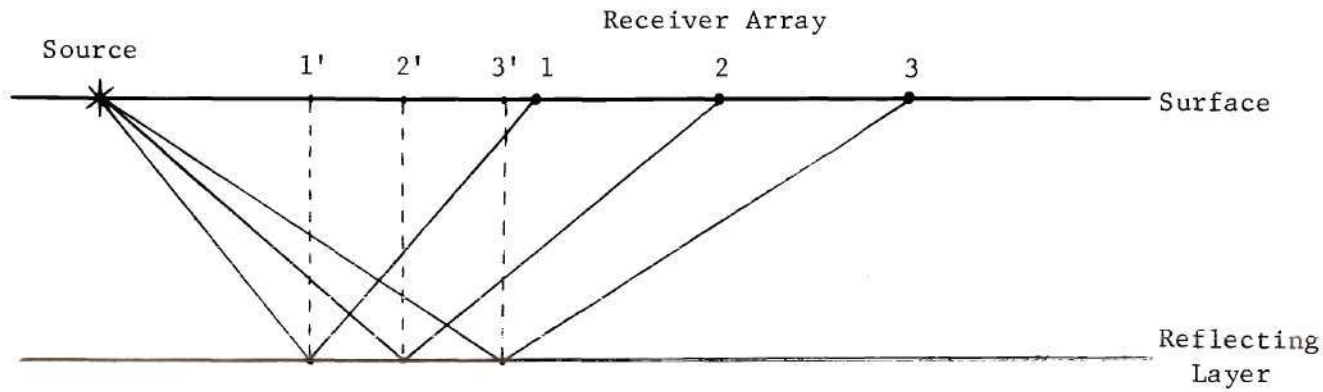

Image Source

Figure 21. Normal Moveout Corrections for Several Reflections

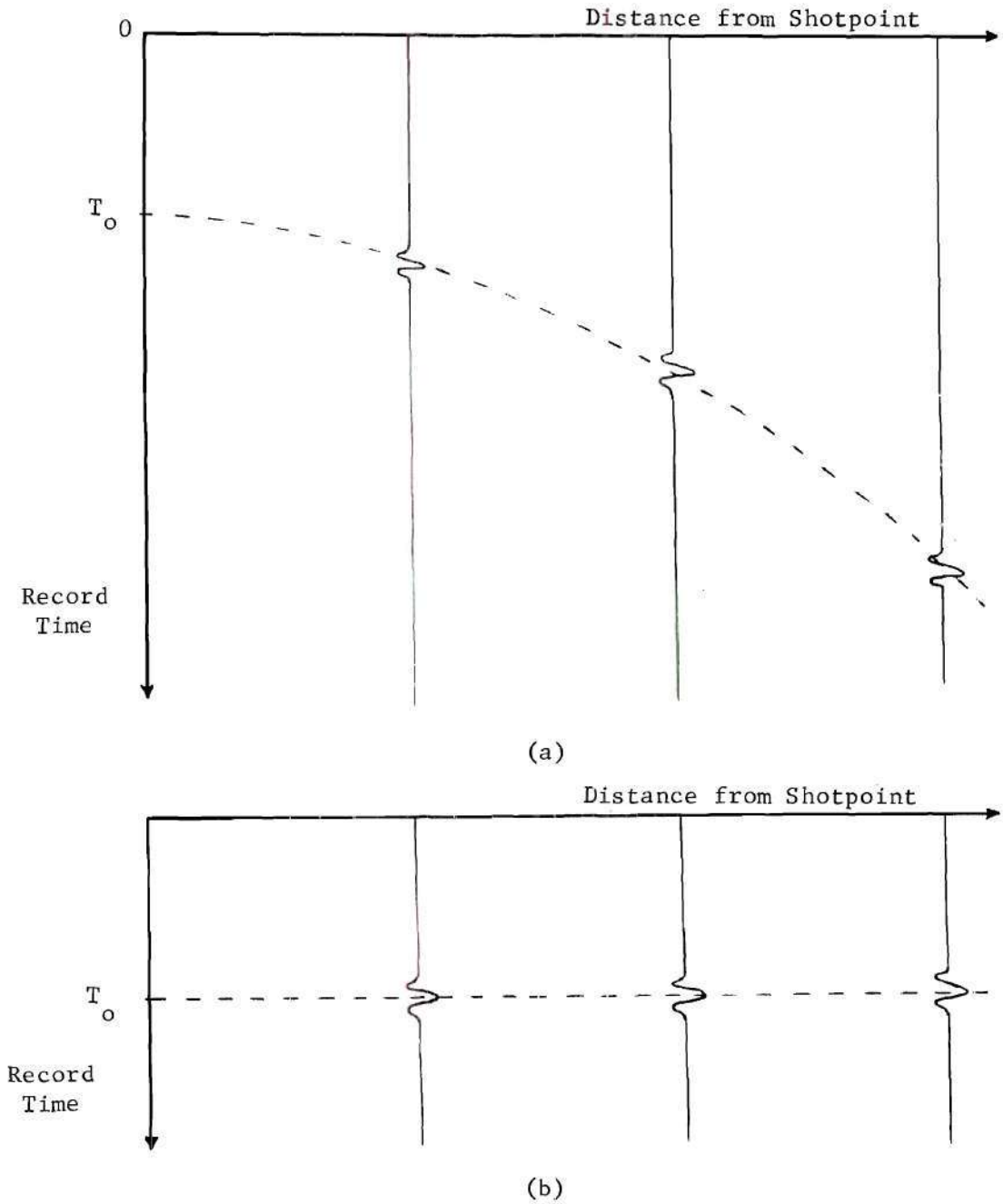

Figure 22. An Event on a Reflection Seismogram
(a) Before NMO Correction
(b) After NMO Correction

T_0 = two-way vertical travel time

X = shotpoint-receiver distance

V = average velocity to the interface

T = actual time of event

they appear to have been both excited and received at points 1', 2', and 3', as shown in Figure 22(b). Of course, the accuracy of the normal moveout correction is very much dependent on how accurately one is able to estimate the average velocity as a function of record time, or depth. And since moveout corrections are eventually applied to nearly all data, obtaining this velocity estimate is a subject of prime importance. An estimate of average velocity is required in other systems, as well as in those employing normal moveout corrections.

In a word, CDP stacking is correcting the traces for moveout and adding them in such a way that primaries reinforce one another and multiples do not. How this is accomplished can best be understood from the example in Figure 23, which is taken from Mayne's original paper on the subject.[15] Wavelets are excited at locations 1, 2, and 3 on the surface, and recorded at the points 1', 2', and 3'. Observe that the shot and receiver points are spaced symmetrically about the point P, so that any primary reflection from a subsurface layer bounces off a point directly below P, and all primaries from the same layer are reflected from the same point. This geometry of excitation and recording is one of the key features of the method; there is no "averaging" effect present due to combining events from many subsurface points. Thus the distinct features of each bounce are preserved.

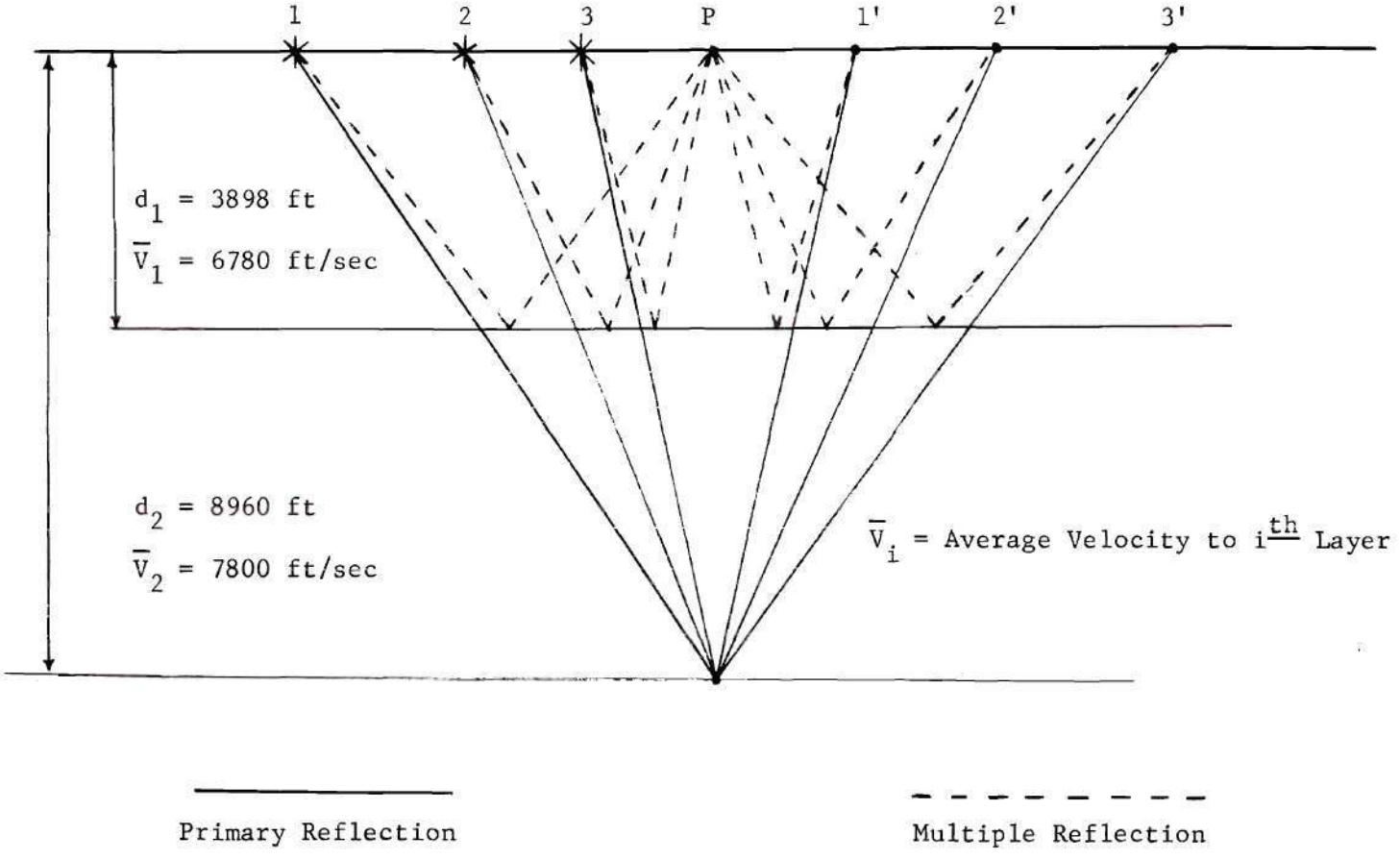

Figure 23. Example Used to Illustrate CDP Stacking

Once the shots at points 1, 2, and 3 have been recorded, they might appear as in Figure 24(a). The actual curvatures shown are exaggerated somewhat for the purpose of illustration. The reason that the multiple reflection exhibits more moveout per trace is that average velocity is generally an increasing function of depth (or record time). If moveout corrections are now applied to each of the traces in the usual way, the result is shown in Figure 24(b). The primaries now all occur at 2.30 seconds, while the multiples still appear at different times. If the traces are now summed, the amplitude of the resultant primary will be three times as large as it was before, while the peak amplitude of a multiple event will be the same as it was before. The summed traces of the example are shown in Figure 24(c). This primary enhancement is the most attractive feature of common-depth-point stacking.

The advantages offered by the CDP process, namely multiple elimination and processing data from a single depth point, are significant. Since the basic technique described above was first proposed in 1962, there has been considerable effort toward improving and refining it. Selected references are given in the Bibliography.[16-19]

Optimum Processing

In its most general sense, the word optimum as used here means any processing method which is derived using the least-mean-square error criterion in any way. In this sense, the finite-length deconvolution filter derived earlier was an optimum filter. In this section, however, some optimum techniques of a bit more sophisticated nature are discussed.

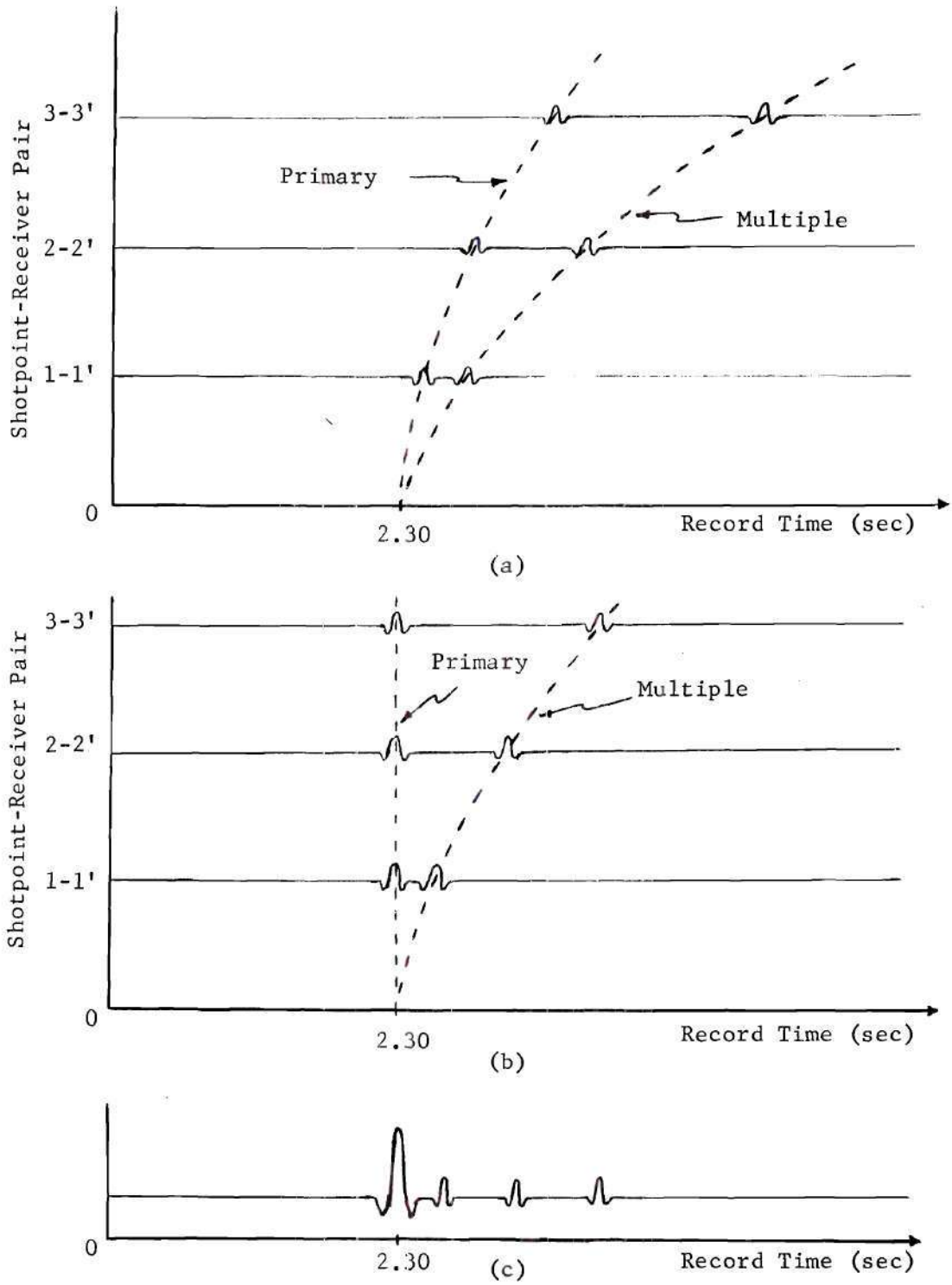

Figure 24. Reflections of Figure 23 (a) Before CDP Stacking, (b) After NMO Corrections, and (c) After NMO Corrections and Summation

Though optimum linear filtering had been a part of communication theory for several years, it was not until 1952 that a small group of geophysicists at M.I.T. recognized that many of the techniques used by communications theorists might be applied to their own seismic problems. This group of professors and graduate students, with financial help from a number of interested petroleum companies, turned out a great deal of research in this area from 1952 through 1957. Though the efforts of the group, known as the Geophysical Analysis Group (GAG), were not immediately put to use in the exploration industry, there can be no doubt that it was they who turned seismic exploration in the direction in which it is now moving.

Robinson's thesis, which was recently published in its entirety in a special GAG issue of *Geophysics*,[20] was the first application of optimum filtering and prediction to seismic problems. In his own words, the research was an attempt at "coordination of statistical methods with knowledge of practical and theoretical seismology." In the thesis he reviewed techniques for finding optimum discrete linear filters and predictors, and applied these to the problem of seismic signal estimation and prediction. His prediction operators actually take the form of the deconvolution filters discussed earlier. Rather than assuming a wavelet shape, however, he uses a least-squares method for estimating this from the seismic trace being used.

Since the demise of the Geophysical Analysis Group there have been a number of attempts to apply least-mean-squares techniques to seismic processing. Burg[21] developed the optimum three-dimensional linear filter, than applied it to the problem of extracting the micro-

seismic signals encountered in earthquake seismology from the noise present.[22] In the usual manner, the development of the least-squares filter required (1) that signal and noise be uncorrelated and (2) that both signal and noise be taken from wide-sense stationary random processes. As in the implementation of any optimum techniques, accurate knowledge of signal and noise power spectra (in this case three-dimensional) are required, and are difficult to actually measure.

Multidimensional least-squares filters have also been used to eliminate *ghost* reflections.[23] These are signals which have traveled from the shotpoint beneath the surface, back to the surface, then back to a subsurface layer and up to the detector. They are present only when using explosives, since only then is the signal excited below the surface. Again, implementation of the linear optimum filter requires the assumptions of stationarity and uncorrelatedness, though the authors admit that the latter cannot be justified, but must be made for analytical convenience.

In a recent paper,[19] least-squares techniques are applied to the derivation of stacking filters. These are filters which are used to perform the stacking operations described earlier. They attempt to provide more rejection of multiples than is available from ordinary stacking by filtering the moveout-corrected traces rather than merely summing them. Presuming a knowledge of the relative locations of primaries and multiples, the optimum techniques are applied in the usual manner and incorporate the usual assumptions.

If the descriptions above seem somewhat cursory, it is partly because the details are familiar and partly because optimum filters

are only optimum if one models the signal and noise processes correctly. This last point is among the topics covered in the next chapter.

CHAPTER V

OBSERVATIONS ON CURRENTLY USED METHODS

In this chapter, the effectiveness of the processing methods of Chapter IV is considered in detail. Several of these techniques make assumptions which are highly dubious; these are discussed,as are strong points in each of the schemes.

Velocity Filtering

It was demonstrated that, if signal and noise spectra lie in separate regions of ω-k_x space, an appropriately designed velocity filter can retain the signal and, to some degree, reject the noise. It was also mentioned that ground roll typically has a velocity much lower than that of any of the desired primaries, and thus can usually be filtered in this manner. A question which now comes to mind is: "Can a velocity filter separate primaries and multiples, i.e., is there a cutoff velocity such that the horizontal velocities of all primaries are greater than this cutoff and those of all multiples are less than the cutoff?" It can easily be demonstrated that no such cutoff exists. Consider Figure 25. A primary and a multiple from the same interface are shown, with the "image" layer for the multiple also included. The two wavelets have traveled through the same medium, but are incident on the receiver at different angles, θ_p and θ_m. Since θ_m is greater than θ_p, the apparent horizontal velocity of the multiple is larger than that of the primary. More likely than not, the next primary will

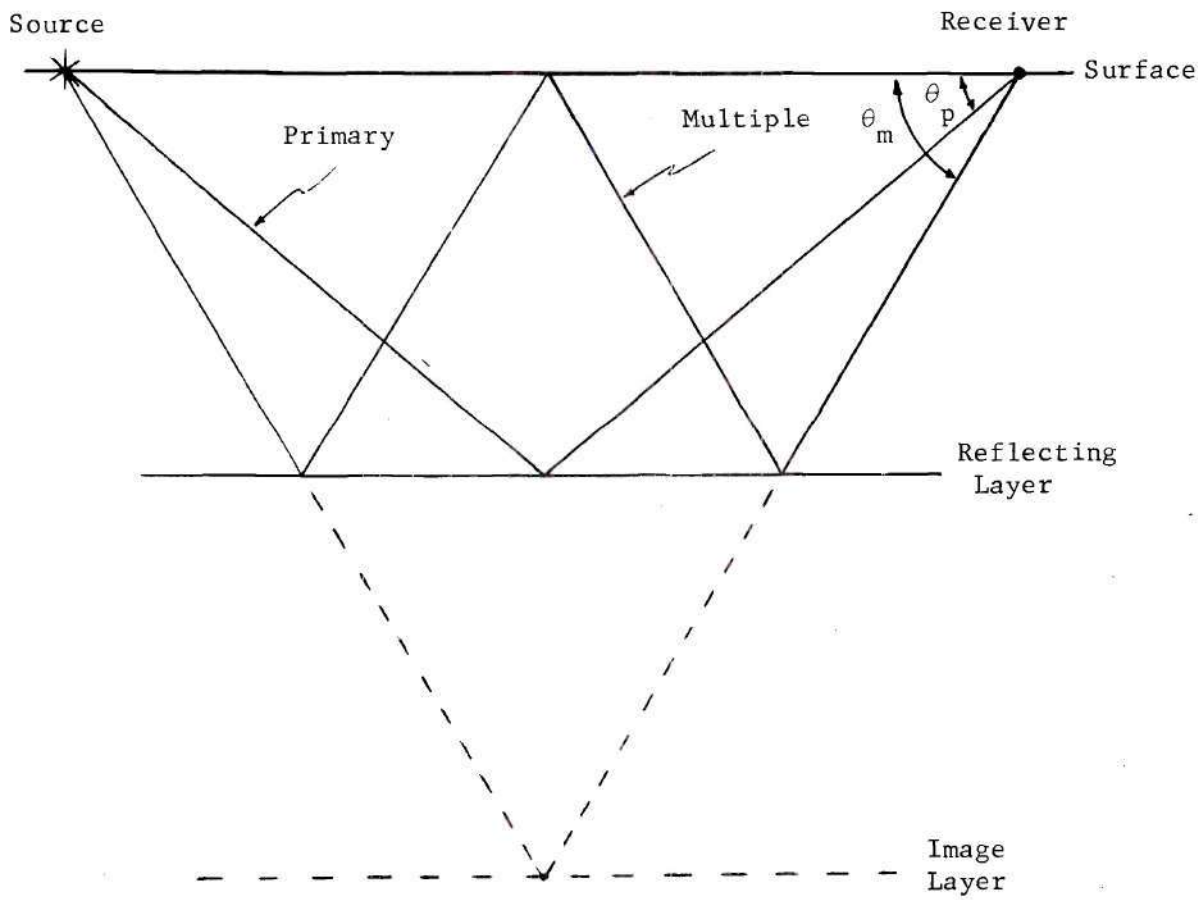

Figure 25. Illustration of the Fact that Multiples Can Have Greater Apparent Horizontal Velocity than Primaries

have a larger apparent horizontal velocity than this multiple, and the horizontal velocities of subsequent multiples will be greater than that of either primary. Consequently it is impossible for a velocity filter like the one described in Chapter IV to achieve separation of primary and multiple events. For this reason, velocity filtering is little used today, and then only to eliminate ground roll.

Deconvolution Filters

Deconvolution filters are widely used by those who actually process data from the field, since the net effect is to "sharpen" all events on a record, tending to make them impulses as closely as possible. But since no noise rejection is included in the filter design, none occurs, and in fact multiples are sharpened just as much as primaries. Another problem encountered with deconvolution, wavelet broadening, has recently been reported.[13] Wavelet broadening is the tendency of the earth to attenuate the higher frequencies in a signal to a greater degree than the low frequencies present. Thus, as shown in Figure 26, a signal which is a spike at record time zero would be broadened if received at two seconds, and broadened still more after four seconds. An inverse filter designed to deconvolve the wavelet received at two seconds into an impulse certainly could not do the same for the wavelet at time four seconds. The reference cited proposed a time-varying deconvolution filter, one which changed its assumed wavelet shape at discrete times, thus continually sharpening all received wavelets. Even so, primaries and multiples alike are enhanced.

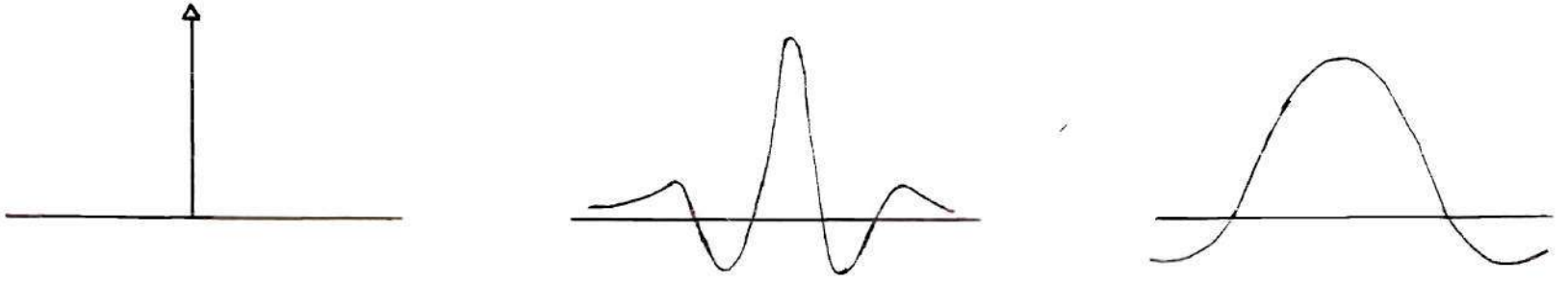

Figure 26. Wavelet Broadening; a Seismic Wavelet
(a) At Excitation
(b) Two Seconds After Excitation
(c) Four Seconds After Excitation

Optimum Techniques

Though the two suboptimum filters mentioned above have inherent problems, and though neither affords any protection from multiple reflections, there are also a number of fundamental problems associated with those methods which have been called "optimum" up to now. The first of these is the determination of the signal and noise power spectra or autocorrelation functions. In optimum linear filtering problems, the final expression for the impulse response function or transfer function characteristic is always in terms of these statistical characteristics; generally they are difficult, if not impossible, to obtain. Further, since primaries and multiples have approximately the same frequency content, it is difficult to see how an optimum one-dimensional filter could afford any separation between them. The same could be said of any multidimensional optimum filters of the usual variety, since primaries and multiples occupy the same regions of ω-k_x space.

Besides the fact that correlation functions are difficult to obtain, it can also be shown that two basic assumptions which are nearly always made in optimum processing techniques cannot be justified in the seismic reflection problem. The first of these is the assumption that noise and desired signal and uncorrelated. It is obvious that disturbances generated by the same source and received at a common point must be correlated to some degree; since multiples and primaries travel much the same path, there should be a very strong correlation between them, and a lesser correlation between primaries and other source-generated noise. In the derivation of the optimum linear filters it is

not required that signal and noise be uncorrelated; but if this is not assumed than one must specify the crosscorrelation function $R_{sn}(t_1,t_2)$, and this is usually even harder than giving the autocorrelation functions. Indeed, in the paper dealing with ghost elimination[23] the authors admit that the assumption is not valid, but declare that it must be used in order to get the desired filter.

A second assumption which is generally made is that signal and noise are sample functions taken from wide-sense (weakly) stationary random processes. Again it is not necessary that one assume this, but otherwise one must again know all correlation functions, which now are of the form $R(t_1,t_2)$ rather than $R(t_1-t_2) = R(\tau)$. Specification of correlation functions of this form is a formidable task. It will now be shown that this assumption is inconsistent with reality in the seismic problem.

If a function is a sample function from a wide-sense stationary random process, its basic character is invariant with respect to time; i.e., its approximate mean, variance, frequency content, etc., are independent of the location of the time origin. It has already been pointed out in the discussion on wavelet broadening that the earth acts as a low-pass filter, and that the longer a wavelet travels through the earth, the lower is its frequency content. Thus the wavelets generated are nonstationary in this sense. In addition to wavelet broadening, the strength of the received signal and multiple noise fades greatly with increasing record time due to attenuation and spherical divergence. It is a necessary, but not sufficient, condition for stationarity of any sense that

$$E\{s(t_1)s^*(t_2)\} = R_s(t_1,t_2)$$

$$= R_s(t_1-t_2)$$

$$E\{s(t_1)s^*(t_2)\} = R_s(\tau) \qquad (5\text{-}1)$$

where $E(\cdot)$ means "expected value of," and * denotes the complex conjugate. This means that the autocorrelation function of a stationary random process is a function only of the time difference, τ, and not of the actual times t_1 and t_2. Letting τ equal zero, this means the variance of the signal is a constant with time. If the signal s(t) experiences fading, though, its variance will not be constant and one might justly conclude the signal is nonstationary. Application of a time-varying gain can restore this signal, but will cause the constant ambient noise to become stronger with time, causing this noise process to be nonstationary.

As a final example of the nonstationarity of the signal and noise processes, consider the two-dimensional signals which the array detects, s(t;x). As has been stated several times before, the apparent horizontal velocity of the received primaries (and multiples) is low at first, then monotonically increases through the record. The fact that this two-dimensional characteristic of the signal varies with time is a heuristic proof of two-dimensional nonstationarity. For a more satisfying illustration, though, consider the following situation. A plane wave is incident on an array which lies on the x-axis. The signal received by the array can be written as

$$s(t;x) = Ae^{j(\omega t - k_x x)}$$

where A is a complex constant. The two-dimensional requirement corresponding to (5-1) is that

$$E\{s(t_1;x_1)s^*(t_2;x_2)\} = R_s(t_1,t_2;x_1,x_2)$$

$$= R_s(t_1-t_2;x_1-x_2)$$

$$E\{s(t_1;x_1)s^*(t_2;x_2)\} = R_s(\tau;\chi) \qquad (5\text{-}2)$$

Examining the plane wave signal received by the array, one has

$$R_s(t_1,t_2;x_1,x_2) = E\{[Ae^{j(\omega t_1 - k_x x_1)}][A^* e^{-j(\omega t_2 - k_x x_2)}]\}$$

$$= |A|^2 \cdot E\{e^{j\omega(t_1-t_2)} \cdot e^{-jk_x(x_1-x_2)}\}$$

$$= P_s(t_1-t_2;x_1-x_2)$$

and the received signal is stationary. Suppose, however, that the angle at which the plane wave is incident on the array changes as a function of time. Then the wavenumber k_x is no longer a constant, but a function of time, $k_x(t)$. Checking now for stationarity,

$$R_s(t_1,t_2;x_1,x_2) = E\{[Ae^{j(\omega t_1 - k_x(t_1)x_1)}][A^* e^{-j(\omega t_2 - k_x(t_2)x_2)}]\}$$

$$= |A|^2 \, E\{e^{j\omega(t_1-t_2)} \cdot e^{-j(k_x(t_1)x_1-k_x(t_2)x_2)}\}$$

It is obvious that in general one can never put this last term in the desired form of (5-2). Since this is a necessary condition for stationarity, one concludes that the signal examined is two-dimensionally nonstationary. Though the signal used for illustration was a plane wave, it is clear that the changing angle of incidence would cause a similar result if something other than a plane wave were considered.

Common-Depth-Point Stacking

Though it has been shown that the assumptions which one generally makes in optimum filtering and processing are not justified, their users appear to be quite satisfied with the results which they obtain. Nevertheless, the fact remains that stacking techniques are currently the only means available for reducing multiple reflections. It is interesting that of the methods discussed here, CDP stacking is both the most intuitive approach to the seismic problem and also the most effective. It is also interesting that *stacking is the only method mentioned which adapts itself to the characteristics of the signal present at each instant of time.* This, of course, is accomplished by correcting the records for moveout in accordance with the current velocity estimate.

But even though stacking can effectively be used to reduce multiples, one would prefer a technique which not only added primaries in such a way that they reinforced one another, but which also weighted multiples in such a way that they interfered destructively with one

another. The research by Galbraith and Wiggins[19] on multichannel stacking filters is an attempt at this, as is the earlier work by Schneider.[24] In each case the data are filtered before stacking in order to produce the destructive interference described. Unfortunately, both processing schemes require some knowledge of the location or probable moveout of the multiples which are to be eliminated. If such information is available and accurate, each technique seems to do the job efficiently.

CHAPTER VI

A NEW PROCESSING METHOD

The method proposed in this thesis is an attempt to reduce multiples in a manner different from any of those described. There are several distinctly attractive features about it. First, it is a filtering operation, to be distinguished from the shift-and-sum operation of normal stacking. As such, it is capable of greater separation of multiples and primaries. Further, it requires no a priori knowledge of the locations or moveout of multiples which might be present, only the velocity estimate required for ordinary stacking. Third, like stacking itself, the method is intuitively pleasing; one's "feel" for what is happening is not obscured by unwarranted assumptions or mathematical complexity. And, finally, the filtering takes place on a processing level where CDP stacking is not usually performed; hence the method is suitable for use in conjunction with stacking, as a form of preprocessing against multiples.

The proposed new filtering technique is a time-varying velocity filter. Its purpose is to process the traces in such a way that multiple reflections are continually rejected while all primary reflections are retained. The motivation for it is somewhat like that used earlier in explaining common-depth-point stacking. Consider the figures used in that discussion, Figures 23 and 24. Since the interval velocity, and hence the average velocity, generally increase with depth, the

moveout per trace exhibited by a primary is usually less than that shown by a multiple which arrives at about the same time. For the example of Figure 23, the difference in moveouts is shown in Figure 24. It is this moveout difference which allows one to enhance primaries in the CDP stacking procedure. But the difference in moveout of primaries and multiples also means that their apparent horizontal velocities are different, and that that of a primary should be greater than that of a multiple present at about the same time, since the moveout per trace is less for the primary. Consequently, a velocity filter whose impulse response changes appropriately with time should be able to continually separate primary events from multiples. The variation should be such that the filter's cutoff velocity is always equal to or slightly less than the estimated apparent horizontal velocity of the primary reflections present. Observe that no actual information about the nature of the multiples is required, only the same velocity estimate which is used in CDP stacking.

It should be explained that the method can be used in conjunction with common-depth-point stacking, since from the above discussion one is inclined to think that both techniques require the same data as an input. The data on which the time-varying velocity filter is used is recorded in the following manner. An array of geophone groups is arranged at a spacing of 300 feet between their centers. Wavelets are then excited, probably by a vibrator unit, at a distance which starts at several hundred feet from the array and is increased by perhaps 15 feet each time a sweep is completed. The output of each geophone group is recorded for each sweep of the vibrator, and it is

this data on which the time-varying velocity filter operates. Ordinarily, a single geophone group will record 20 sweeps, then simply sum these to produce a single output trace, using the philosophy that some random noise will be cancelled in the process. Thus, if one has 24 groups and 20 sweeps are made, 480 traces are initially recorded. Currently these are summed in the field, so that 24 records would return to the lab; under the proposed method, 480 records would go to the lab for processing. This is a drawback to the time-varying velocity filter approach, but one which is surely offset if the multiple cancellation is effective.

The traces which are the result of summation in the field, called gathered traces, are what is generally used as the input to the stacking procedure (perhaps after sharpening with a deconvolution filter). With the new processing method, the 20 traces which were formerly summed are now processed with the time-varying velocity filter to produce a single output trace. This trace is now ready to be used in the CDP procedure, but is presumably more free from multiples than the gathered trace. Thus time-varying velocity filtering will not replace common-depth-point stacking, but rather will complement that process.

Two principal problems immediately become apparent. First, exactly how does one create a time-varying linear filter? Though much is written where the impulse response function is left in the form $h(t_1,t_2)$, very little is actually said about the subject of how one chooses such a function, whether or not it has a meaningful transfer function (Fourier transform), and how such a system is realized or implemented. After examining the literature, and in particular two

excellent articles by Kailath[25] and Zadeh,[26] it was concluded that the problem of physical realizability is probably the main reason so little has been done in the area. Since this is not a factor in the seismic problem (all filters are non-real-time computer realizations), the implementation of a time-varying filter produced no major difficulties other than adding another dimension to the velocity filters used. In the stationary case, one uses functions of two variables to describe the filter, the impulse response function, $h(\tau;x)$, and the transfer function, $H(\omega;k_x)$; in the time-varying case the impulse response function, $h(t,\tau;x)$, and the transfer function, $H(t,\omega;k_x)$, are functions of time as well. The time variation of the filter is evidenced through the variable t, while the variables τ and x as usual define the distance in time and space from the point of excitation. Thus, in Equation (4-1), the parameter p is a function of a third index which describes time variations, p(i).

Another problem in the implementation of the time-varying velocity filter is the provision of a good velocity estimate. As is true in stacking techniques, the output of the time-varying filter will only be as good as the velocity information on which its variations are based. Initially it was thought that a technique which employed crosscorrelation of traces in various ways might be the best way to obtain the velocity estimate. Indeed, this avenue of attack had been exploited[27] with reported success. However, the Atlantic Richfield Company uses another technique for sensing average velocity, and it was this method which was used in this work. Of course, the manner in which

the estimate is obtained is immaterial, its accuracy being of prime concern.

To understand how the Atlantic Richfield method works, consider Figure 27. It has been shown in Appendix A that the actual time of arrival of a primary wavelet at a receiver location a distance X from the shotpoint is

$$T = \sqrt{T_0^2 + \left(\frac{X}{V_{av}}\right)^2}$$

where T_0 is the two-way vertical travel time, and V_{av} the average velocity, to the point of reflection. The curves shown in Figure 27 are those of T versus X for the labelled values of average velocity, V_{av}. The technique used to sense the velocity is what might be called a "power-window" method. One attempts to measure the power in a "window" about a given velocity. For instance, the dotted lines in the figure represent such a window about the average velocity V_3. The samples of each trace which fall within the window are summed, after appropriate time shifting, and the integral of the square of the resultant function is a measure of the power in the velocity V_3. Once this is done for enough velocities, the two-way vertical time T_1 is considered, and so on. At length one can make plots such as those seen in Figure 28. Each vertical plot on the lower figure shows the power in the various average velocity windows for a particular value of two-way vertical record time. The upper figure is a plot of the maximum power detected at that time, no matter what the velocity. The data used

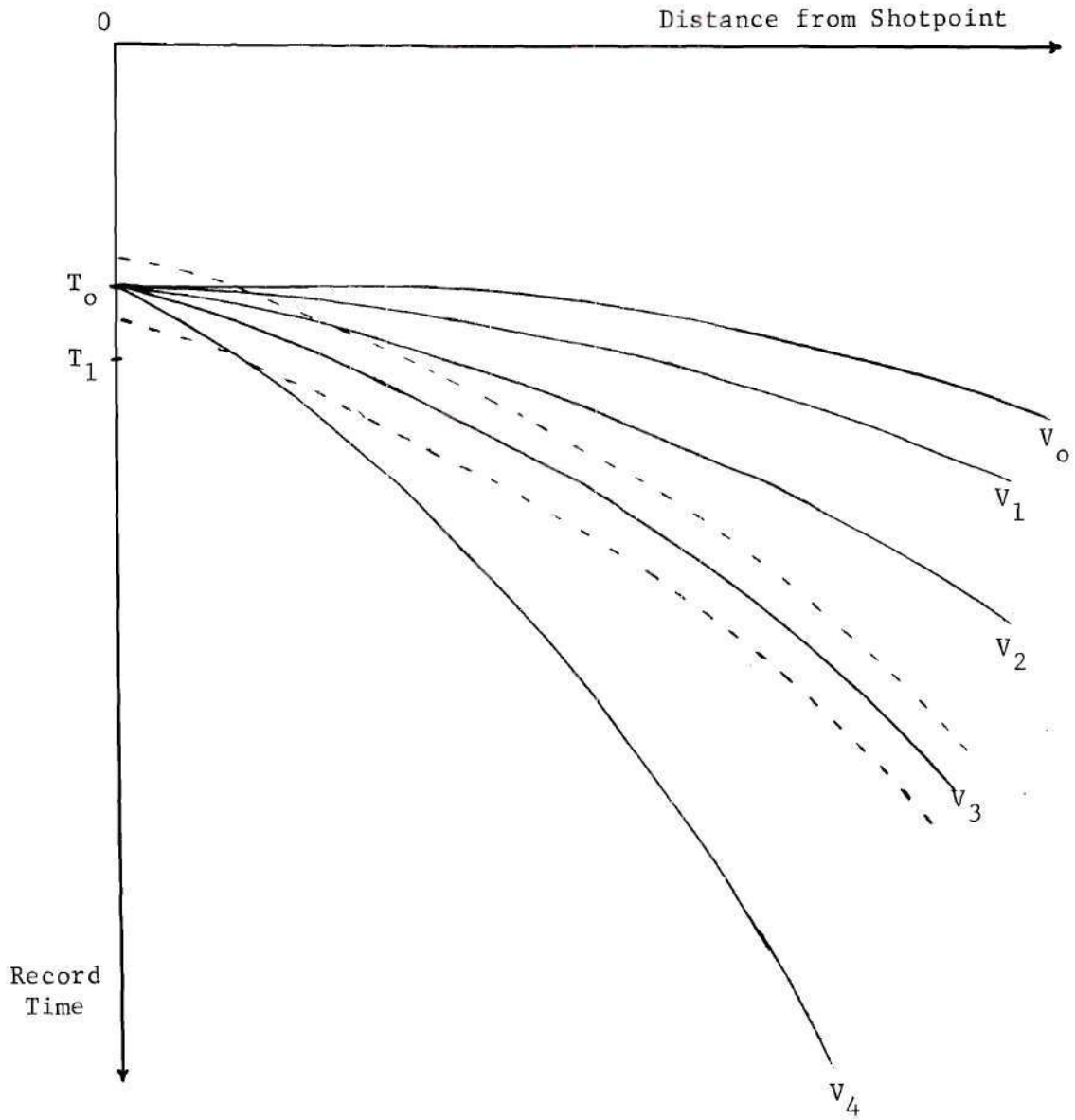

Figure 27. The "Power-Window" Method of Velocity Analysis

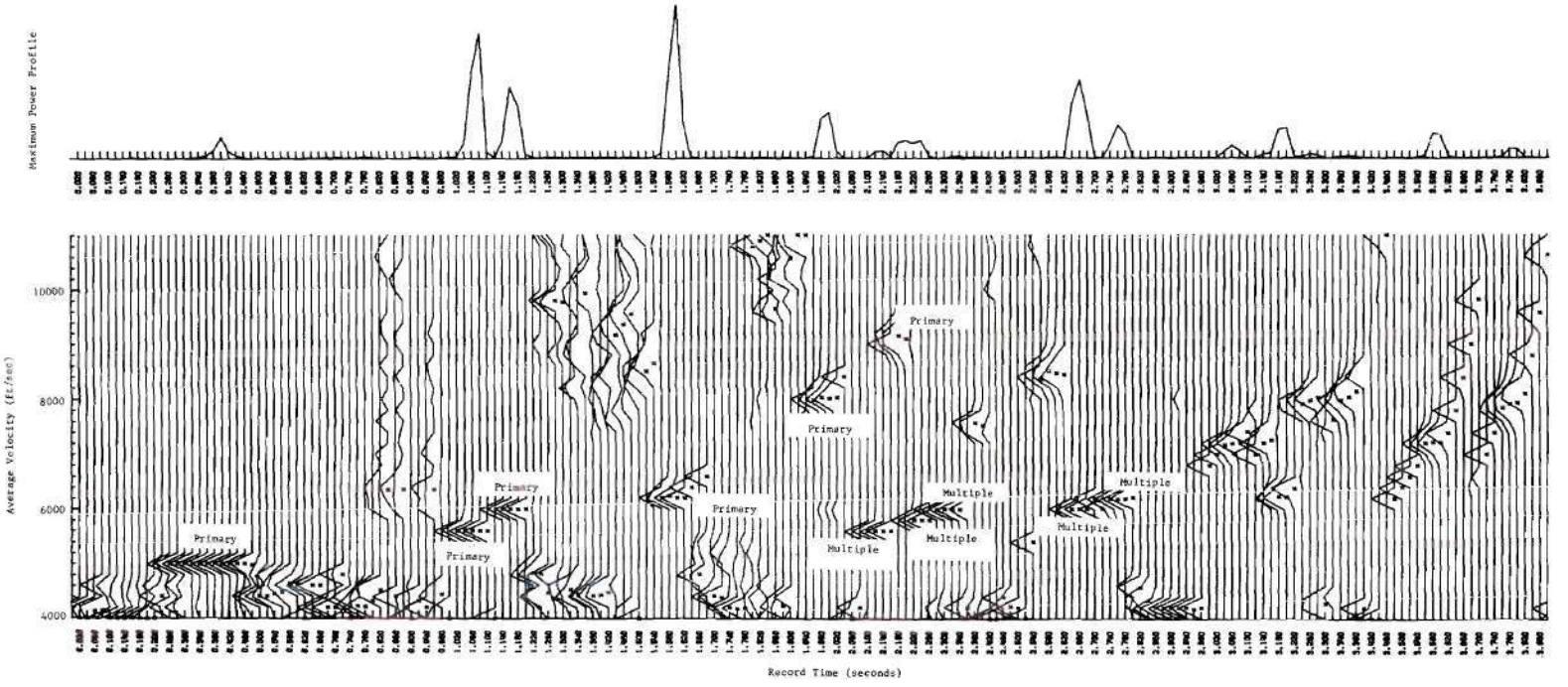

Figure 28. A Velocity Analysis Plot; Each Curve Normalized to its Maximum Value

for this particular velocity analysis were synthetic, and consisted only of primary and multiple reflections resulting from a six-layer synthetic earth profile. Locations of all the primaries and several of the multiples have been marked on the lower figure, where one observes that, at a given time, the average velocities of primaries are greater than those of multiples.

In the presentation of Figure 28, the velocities plotted were normalized for each time; that is, each velocity curve was normalized relative to the maximum value on that particular curve. In Figure 29, the velocities were normalized relative to the maximum velocity on the entire record. Often one must consider both presentations as well as the maximum power curve in order to make an accurate assessment of the average velocity profile.

From these figures one might ask why this information is not used as the final product, for isn't one primarily interested in a velocity profile such as that given? The first reason why this cannot be done is noise. When one analyzes data from the field, the velocity plots are not nearly so clean, and are thus much more difficult to interpret. But in some respects more important than this is the factor of time; velocity analyses such as these require a great deal of time to perform, and could therefore never be used on the scale necessary to give the proper mapping.

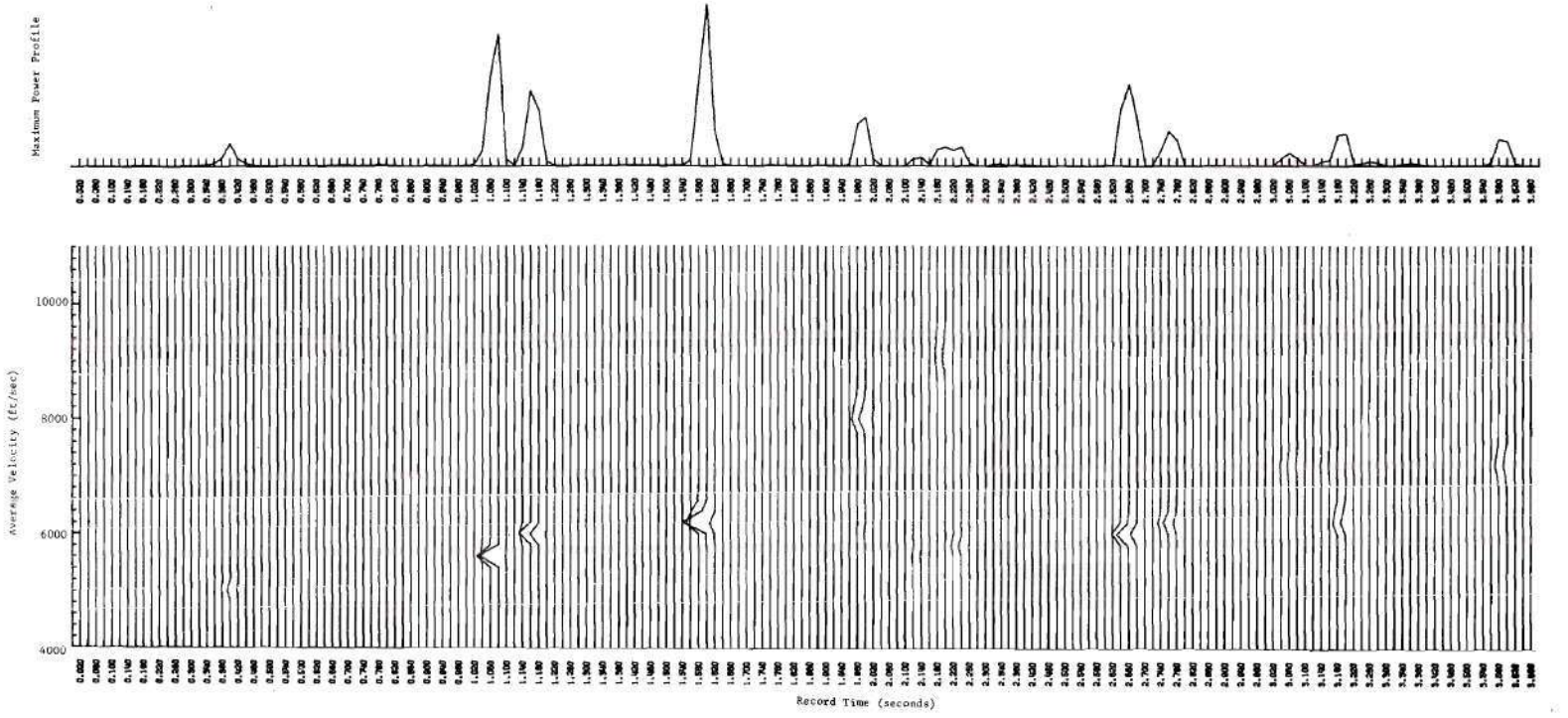

Figure 29. A Velocity Analysis Plot; Each Curve Normalized to the Maximum Value on the Entire Plot

CHAPTER VII

RESULTS OF THE RESEARCH

Time-Invariant Velocity Filters

Before considering the implementation of the time-varying velocity filter, a thorough knowledge of all aspects of time-invariant velocity filtering was necessary, since the time variations require the filter to assume a variety of transfer functions. With the aid of the Atlantic Richfield Company's three-dimensional plotting routine, these filters were studied with respect to variations in a number of parameters, namely the length of truncation, the use of windows for truncation, and the narrowing of the "pie-slice" characteristic in ω-k_x space. The results of variations in each of these will now be discussed.

In considering the effect of changing the lengths at which impulse responses are truncated, the sample spacing in time and distance remain fixed from one example to the next; thus the length of truncation is equivalent to the number of time- and space-sample point operators used. Before considering specific examples, recall that truncation is simply the multiplication of the function by a gate. In the following discussion, the gate used is a rectangular gate, extending from -NT to NT in time and from -MX to MX in space. T is the distance between time samples and X the distance between space samples; there are (2N+1)

time-sample point operators and 2M space-sample point operators.* Then the truncated impulse response function is

$$h_t(nT;mX) = h(nT;mX) \cdot g_{NT,MX}(nT;mX)$$

and its Fourier transform is

$$H_t(\omega;k_x) = H(\omega;k_x) \circledast [\mathrm{Sinc}(N\omega T) \cdot \mathrm{Sinc}(Mk_x X)]$$

since, as previously stated, multiplication of two functions is equivalent to convolution of their Fourier transforms. The function Sinc (•) is the sine cardinal function. This convolution of the desired transfer function $H(\omega;k_x)$ with the two-dimensional sine cardinal is what causes $H_t(\omega;k_x)$ to deviate from the ideal. As N and M become very large, the sine cardinal becomes impulsive in nature, since

$$\lim_{M,N\to\infty} \int_{-\omega_0}^{\omega_0} \int_{-k_0}^{k_0} \mathrm{Sinc}(N\omega T)\mathrm{Sinc}(Mk_x X) \frac{d\omega}{\pi} \frac{dk_x}{\pi} = 1$$

Thus $H_t(\omega;k_x)$ approaches $H(\omega;k_x)$ as N and M become very large; but for finite N and M there will not be a well-defined cutoff velocity nor a reject region in ω-k_x space where the response is zero.

Two sets of examples illustrate the effect described above. In each set, 25 time-sample point operators were used. It was found that

---

*The difference is due to there being no spatial operators along the x = 0 axis, a step taken to avoid singularities in the impulse response function at the t - x origin.

this number could be increased as much as desired, but that for the filters used here, the coefficients beyond this point were small enough that including them had little effect on the transfer function. However, increasing the number of space-sample point operators beyond a given amount is not permissible for two reasons. First, since the data filtered are not from a common depth point, using too many traces tends to "smear" the detailed structure of a layer. And second, because the wavelets propagate on a spherical front and therefore have no single apparent horizontal velocity, discrimination on the basis of a difference in apparent horizontal velocities becomes less effective as the number of traces filtered increases. Ultimately, therefore, one must decide on a number which is a compromise between the considerations just stated and a desire to best duplicate the ideal filter transfer function.

The first pair of examples are shown in Figures 30 and 31. Figure 30 is the transfer function of a non-ideal velocity filter truncated at M = 8 (number of spatial operators) and N = 25; the point of observation is above the third quadrant in ω-k_x space, and the part of the transfer function being viewed is just that shown in the first quadrant of Figure 16. The coefficient p, which gives the degree of closure of the transfer function and which is defined by

$$p = \frac{\omega_{max}/k_{max}}{V_{cutoff}}$$

$$= \frac{\Delta x/\Delta t}{V_{cutoff}}$$

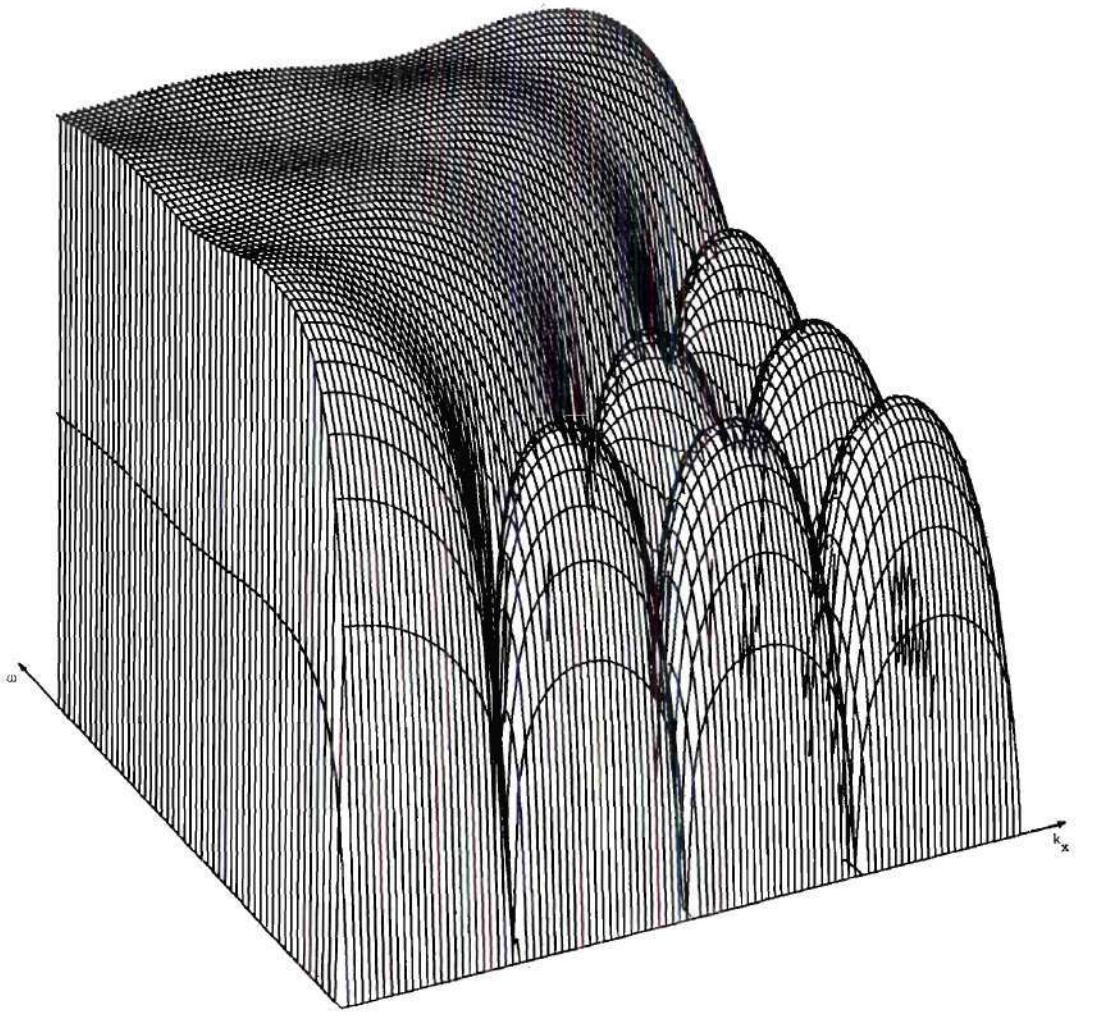

Figure 30. Transfer Function of Velocity Filter; 25 Temporal Operators, Eight Spatial Operators, Rectangular Gate, p = 1.0

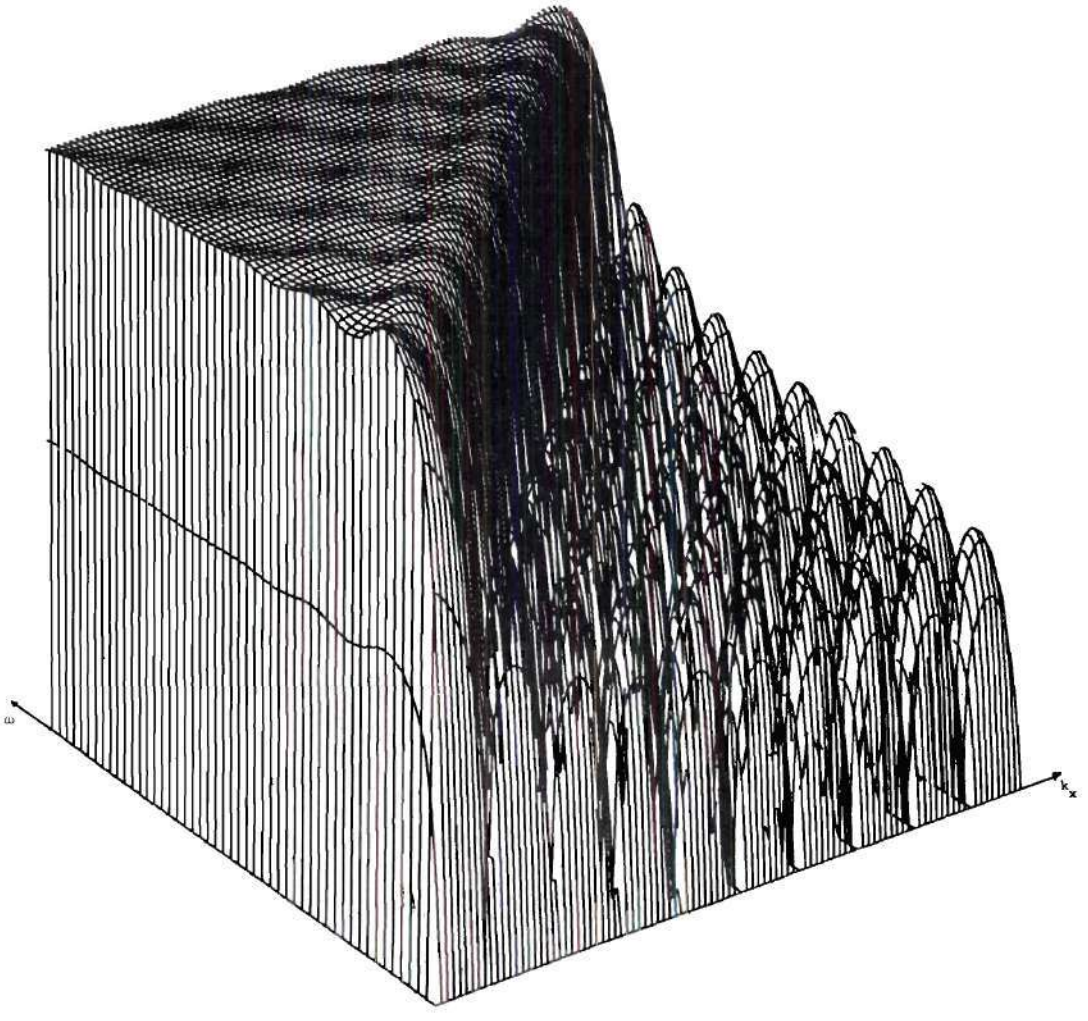

Figure 31. Transfer Function of Velocity Filter; 25 Temporal Operators, 20 Spatial Operators, Rectangular Truncation Window, p = 1.0

is 1.0 in this case. Figure 31 is identical except that 20 spatial operators were used in this case. A number of observations can be made on comparing the two. First, there is no sharp cutoff velocity for the filter which uses 8 operators; in contrast, the 20-operator filter has a fairly well-defined dropoff along the 45° line. Second, the "side-lobes" which appear in the reject region of the 8-operator filter are at least 18 db below the amplitude of the pass region; in the filter with 20 spatial operators, these are a minimum of 25 db down. Finally, the amplitude of the response near the origin in the pass region, which should be identical to the response anywhere else in the pass region, is a good deal lower than it should be. For the 8-operator filter the near-origin response is down as much as 20 db below other parts of the pass region; for the filter with 20 operators, the difference is greater than 10 db.

Figures 32, 33, and 34 further illustrate the effect of increasing the number of spatial filter operators. In each figure, the parameter p is 0.25, and 25 temporal filter operators are used. In Figure 32, 20 spatial operators are used, in Figure 33, 30 are used, and in Figure 34, 40 are used. Though more operators do make a visible difference, the improvement is not outstanding. This, coupled with the reasons mentioned for keeping the number of filters low, led to the decision that in most instances, 20 spatial operators would be a good compromise. Experience has proved this to be true.

The subject of truncation windows (gates) was one which received considerable attention. It was felt that convolving the ideal transfer function with something other than a two-dimensional sine cardinal

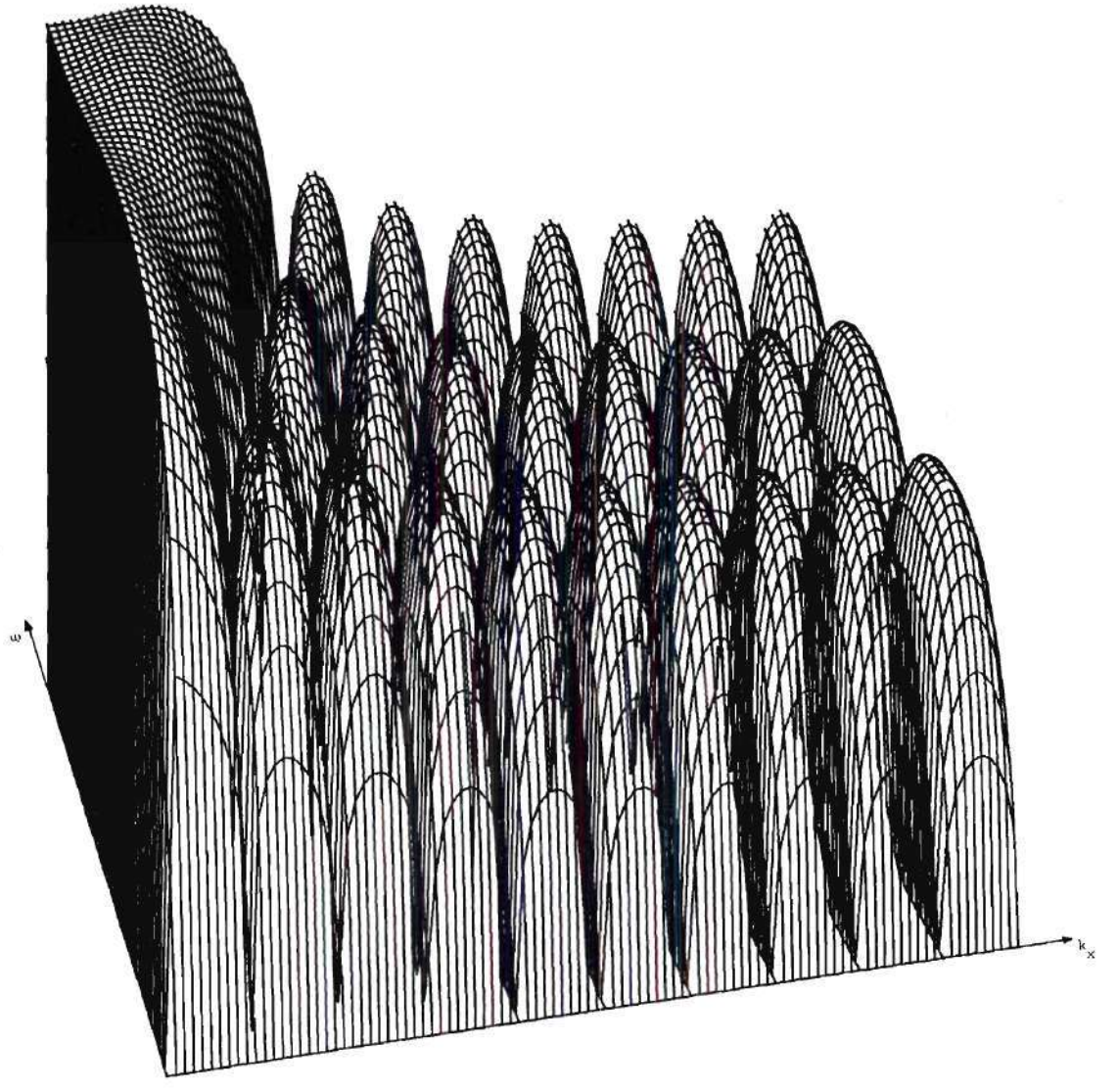

Figure 32. Transfer Function of Velocity Filter; 25 Temporal Operators, 20 Spatial Operators, Rectangular Gate, p = 0.25

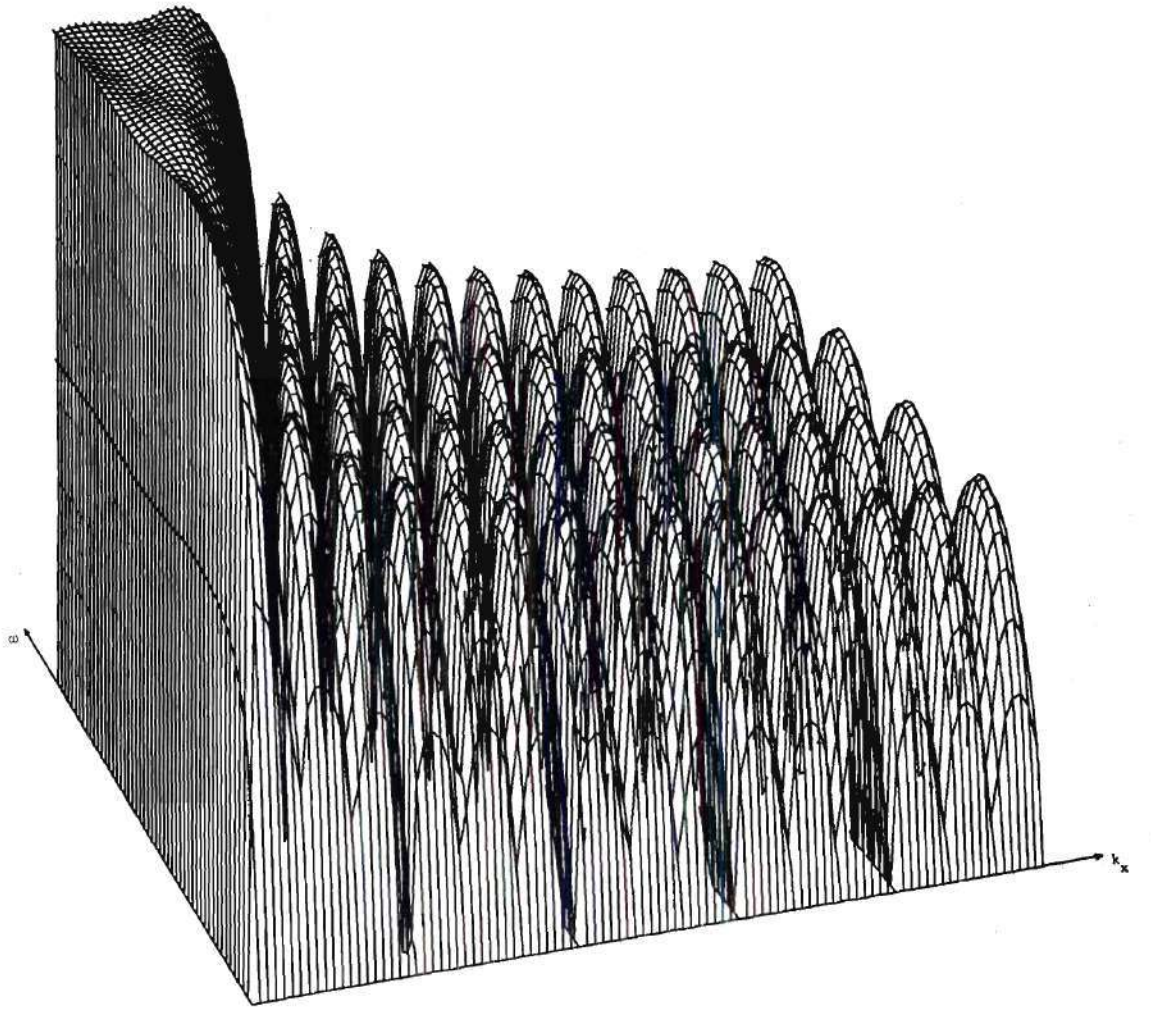

Figure 33. Transfer Function of Velocity Filter; 25 Temporal Operators, 30 Spatial Operators, Rectangular Gate, p = 0.25

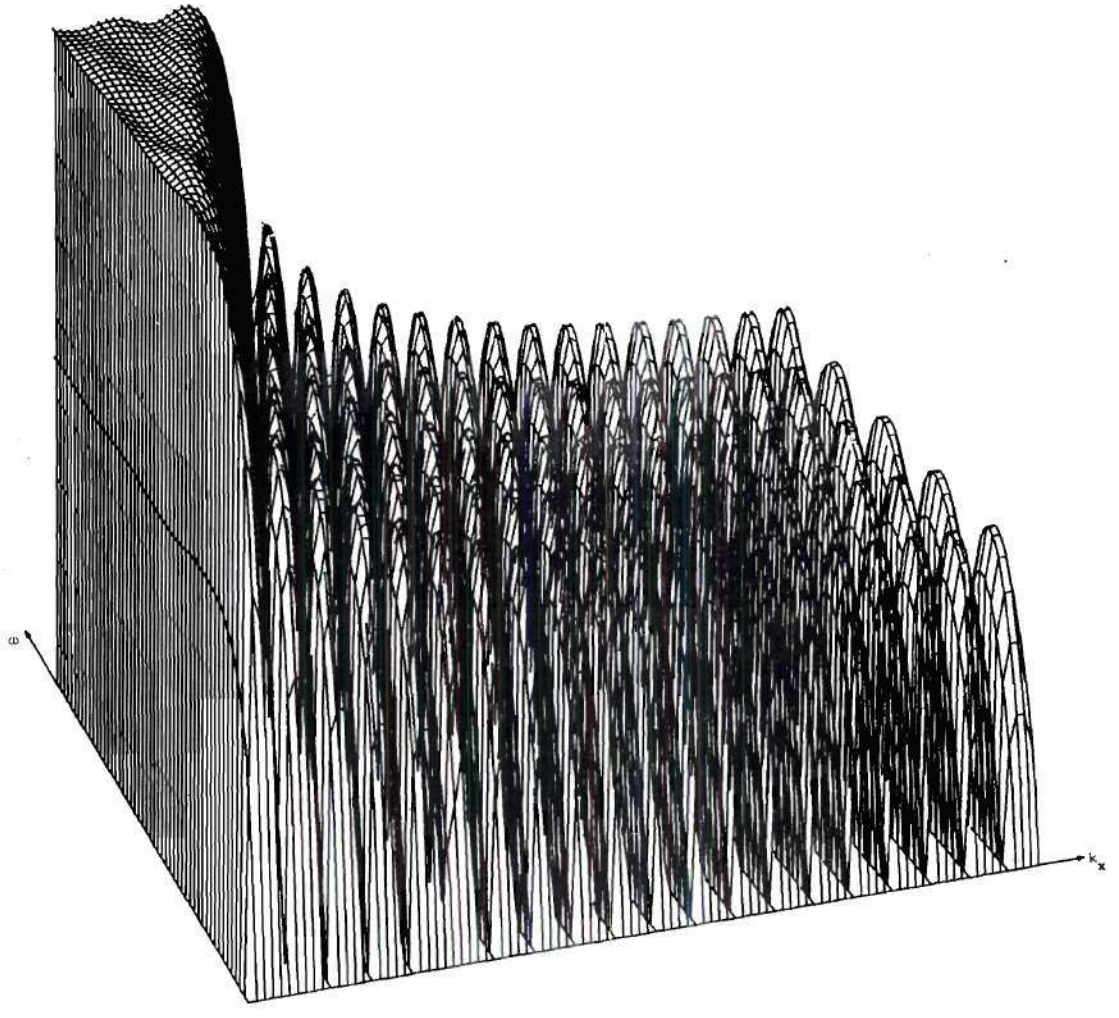

Figure 34. Transfer Function of Velocity Filter; 25 Temporal Operators, 40 Spatial Operators, Rectangular Gate, p = 0.25

might result in a transfer function better suited to the particular problem at hand. In one case this proved true, though not in the manner one might expect.

The first window examined was a two-dimensional Hanning window,[28] which is given by

$$w_h(t;x) = \frac{1}{4} \cdot \left[1 + \cos \frac{\pi t}{T_m}\right] \cdot \left[1 + \cos \frac{\pi x}{X_m}\right]$$

for

$$|t| < T_m, \qquad |x| < X_m$$

Bruce[29] examines this and other windows in great detail. The Fourier transform of this gate is like the sine cardinal in that it has a large lobe at the origin in ω-k_x space and sidelobes in areas away from the origin. However, there are two important differences in these two convolving functions. First, the principal lobe of the sine cardinal falls to zero in half the distance required by the Hanning window transform. Second, the sidelobes of the Hanning window transform are at least 20 db below those of the sine cardinal. From these two facts one can predict that if the truncation is performed by a Hanning gate, the sidelobe structure in the reject region should be improved over that of Figure 31. This is indeed the case, as evidenced by Figure 35, a velocity filter of 25 temporal and 20 spatial operators which is truncated by a Hanning gate. The "floor" introduced is 58 db below the level of the passband, a significant improvement from the 25 db obtained

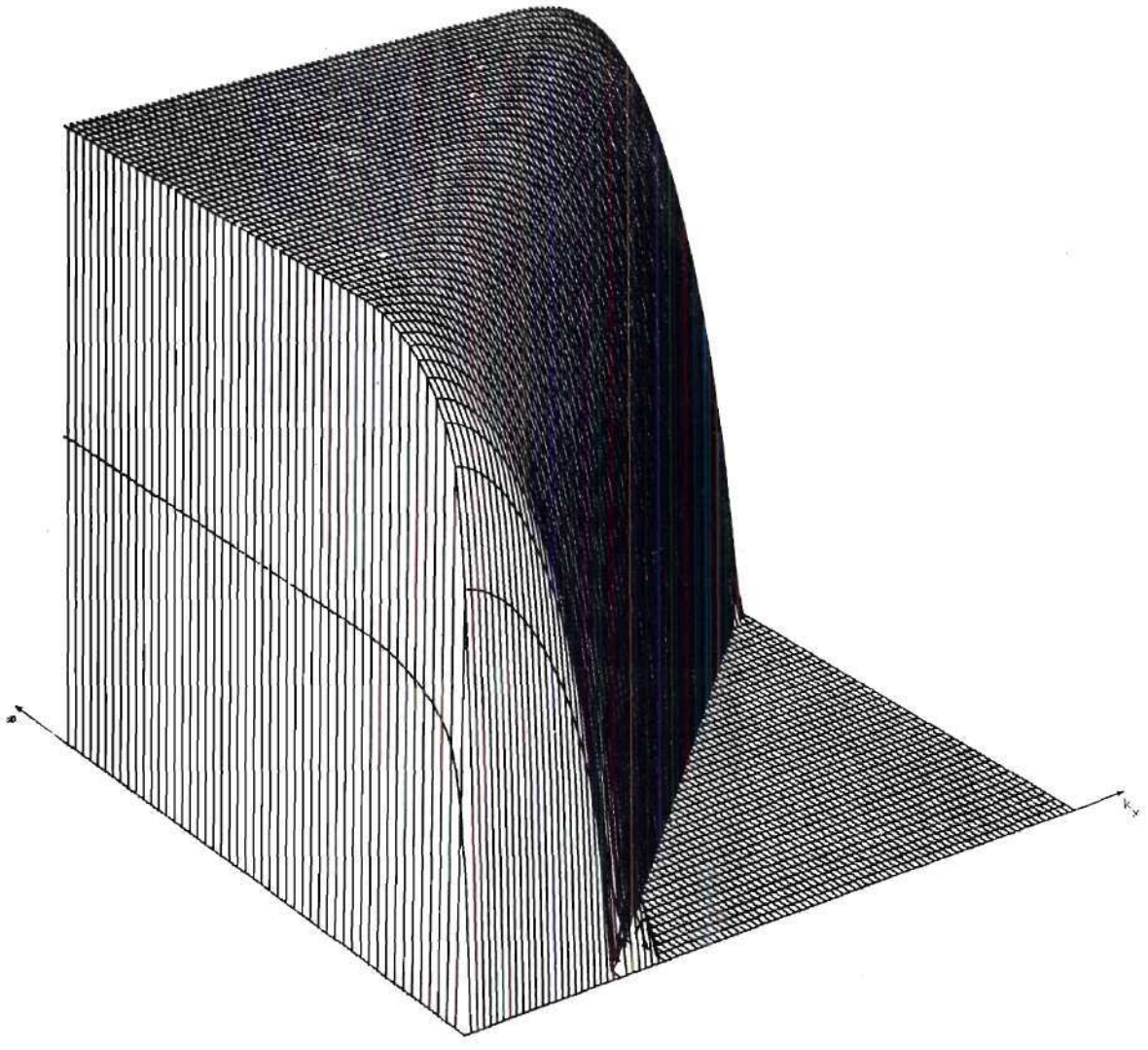

Figure 35. Transfer Function of Velocity Filter; 25 Temporal Operators, 20 Spatial Operators, Hanning Truncation Window, p = 1.0

using a rectangular truncation window. A significant drawback to the use of the Hanning window is also evident from a comparison of the two figures: the cutoff along the 45° line is much sharper with a rectangular truncation than with a Hanning truncation. An even better indication of these properties can be seen in Figures 36, 37, and 38, which show the ideal transfer function, that obtained with a rectangular gate, and that obtained with a Hanning gate, respectively. Again the Hanning truncation exhibits low sidelobe structure at the expense of sharpness in cutoff. In situations in which the separation between signal and noise is considerable, a filter using a Hanning window for truncation would obviously be more desirable. Such a situation might be one in which the low-velocity ground roll is extremely strong, so strong that the elimination characteristics of Figure 37 would not be enough. The cutoff characteristics of Figure 38 would cause no problems here, since the apparent horizontal velocities of all primaries would be very much greater than that of ground roll. However, when trying to separate primaries from multiples, the sharpness of cutoff is of prime concern. At a given time the difference in the apparent horizontal velocities of the two may be relatively small, so much so that one often is faced not with the problem of *how much* rejection can be had, but rather with whether *any* rejection of multiples can be effected. Since the primary purpose of the time-varying velocity filter is to reject multiples, the use of a Hanning or other window which smoothed sidelobe structure was deemed not usually desirable.

One familiar with the use of smoothing windows in antenna pattern synthesis might inquire, "Why not increase the size of the receiver

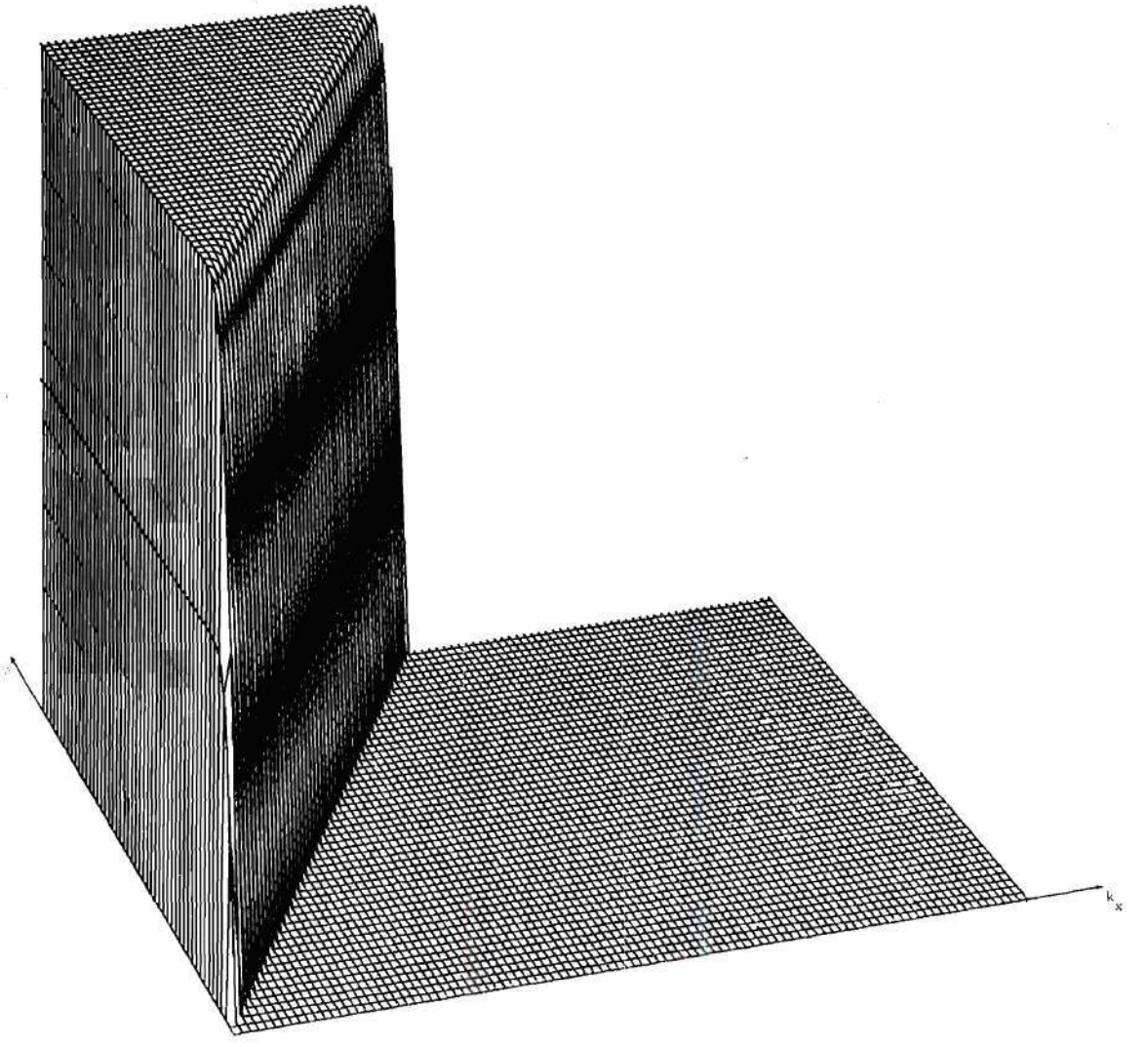

Figure 36. Ideal Transfer Function of Velocity Filter; p = 0.5

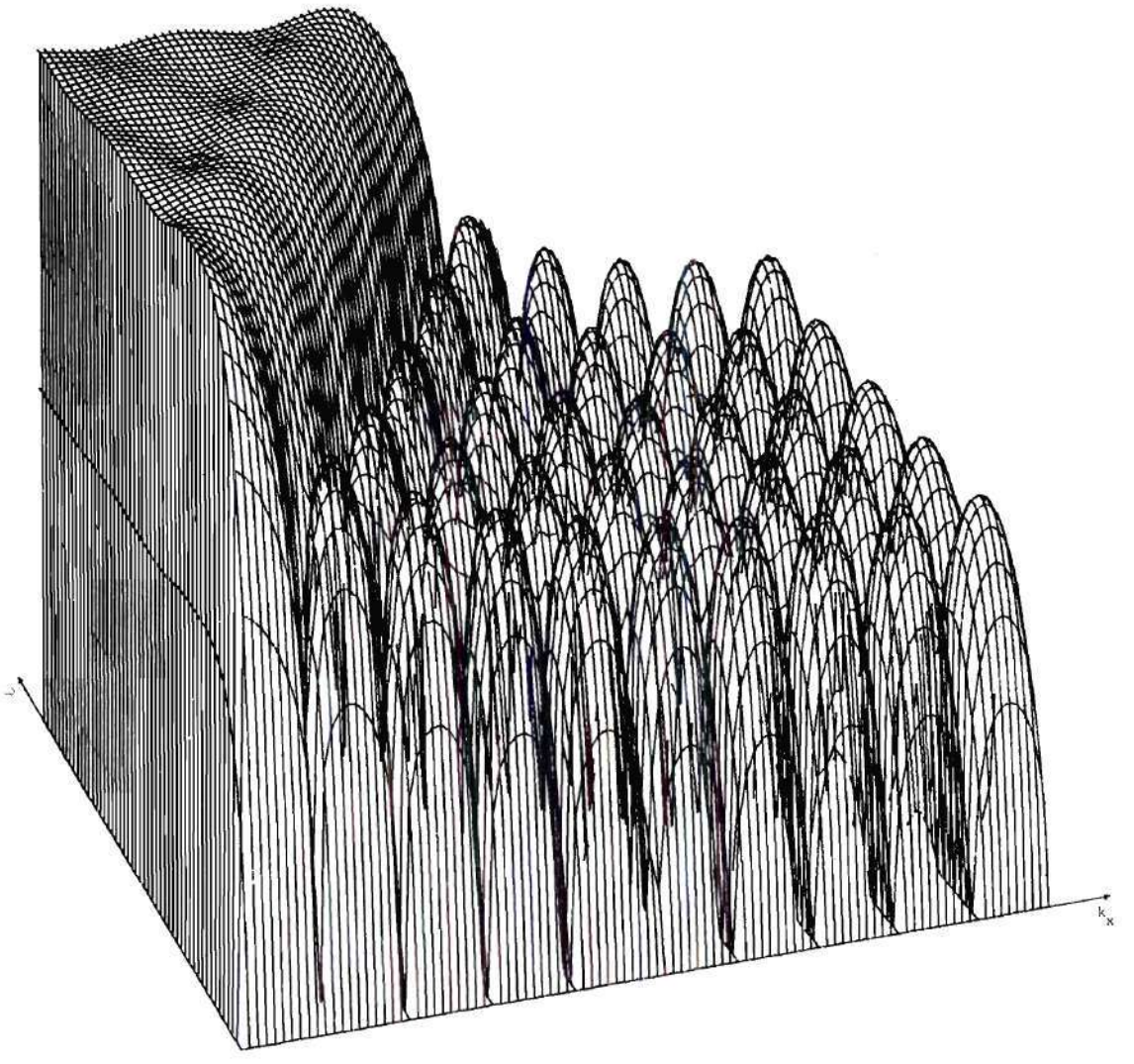

Figure 37. Transfer Function of Velocity Filter; 25 Temporal Operators, 20 Spatial Operators, Rectangular Truncation Gate, p = 0.5

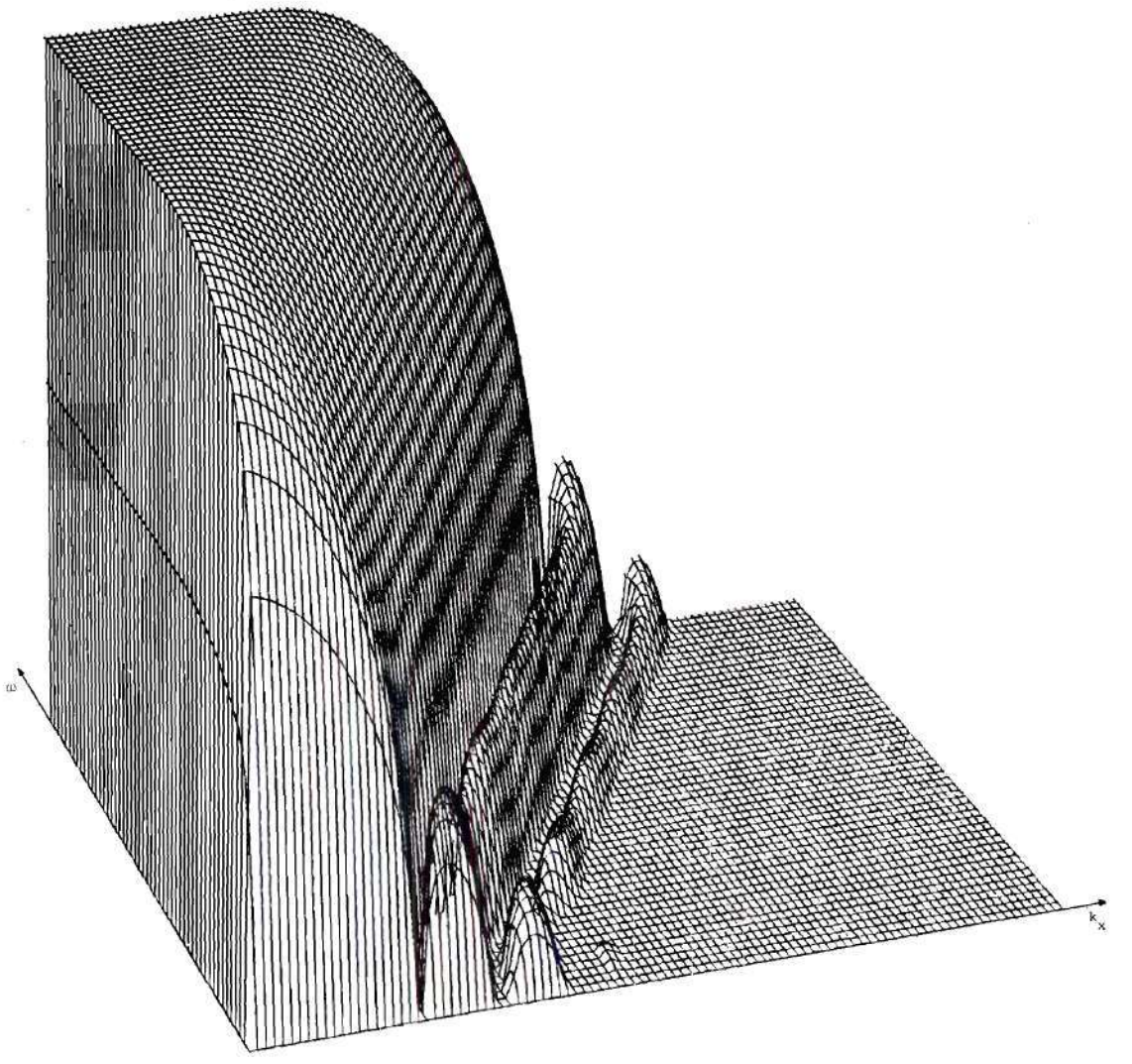

Figure 38. Transfer Function of Velocity Filter; 25 Temporal Operators, 20 Spatial Operators, Hanning Truncation Window, p = 0.5

aperture until the desired sharpness of cutoff is obtained?" In this case, increasing the number of operators by 50 to 100 per cent should produce cutoff characteristics when using the Hanning window which are equivalent to those obtained by rectangular truncation. However, as was just discussed, this demands an increase in the number of spatial operators from 20 to 30 or 40, and this is generally undesirable for the reasons stated above.

When comparing the characteristics produced by truncating the impulse response with rectangular and Hanning gates, one might wonder if the apparent compromise between sidelobe structure and sharpness of cutoff might be exploited farther. That is, can one desive some sort of "inverse" window which will sharpen the descent of the amplitude response at cutoff, at the expense of increasing the heights of the sidelobes? The answer is Yes, by applying a window function, the amplitude of which increases as one approaches the truncation points. The function $e^{\alpha|x|}$ might be such a window. The window which was used here, though, was simply a spatial window formed by normalizing the maximum value of each of the 20 individual filters in the impulse response function of the velocity filter to the same value. By "individual filter" it is meant one of the 25-point arrays which is convolved with an input trace. The resulting transfer function characteristics are displayed first in Figure 40. Although the three-dimensional plots are helpful, in this case a more quantitative plot is required; hence the amplitude response of the filter along a line through the cutoff is shown. The responses shown are those resulting from the three windows discussed, when the coefficient p has a value

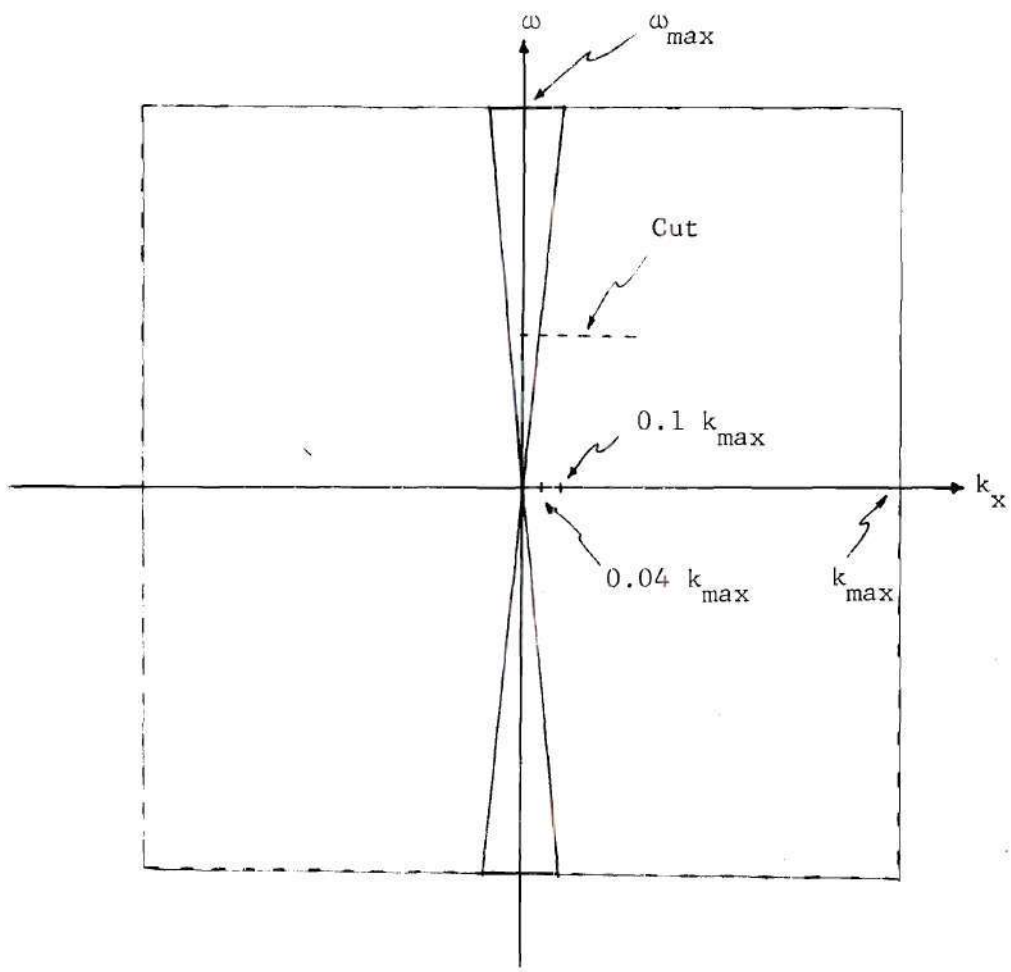

Figure 39. Portion of Velocity Filter Transfer Function Shown in Figure 40

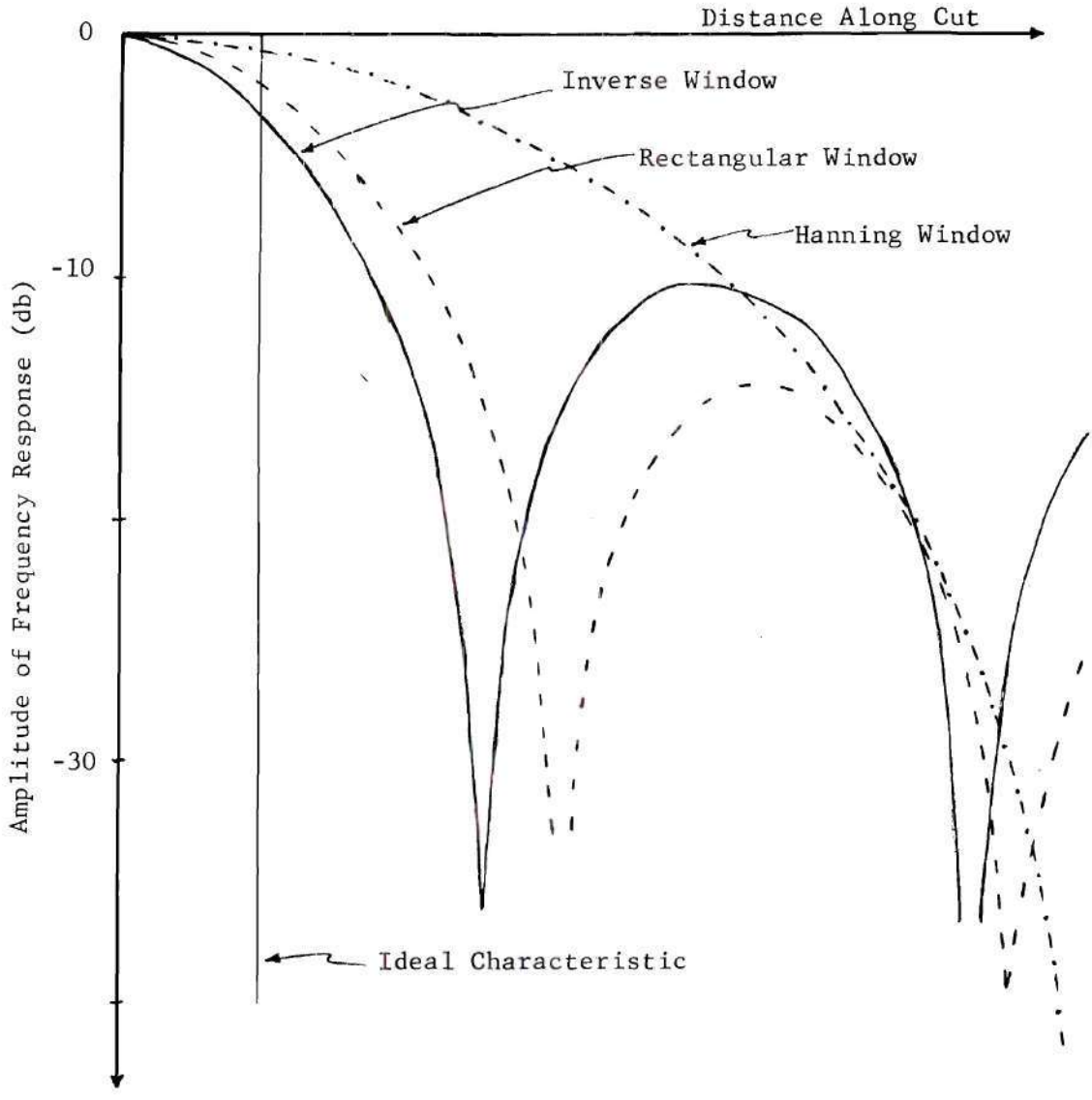

Figure 40. Transfer Functions of Velocity Filters, Truncated by Hanning, Rectangular, and Inverse Gates; p = 0.1

of 0.1. The line through the cutoff is shown as a dotted line in Figure 39. First note that the cutoff properties of the Hanning window are unquestionably bad. Then one observes that the sidelobe structure of the inverse-window filter is worse than that of the rectangular-window filter. But in the area around cutoff, the inverse-window filter has a more desirable falloff characteristic than does the rectangular-window filter. In applying time-variations to the velocity filter, the locations of expected primaries are by design always just inside the cutoff, and multiples usually fall just outside there. Consequently, in discrimination between primaries and multiples, this filter may prove to be of more value in some cases than that formed using a rectangular window for truncation. The question of whether or not such a gate function is required is dependent on the particular data with which one is working.

The behavior of the actual transfer functions as the pie-slice shape becomes narrower, i.e., as the coefficient p becomes small, is crucial in some cases. Though in many instances the time variations are such that the transfer function wedge is not required to become very narrow, there are instances where a narrow shape is reached almost immediately. Hence a knowledge of the effect of narrowing the beam is essential if one is to judge when the filtering will be effective. Figure 32 and Figures 41, 42, and 43 show what happens when this is done. Figure 32 is the result of rectangular truncation, 20 spatial operators, and p = 0.25; Figure 41 is the same for p = 0.175; and Figure 42 is the same when p = 0.10. The fact that the transfer function of Figure 42 bears little resemblance to the ideal

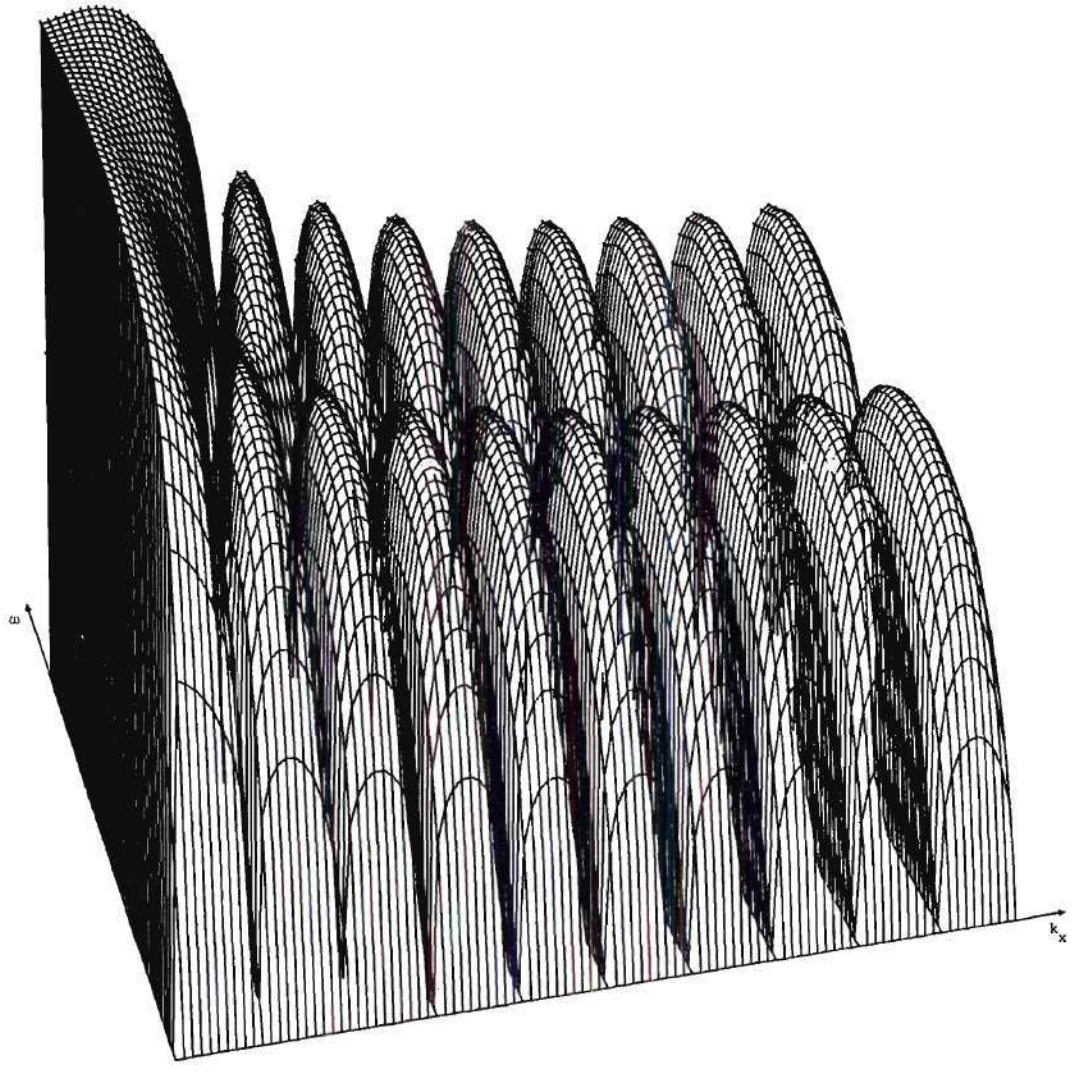

Figure 41. Transfer Function of Velocity Filter; 25 Temporal Operators, 20 Spatial Operators, Rectangular Gate, p = 0.175

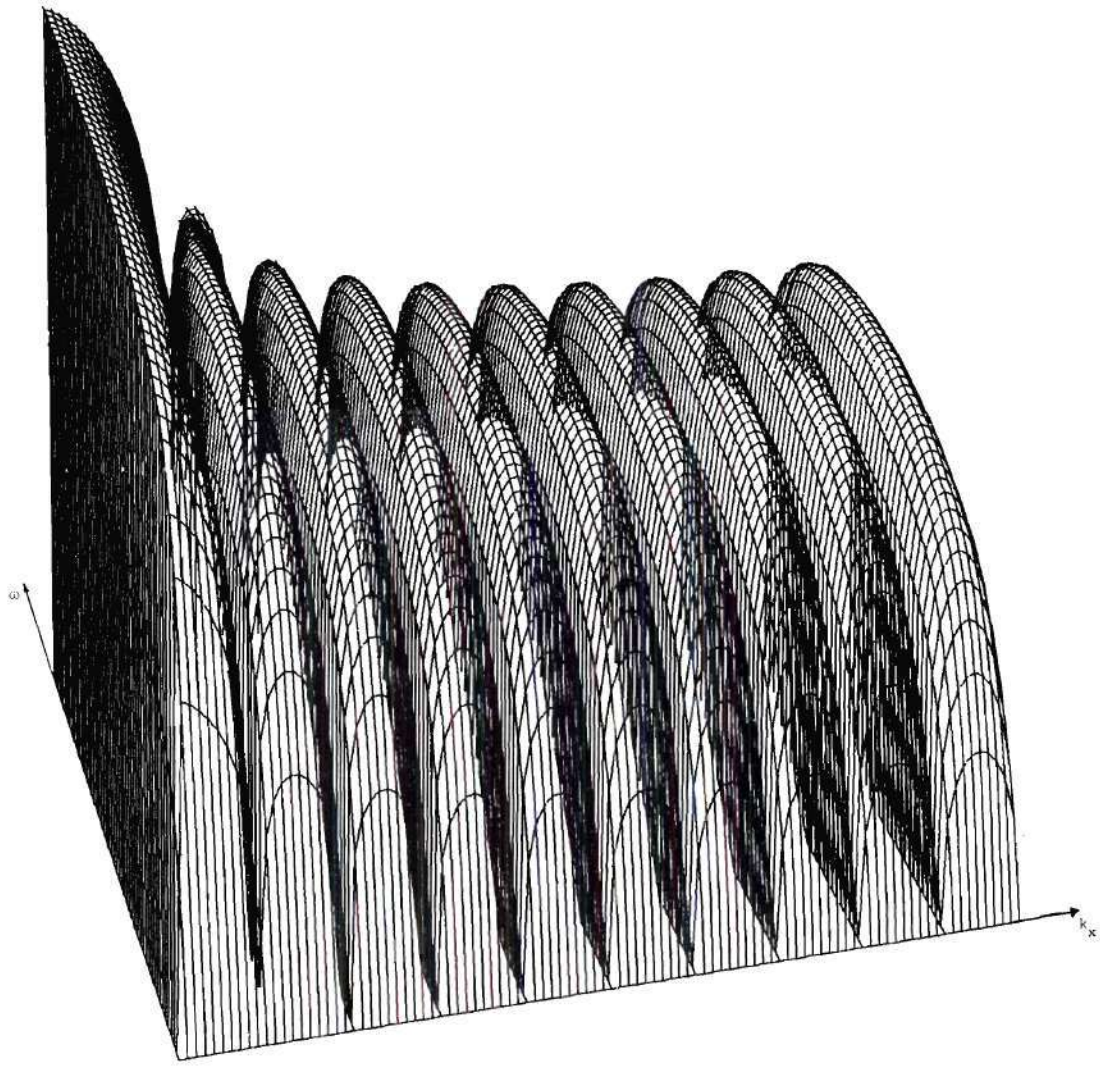

Figure 42. Transfer Function of Velocity Filter, 25 Temporal Operators, 20 Spatial Operators, Rectangular Window, p = 0.10

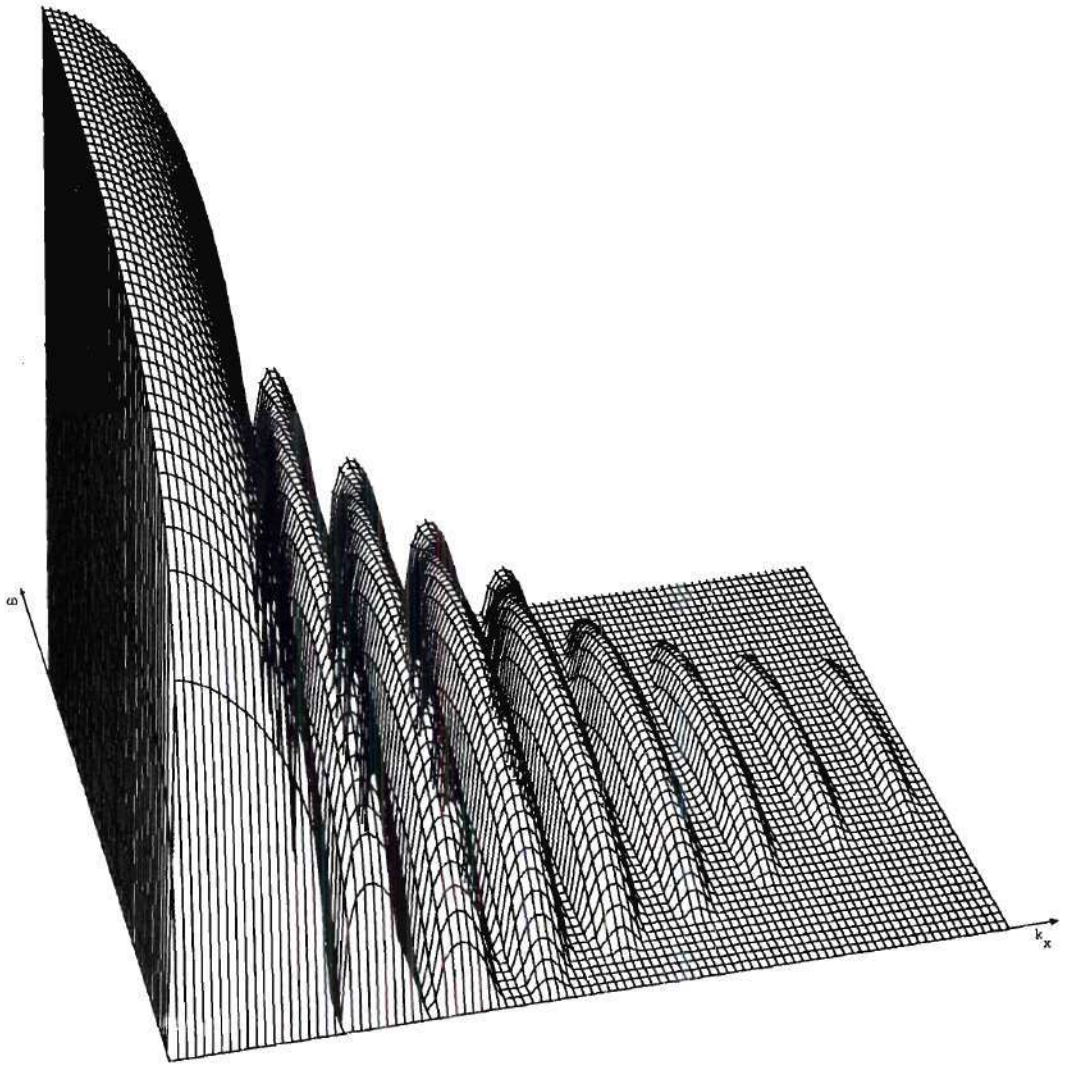

Figure 43. Transfer Function of Velocity Filter, 25 Temporal Operators, 20 Spatial Operators, Hanning Window, p = 0.10

characteristic results from the fact that the dimensions of the ideal filter are now smaller than those of the convolving function; therefore the dimensions of the result of convolution will be no less than the dimensions of the main lobe of the convolving function. This is also apparent from Figure 43, which is the transfer function of a 20-operator filter, truncated with a Hanning window, for which p = 0.1. The pass region of this filter is considerably broader than that of Figure 42, since the main lobe of the Fourier transform of the Hanning window is twice as wide as the principal lobe of the sine cardinal. This is another reason why the Hanning window is not suitable for use in the time-varying filter.

Data Processed

Both synthetic data and actual field data were used in the evaluation of the time-varying velocity filter as an instrument for eliminating multiple reflections. It was decided that the use of a typical synthetic example would be valuable for two reasons. First, in examining synthetic data one *knows* which events are primaries and which are multiples; in contrast, when looking at data recorded in the field, one can never be absolutely sure if a given event is a primary or a multiple reflection. In addition, since the data generated consist only of primaries and multiples, with no other noise of any kind, one can observe exactly how much the multiple events are attenuated by the process. A second reason for looking at a synthetic example is that the velocity log (profile) assumed is probably more typical of the structure of most parts of the world than is the

velocity profile of the area from which the field data used in this thesis were obtained. Unfortunately, since the traces recorded in the field at spacings of 15 feet are ordinarily summed before they are brought in, there is very little data recorded at this spacing which is available for processing. Nevertheless the Atlantic Richfield Company did have one set of data which was recorded at this spacing in an area of West Texas. However, this part of Texas is what might be called a high-velocity area, since much of the subsurface is composed of layers with extremely high interval velocities. Consequently, the synthetic example used gives an indication of how the technique works under more "normal" conditions.

Synthetic Data

This example used here is shown in Figure 44. It was suggested by Dr. C. Floyd George, head of the Seismic Analysis Research Group of the Atlantic Richfield Company's Research and Development Laboratory. Since there are six subsurface interfaces, there will be six primary reflections which are to be received. The time of arrival of a primary at a particular receiver point is given by the familiar equation

$$T = \sqrt{T_0^2 + \left(\frac{X}{V_{av}}\right)^2}$$

or by

$$T = T_0 \sqrt{1 + \left(\frac{X}{2Z}\right)^2}$$

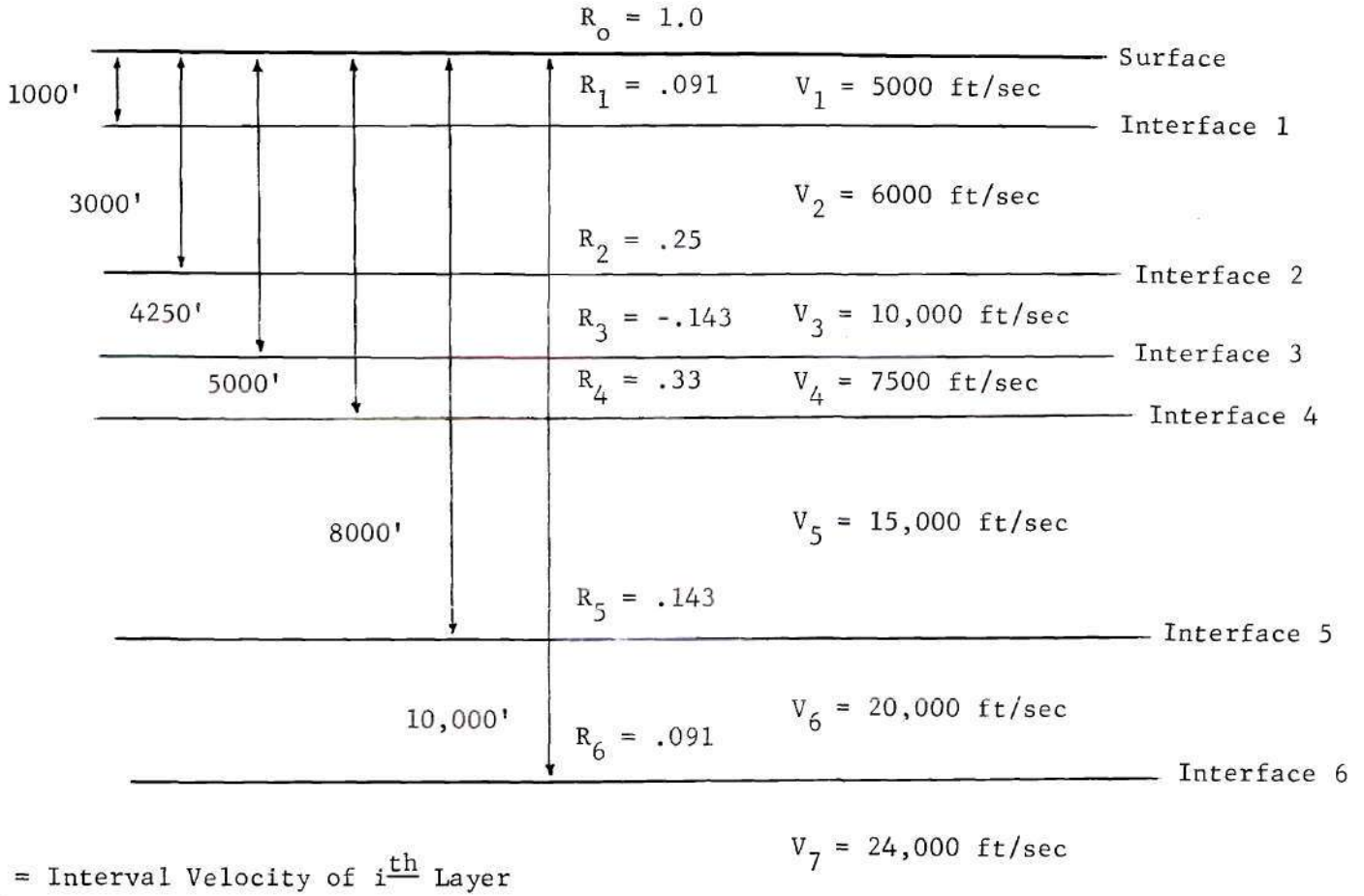

V_i = Interval Velocity of $i^{\underline{th}}$ Layer

R_i = Reflection Coefficient of $i^{\underline{th}}$ Interface

Figure 44. Velocity Profile Used to Generate Synthetic Seismogram, Showing Reflection Coefficients at Interfaces

where T_0 is the two-way vertical travel time, Z is the depth of the layer, X is the shotpoint-receiver distance, and V_{av} is the average velocity to the layer.

Since, in even the simplest layering problem, there are an infinite number of multiple reflections which can be excited, some limitation on the generation of these was necessary. Thus, only three-bounce surface multiples were included. These are multiple reflections which have been reflected three times, the second reflection being from the surface. Assuming the surface reflection coefficient is unity, a three-bounce surface multiple is diminished only by the product of the reflection coefficients of the two reflecting layers giving rise to the multiple; all other possible multiples are prefaced by the product of at least three reflection coefficients, and should therefore usually be smaller than the three-bounce surface multiples. Since there are six reflecting layers, there are 36 ways a three-bounce surface multiple can be excited. The moveout of a particular multiple is shown in Appendix A to be

$$T = (T_{oi} + T_{oj}) \sqrt{1 + \left[\frac{X}{2(Z_i+Z_j)}\right]^2}$$

where T_{oi} is the two-way vertical travel time to the ith layer, Z_i is the depth to the ith layer, and X is the shot-point-receiver distance.

No provision is made in the example for the effects on the wavelet amplitudes of spherical divergence and attenuation in the earth. The amplitudes of the primary and multiple events are dependent solely on the reflection coefficients by which they are multiplied. The

waveform representing each event is the same, that of Ricker wavelet,[30] which is defined by

$$r(t) = \frac{\sqrt{\pi}}{2} \cdot (\sqrt{6}\,\pi f_0 t^2 - 0.5) \cdot \exp[-\sqrt{6}\,\pi f_0 t^2]$$

The parameter f_0 is the peak frequency, that is, the frequency at which the Fourier transform of the wavelet has its peak. This frequency was chosen to be 45 Hertz for the example at hand.

Figure 45 shows all the primary events and most of the multiple events received at points 300 feet apart at distances of 5100 to 8400 feet from the shotpoint. Since the 240 traces used for processing were spaced at 15 feet, those shown in Figure 45 represent every 20th one of the 240. Because the vibrations of the earth are only recorded for about four seconds, a few of the very late-arriving multiples are not shown. Primary events on the record are those marked with a P, multiples are those marked with an M.

Figure 46 illustrates what happens when a time-varying velocity filter is applied to the synthetic traces. The real evidence of how well the method works is seen from the events which occur on the trace at 4800 feet between 1.80 seconds and 3.00 seconds. In this range fall two primary events, at times 2.01 seconds and 2.19 seconds, whose amplitudes on the unfiltered traces are about the same as those of multiples present in that interval. On the traces which have been filtered by the time-varying velocity filter, however, these two events stand out as the two strongest reflections in the interval, especially on the upper

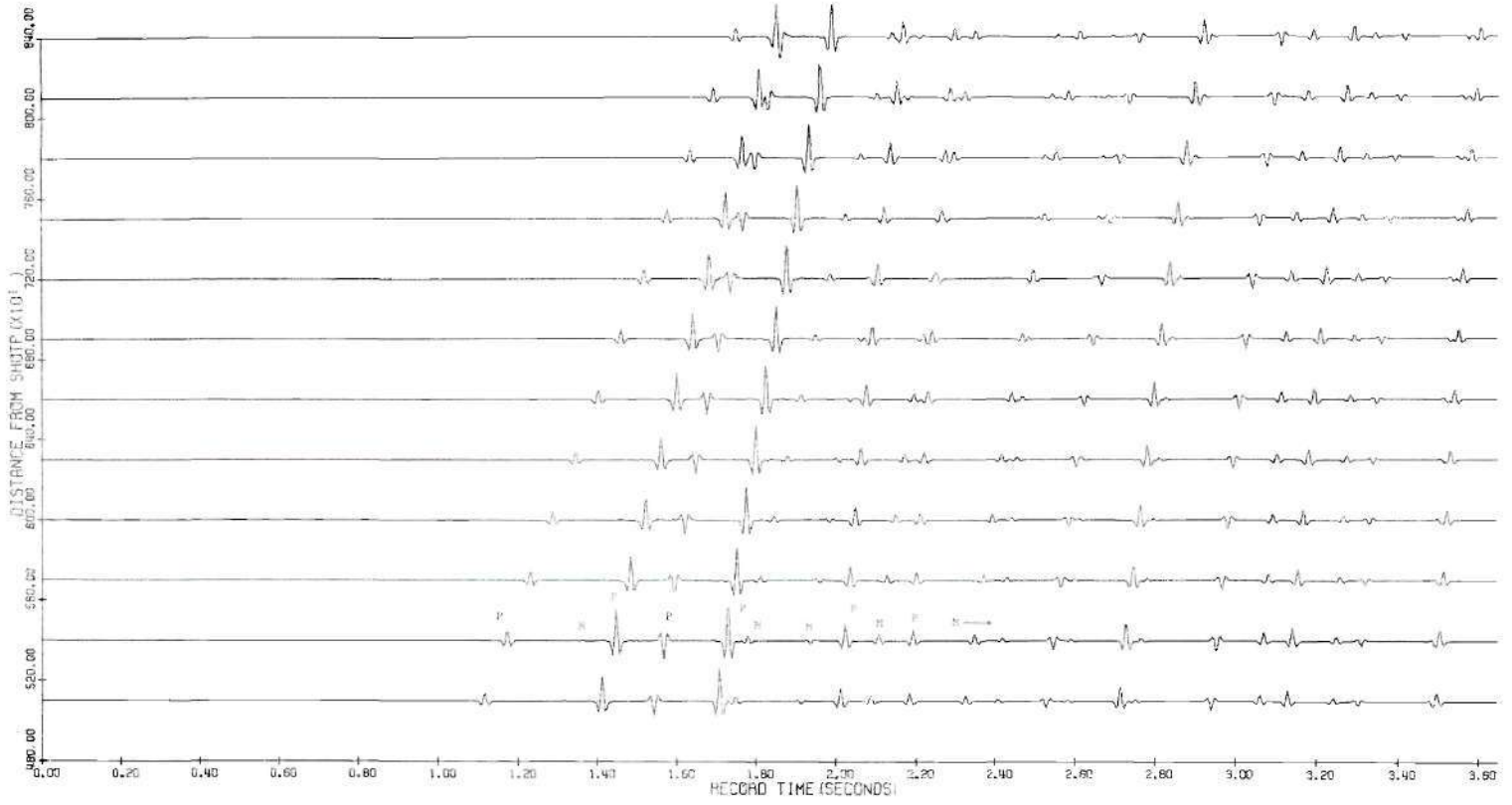

Figure 45. Synthetic Seismogram Generated by Velocity Profile of Figure 44

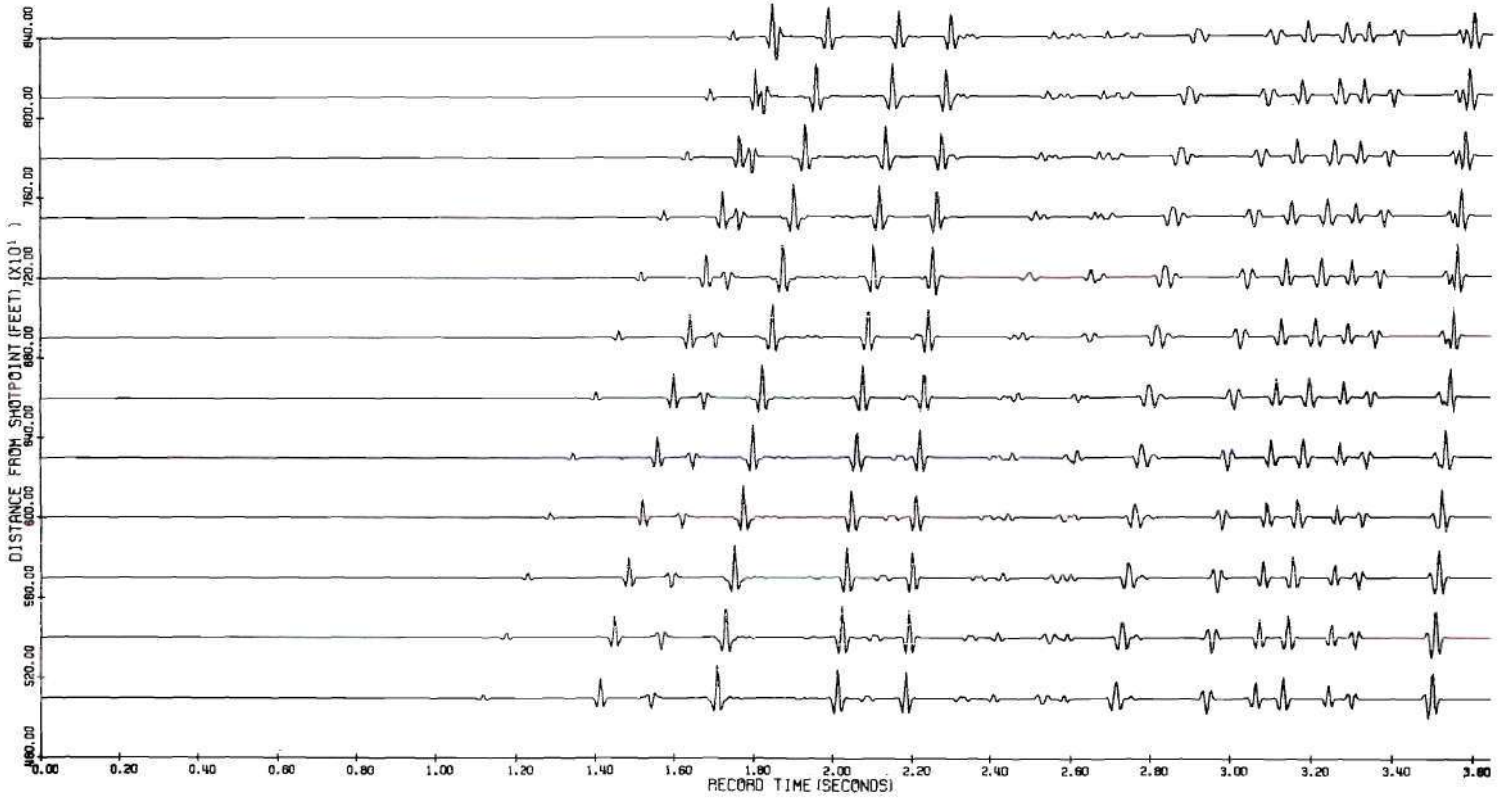

Figure 46. Result of Time-Varying Velocity Filtration of Synthetic Example of Figure 44, Using Rectangular Truncation Window

traces. After 3.00 seconds, measured on the trace at 4800 feet, the multiples which are received have as high an apparent horizontal velocity as the last primary received, consequently they fall within the passband of the time-varying velocity filter and are amplified like a primary. They occur so late in the record, though, that a crafty geophysicist would probably ignore them.

Figure 47 shows 12 output traces which have been processed by a time-varying velocity filter which uses a Hanning truncation window. In the same time interval considered previously, the primaries occurring at 2.01 seconds and 2.19 seconds on the lowest trace show some gain over the multiples in the interval. However, the improvement here is not as great as before, and the primary at 2.19 seconds is actually smaller than the multiple at 2.71 seconds. This substantiates the prediction that, in most instances, the use of Hanning window for truncation of the time-varying velocity filter is undesirable.

Seismic Field Data

Since it is not common practice to record the data at 15-foot spacings and return it to the laboratory in that state, only one set of such data was available with which to test the time-varying velocity filter. The data were recorded in an area of West Texas where the subsurface is usually composed of materials which propagate acoustic waves at very high velocities. It is also known that generally the subsurface structure of the region is such that two major primary reflections will ordinarily be received--the first off an interface known as the Delaware Line, and the second from the layer known as the Devonian. Knowing a

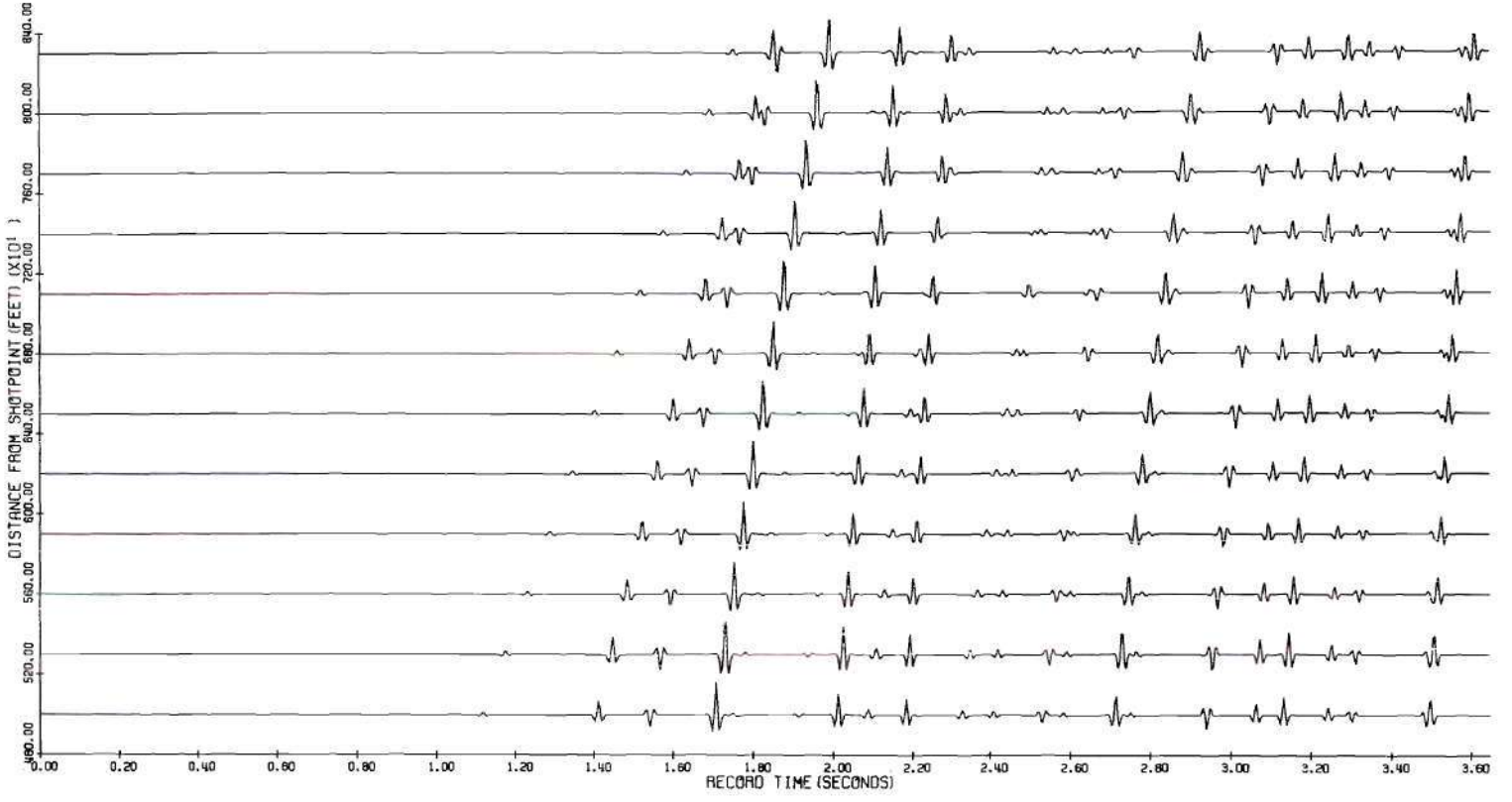

Figure 47. Result of Time-Varying Velocity Filtration of Synthetic Example of Figure 44, Using Hanning Truncation Window

little about the usual features of the area is almost imperative, no matter how the data are processed.

Figure 48 is a variable density presentation of the particular set of traces used. There were 23 groups of geophones, the centers of which were about 300 feet apart. The vibrators were moved 15 feet at a time, hence there are 460 traces spaced at 15 feet. One can immediately see that the 20 traces recorded by the 6th closest group to the source are faulty, and that the first 5 groups appear to have recorded less usable information than those farther out. It can also be seen that ground roll is not an overpowering factor here, since events of some sort can clearly be seen on the record.

The data shown in Figure 48 were processed by simply gathering the traces, by time-invariant velocity filtering, and by time-variant velocity filtering. Before showing the results of these, obtaining the velocity estimate required by the time-varying processor is considered. The Atlantic Richfield Company's velocity analysis program was first run on every 20th trace of the 460, then on 23 traces obtained by processing the 460 with a time-invariant velocity filter. The latter proved to be the more rewarding analysis; the velocity analysis plots are shown in Figure 49 where the individual plots have been normalized relative to the maximum value on the entire chart. Three parts of the plot which are marked with dotted lines were used for the interpretation. The first dotted line, through the three small peaks around 0.80 seconds, is what was presumed to be evidence of the Delaware Line reflection. One indication of this is the fact that it is a high-velocity event which appears on three consecutive individual plots.

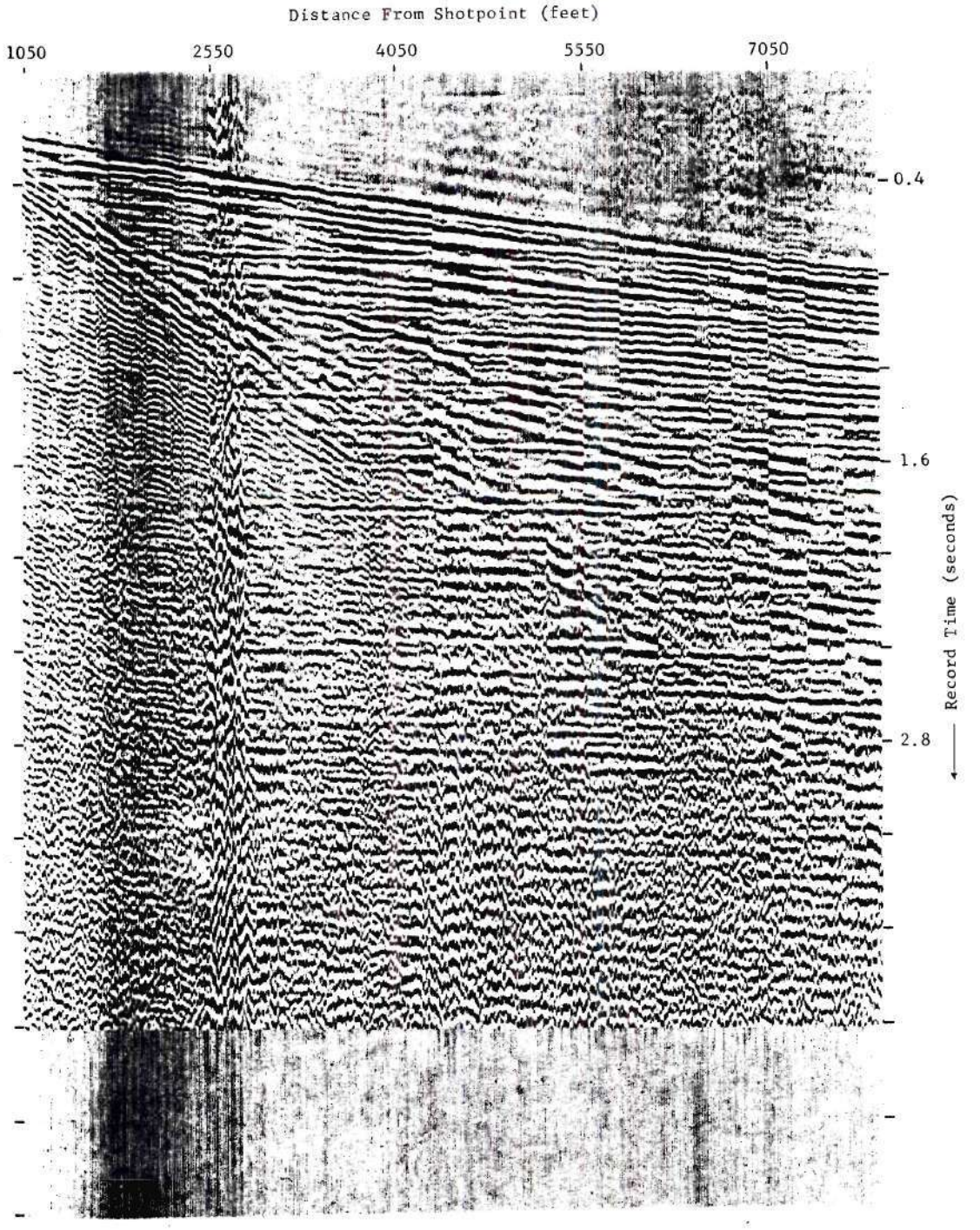

Figure 48. Correlated Vibroseis Traces Recorded at a Spacing of 15 Feet

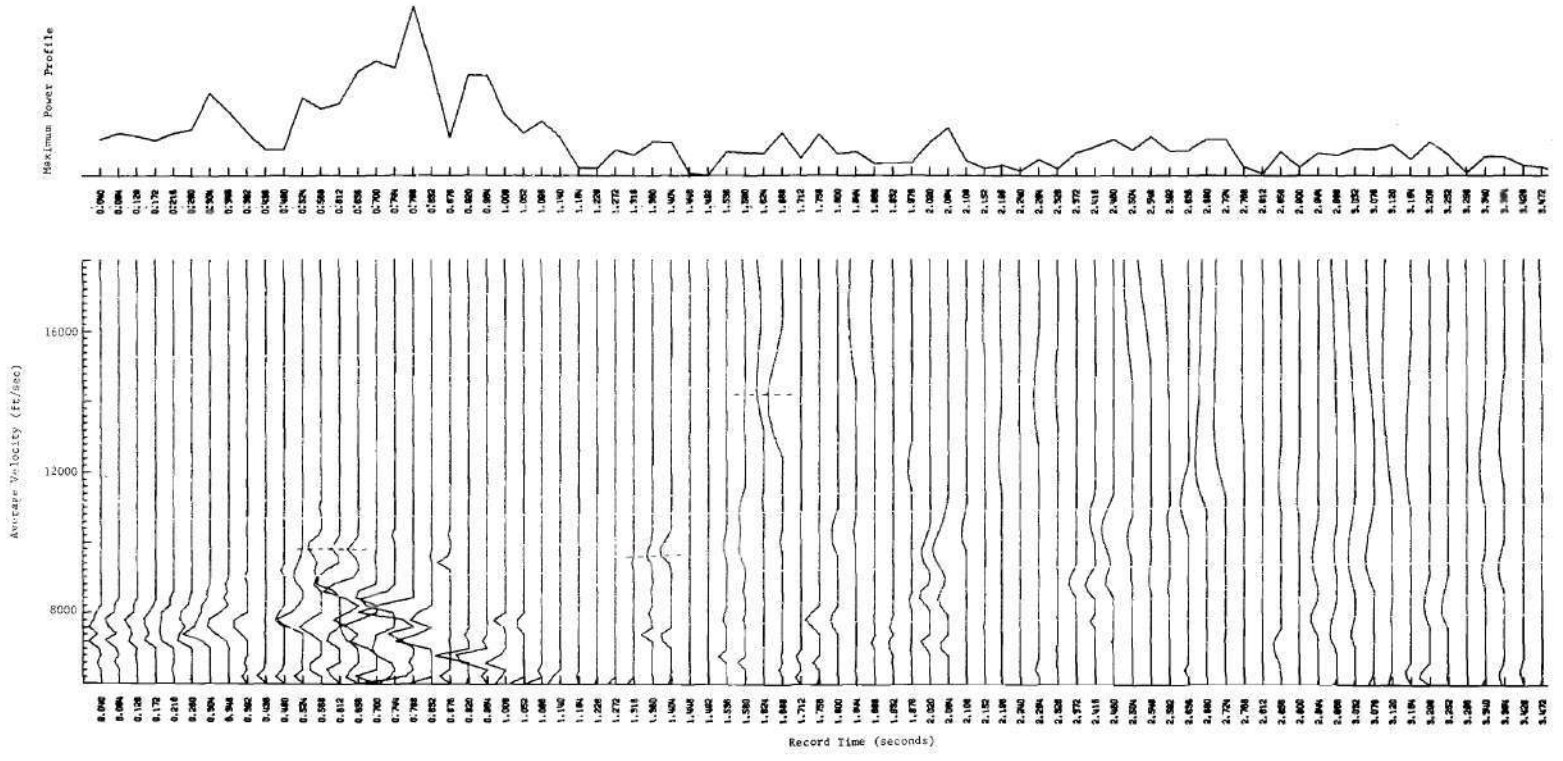

Figure 49. Result of Velocity Analysis on Traces Obtained by Time-Invariant Velocity Filtering the Records of Figure 48

It is unlikely that the event could be a multiple, since it appears so early, and its average velocity of about 10,000 feet per second is probably higher than that of first breaks, which is probably responsible for the coherence at about 8000 feet per second early in the record. A second reason why this is chosen to be a valid reflection is that at slightly more than twice the time of occurrence of the first event one finds a similar event at the same average velocity. A three-bounce surface multiple which is reflected twice from the same interface will have the same average velocity as a primary from this interface, and after application of normal moveout corrections will occur at twice the two-way vertical travel time of the primary. Therefore the event which occurs at about 1.35 seconds was interpreted as a multiple of the earlier event. Finally, the dotted line through the coherence at about 1.65 seconds shows what was assumed to be the reflection from the Devonian. Its high velocity, about 15,000 feet per second, was the main reason this was assumed, coupled with the fact that it appeared on several such analyses with a good deal of coherence. The velocity estimate with which the filter variations were determined was thus obtained.

Figures 50, 51, and 52 illustrate the results of the various kinds of processing. In Figure 50(a), the traces have been gathered in groups of 20 to produce 23 output traces spaced at 300 feet. This is what is ordinarily retained in the field and sent to the laboratory for processing. As can be seen, the background noise level is high, and there are many events present, i.e., events which might well be a primary or multiple reflection. Reduction of the amplitudes of the

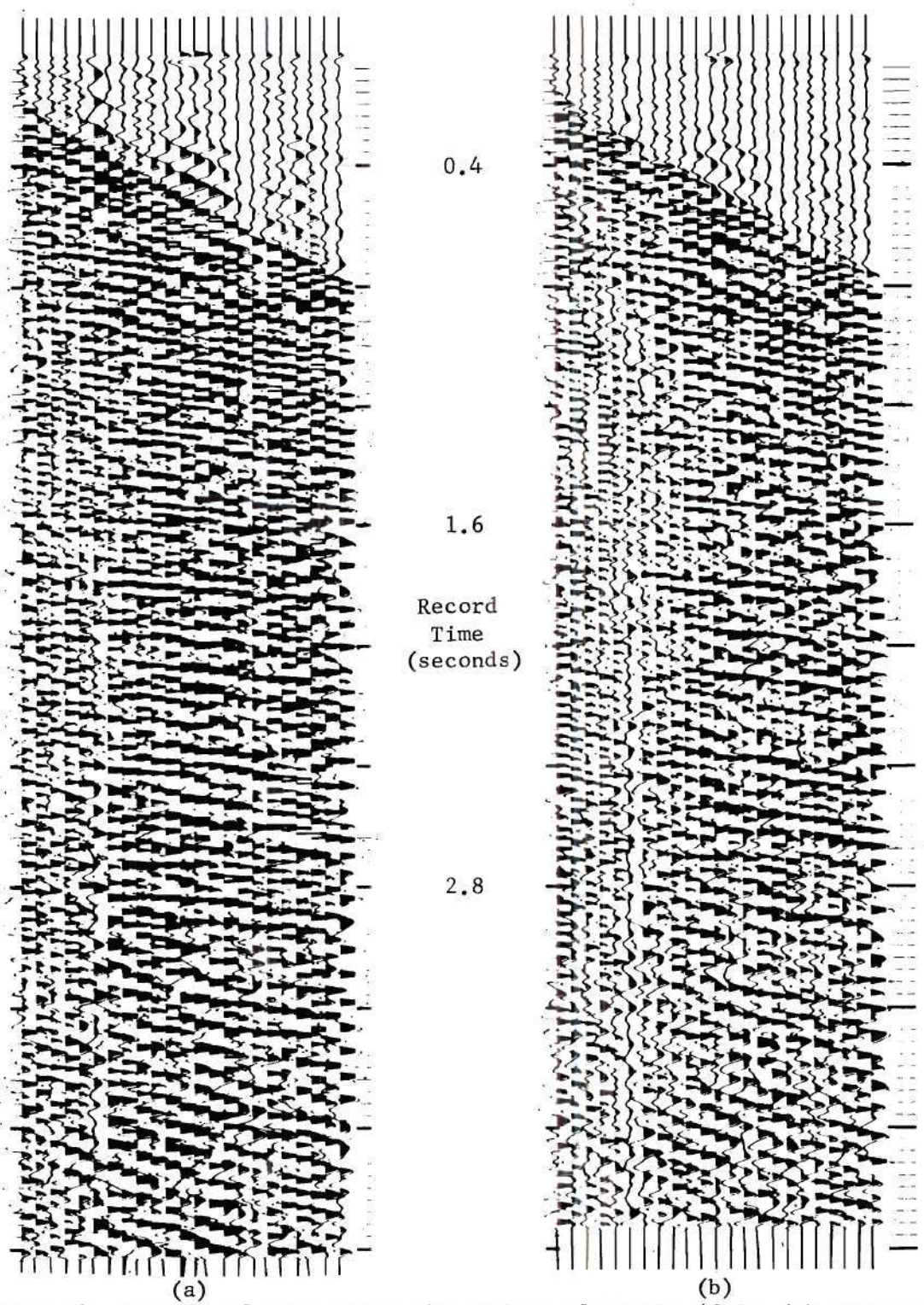

Figure 50. Result of Processing the Traces of Figure 48 by (a) Gathering the Traces in Groups of 20 and (b) Time-Invariant Velocity Filtering in Groups of 20 with p = 0.75.

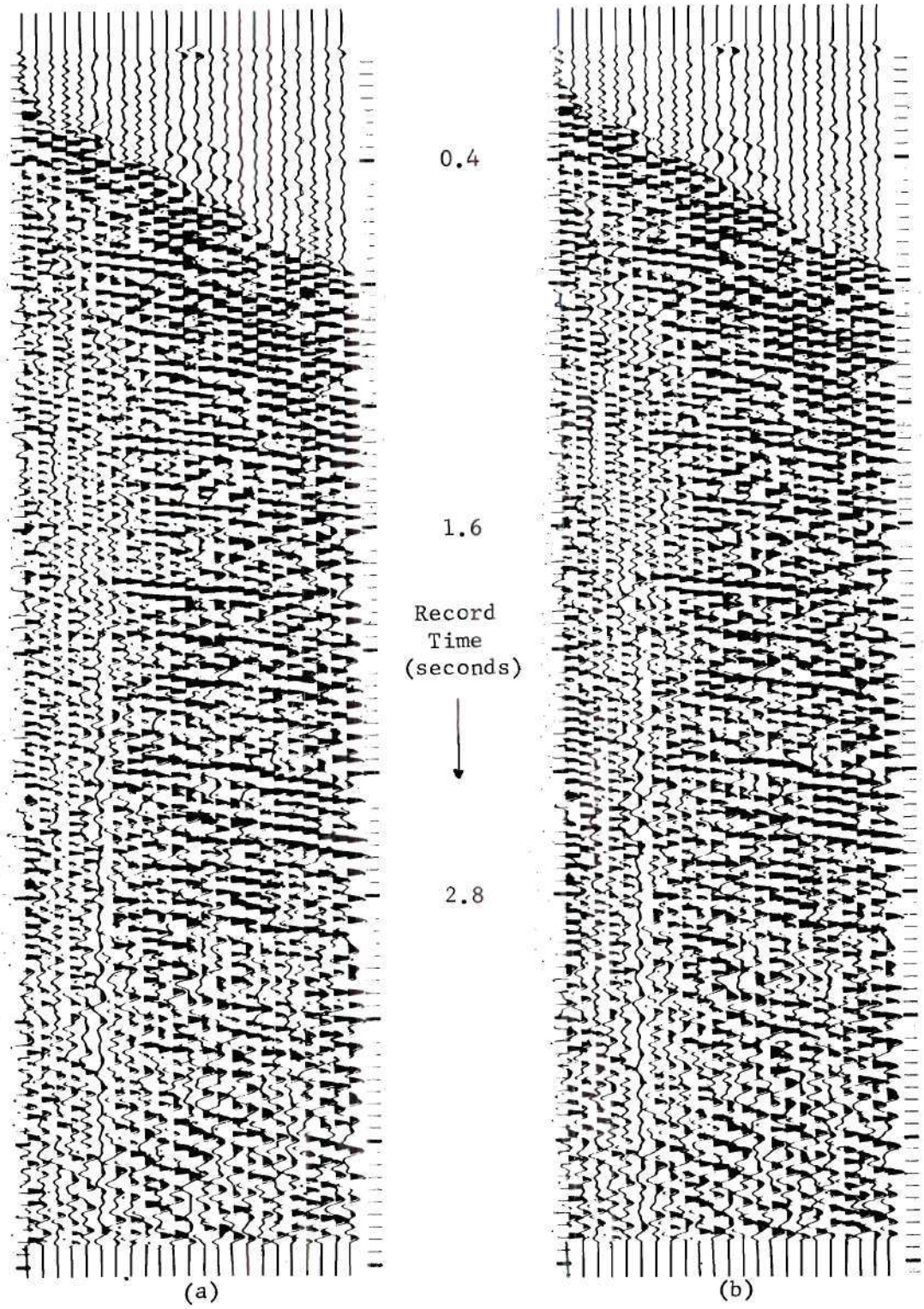

Figure 51. Result of Time-Invariant Velocity Filtering the Traces of Figure 48 with p = 0.4 Using (a) a Rectangular Gate and (b) a Hanning Window.

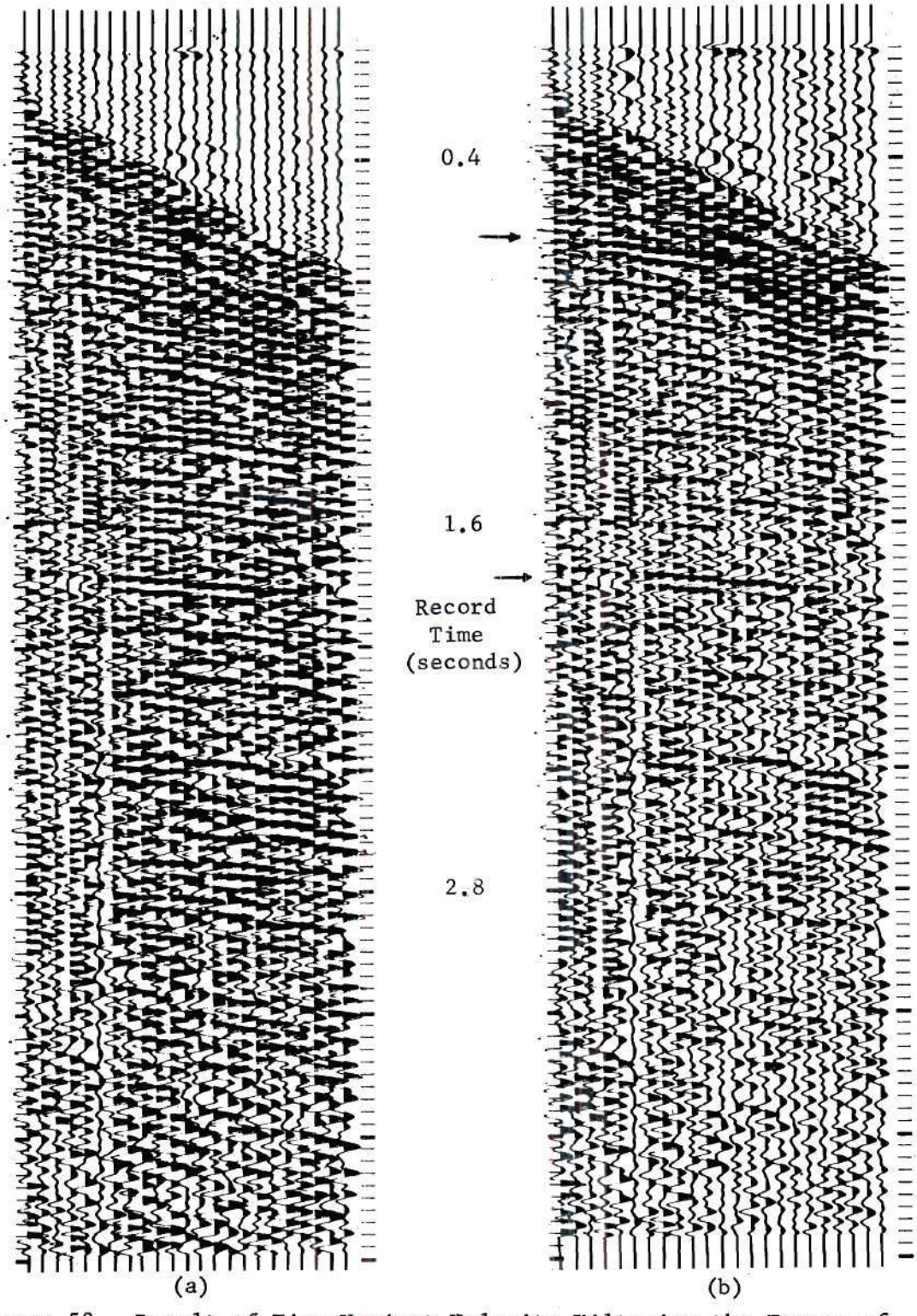

Figure 52. Result of Time-Variant Velocity Filtering the Traces of Figure 48 Using (a) a Rectangular Window and (b) an Inverse Window.

traces might prove favorable in reducing the amount of background noise displayed, but it is doubtful if this would help in the separation of the coherent events on the record.

The 23 traces of Figure 50(b) have been time-invariant velocity filtered, using 25 temporal and 20 spatial filter operators. Since the data were sampled every 15 feet in space and every four milliseconds in time, letting the coefficient p be unity results in a filter with a cut-off velocity of 3750 feet per second, a figure which ordinarily will suffice for the intended purpose. The traces shown were processed with a filter which was truncated with a rectangular window, and whose coefficient p was 0.75. Because the data obviously were of a high velocity nature, it was then decided to set p to 0.40 in order to see if any advantage was to be gained thereby, realizing that all primaries and multiples should have greater apparent horizontal velocities than the cutoff of 9375 feet per second this would produce. The result of this filtering is displayed in Figure 51; part (a) of the figure is the result of velocity filtering with a rectangular truncation gate, and part (b) is the result when a Hanning window is used for truncation. One observes that there is not a great deal of difference in the three velocity filtered outputs, though each appears to be more intelligible than the display of the gathered traces. However, there are still several events remaining on each set of traces.

Figure 52(a) shows 23 output traces which are the result of filtering the data with a time-variant velocity filter. Truncation was performed using a rectangular gate which left an impulse response function with 20 spatial operators and 25 temporal operators. In this case,

any improvement over the outputs of the time-invariant velocity filters is not evident; the background noise, in fact, appears to be greater in Figure 52(a) than in Figure 50(b) or in either Figure 51(a) or (b). This is not unexpected. Due to the high velocity data, and to the fact that the data recorded at sampling rates of four milliseconds and 15 feet, the pie-slice transfer function becomes very narrow almost immediately, and quickly reaches the stage where further change in the coefficient p produces little change in the actual transfer function obtained.

Now recall that an inverse truncation window produced a transfer function with poorer sidelobe structure and sharper cutoff characteristics than that which is the result of rectangular truncation. The inverse window described previously was applied to the time-varying velocity filter which was designed for this set of field data; the results of applying this filter to the data are shown in Figure 52(b). The 23 output traces are the cleanest of all those displayed here. And, most important, the events indicated by arrows stand out as the two strongest events on the record. One can still see remnants of filtered events, but these are not as strong as on the other output records.

In order to get some comparison of how effectively the time-varying processor worked, compare the traces of Figure 52(b) with the record sections of Figure 53. Those shown in the latter figure are the result of processing a large number of sections, such as those in Figure 48, which were taken from the same place in West Texas; the traces shown represent the final product which was turned over to a geophysicist for interpretation. The processing in this case consisted

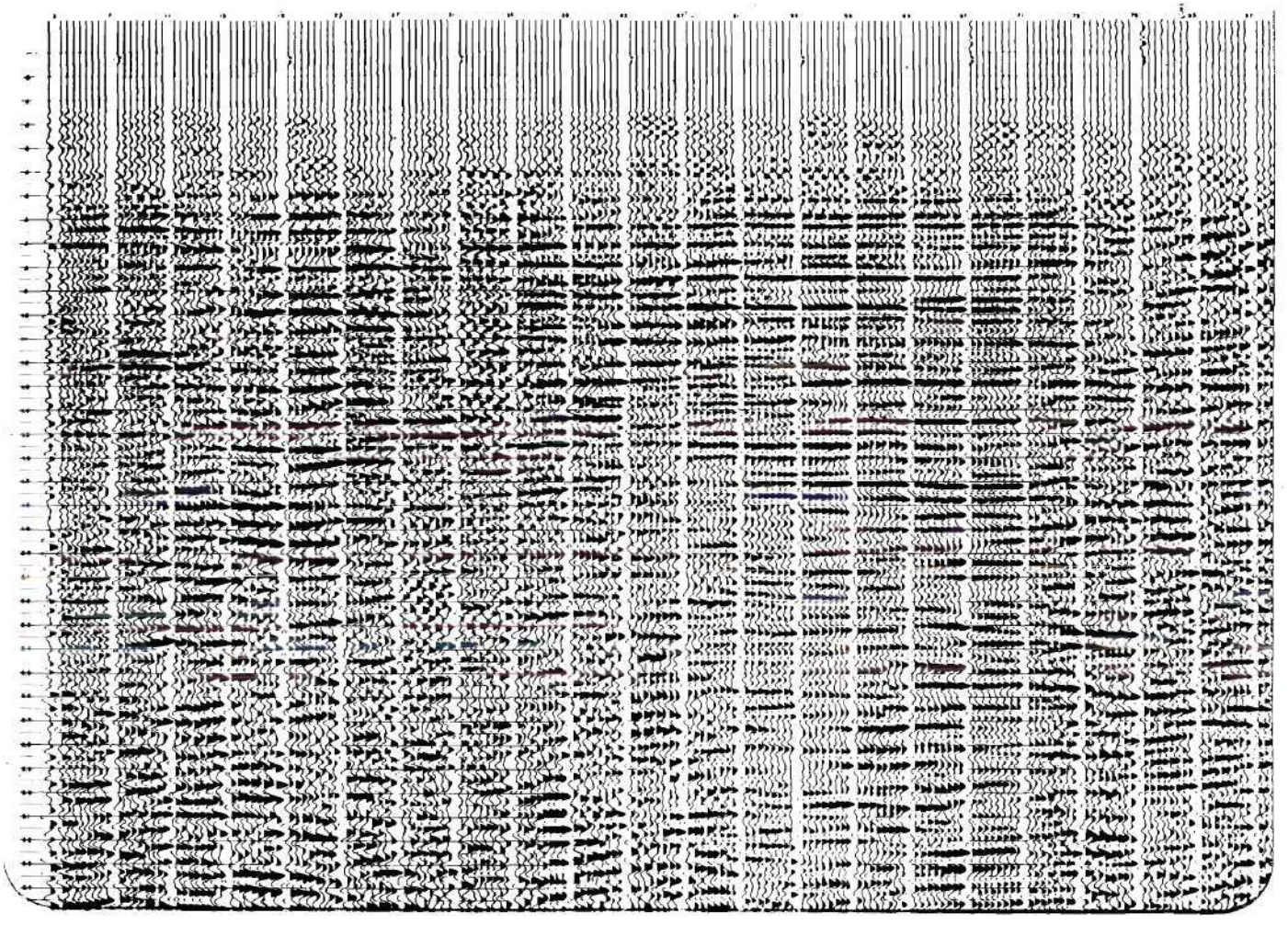

Figure 53. Result of Conventional Processing of Many Record Sections Recorded in the Same Area as Those Shown in Figure 48

primarily of stacking the traces. Though the two sets of processed data cannot be compared directly, since they were processed in different ways, it is fairly obvious that much more than just a pair of well-defined events is displayed on the traces of Figure 53. Even if more primary events than just two are actually present, it is doubtful if there are as many as shown in Figure 53.

CHAPTER VIII

SUMMARY

The research reported here has been an attempt to improve the estimation of seismic primary reflections through the continuous elimination of multiple reflections. First, the basic seismic reflection process was examined in detail. Next, some of the theoretical aspects of seismic wave propagation and reception were considered. Processing methods currently used in the exploration industry were then discussed, and the flaws or disadvantages in these were brought out. Since the signal and noise processes were obviously nonstationary, a time-variant processor of some kind was needed to take advantage of the changing characteristics of the signals and noise. Once the two-dimensionally nonstationary nature of the problem was understood, the solution was obvious, and straightforward in application. A time-varying velocity filter was proposed in order to continually separate primaries from multiples on the basis of the difference in their apparent horizontal velocities. The proposed filter is unique in two ways. First, it is the only reported technique for filtering multiple reflections which requires no a priori information on the positions or moveouts of the multiples. Second, it is the only known method for eliminating multiples applied early enough that CDP stacking may be applied later. This filter was implemented on the digital computer, and both synthetic and field data were processed by it. Results were favorable, and indicate

that the time-varying velocity filter is an effective pre-processing scheme to be used in conjunction with common-depth-point stacking.

The results obtained in this research have demonstrated the feasibility of the approach. However, little effort was spent in optimization of the method. Future effort can be spent in trying to improve the characteristics of the filters being used to effect the separation of primaries and multiples. One area which deserves investigation is that of sharpening cut-off characteristics using inverse truncation windows; only one such window was considered here. Another problem in velocity filtering is the dip in the amplitude response of the transfer function near the origin in ω-k_x space; means of eliminating this effect are currently being studied. The very fact that the method developed here was aimed solely at elimination of multiple reflections raises another question. Can one devise a time-varying processor with not only elimination of multiple reflections in mind, but with the purpose of simultaneously rejecting other types of noise in the best possible way?

It is felt that two other aspects of seismic reflection prospecting deserve as much, if not more, attention as improved filtering and processing methods. The first of these is the design of suitable waveforms for transmission into the earth through vibrators. The "chirp" signal mentioned in Chapter II does a good job; there may be other signals which do considerably better. A second area in which effort could profitably be spent is that of velocity estimation; in the communication theory literature it is not difficult to find methods for estimating one or more randomly-varying signal parameters.[31]

These techniques might profitably be brought to bear in the seismic reflection problem.

Finally, there is a distinct possibility that the processing methods used in seismic studies may be applicable in other areas, and vice versa. For instance, consider a phased array antenna of N elements. Ordinarily its purpose is to focus a beam in a given direction, and to this end N complex weights are applied to the N sensors. The weighted signals are summed. In light of what has been discussed on two-dimensional filters, one can see that the phased array is actually such a filter, with N spatial operators and one temporal operator. In view of this it seems only natural that increasing the number of temporal operators can only improve the characteristics of the array processing. In addition, the use of narrowband signal waveforms and proper group spacing might allow the exploration geophysicist to use techniques developed in the theory of phased array antennas. It is felt that this cross-application of techniques might prove profitable to both parties.

APPENDIX A

DERIVATION OF STRAIGHT-RAYPATH FORMULAS

In this appendix are derived a number of simple, useful formulas which can be applied when using the straight-raypath approximation. In the following, the equations which are numbered are those judged to be most useful. Consider Figure 54, which shows a primary reflection from a subsurface boundary. The symbols used in the equations which follow are now defined.

T_0 = two-way vertical travel time to reflecting layer.

Z = distance to reflecting layer.

V = average velocity to reflecting layer.

X = distance from shotpoint to receiver.

T = time of reception of wavelet.

The distance the wavelet of Figure 54 travels is

$$d = 2 \cdot \sqrt{Z^2 + \left(\frac{X}{2}\right)^2}$$

$$= \sqrt{(2Z)^2 + X^2}$$

The travel time of a wavelet propagating from the source to the receiver is then

$$T = \frac{d}{V}$$

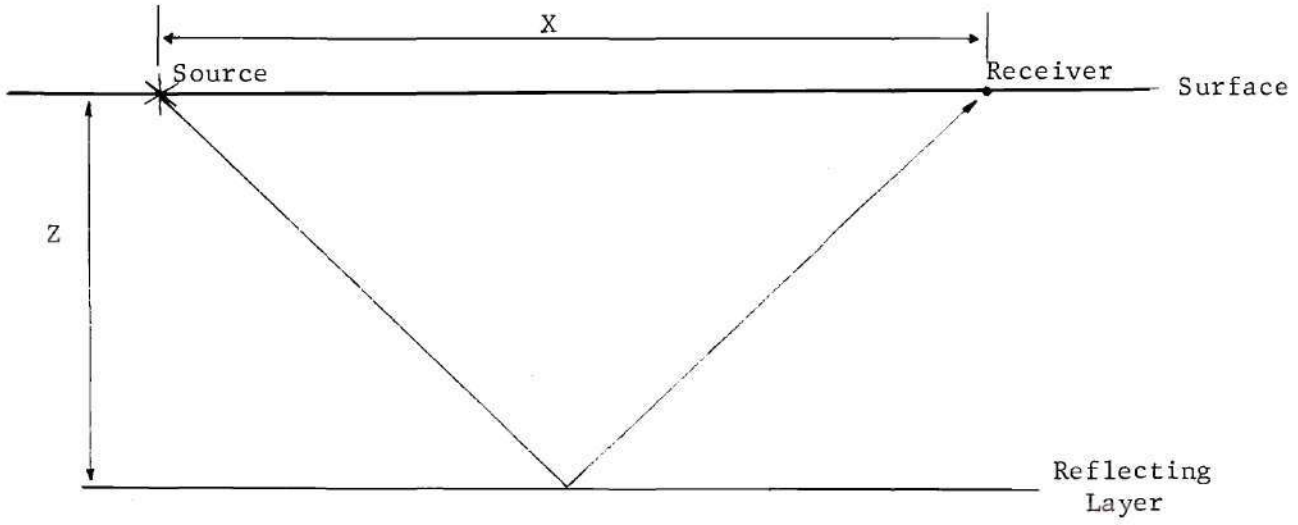

Figure 54. A Primary Reflection

$$= \frac{\sqrt{(2Z)^2 + X^2}}{V}$$

$$= \sqrt{\left(\frac{2Z}{V}\right)^2 + \left(\frac{X}{V}\right)^2}$$

$$T = \sqrt{T_0^2 + \left(\frac{X}{V}\right)^2} \qquad \text{(A-1)}$$

This last is by virtue of the substitution $2Z = VT_0$. Using this again, one has

$$T = T_0 \sqrt{1 + \left(\frac{X}{VT_0}\right)^2}$$

$$= T_0 \sqrt{1 + \left(\frac{X}{2Z}\right)^2} \qquad \text{(A-2)}$$

The two-way vertical travel time formulas used for moveout corrections are then

$$T_0 = \sqrt{T^2 - \left(\frac{X}{V}\right)^2} \qquad \text{(A-3)}$$

and

$$T_0 = T \sqrt{1 - \left(\frac{X}{2Z}\right)^2} \qquad \text{(A-4)}$$

Turn now to the problem of travel times of three-bounce surface multiples, illustrated in Figure 55. The subscripts 1 and 2 on the symbols

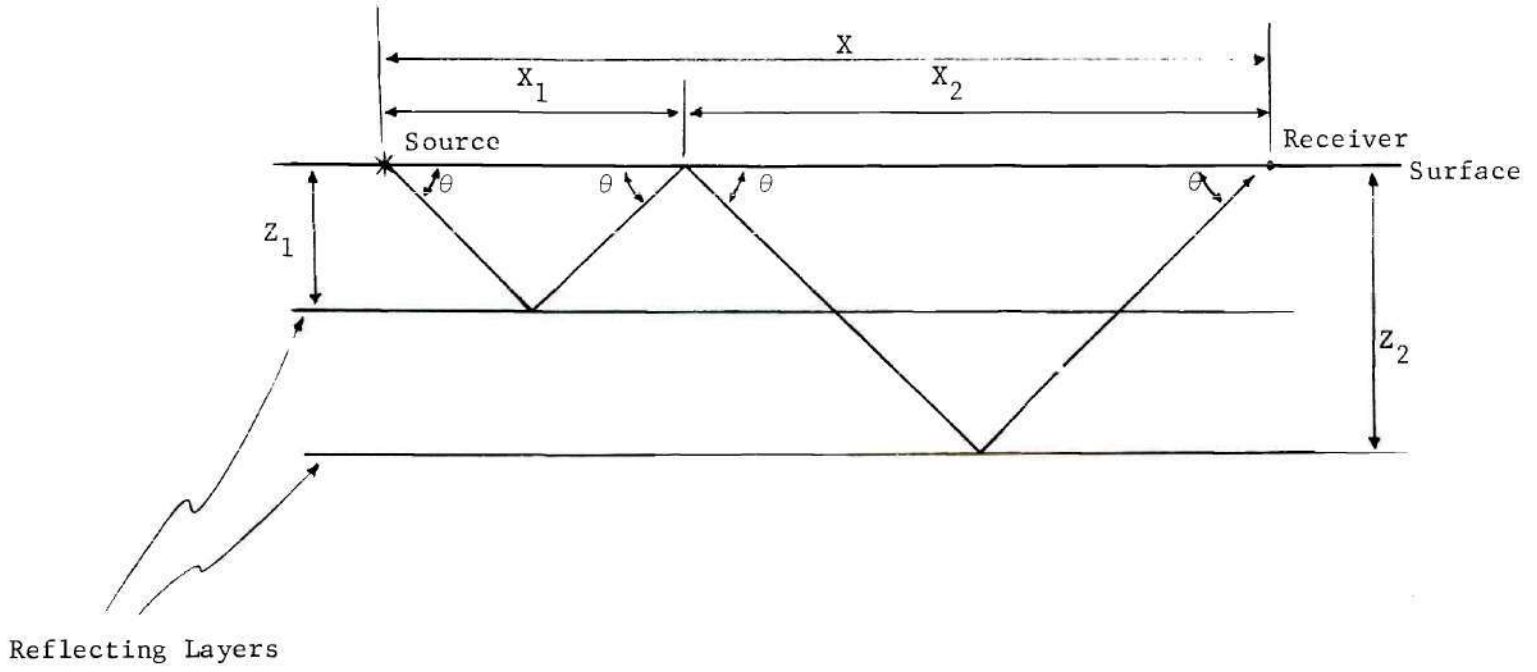

Figure 55. A Three-Bounce Surface Multiple Reflection

modify the definitions of the first page to association with the first or second subsurface reflection. Since all the angles of incidence are equal by virtue of Snell's Laws, one can write

$$\tan \theta = \frac{2Z_1}{X_1}$$

$$= \frac{2Z_2}{X_2}$$

$$\frac{2Z_1}{X_1} = \frac{2Z_2}{X-X_1}$$

Solving this for X_1 yields

$$X_1 = \frac{XZ_1}{Z_1 + Z_2}$$

Similarly,

$$X_2 = \frac{XZ_2}{Z_1 + Z_2}$$

The time of arrival of a multiple is then

$$T = T_1 + T_2$$

$$= \sqrt{T_{01}^2 + \left(\frac{X_1}{V_1}\right)^2} + \sqrt{T_{02}^2 + \left(\frac{X_2}{V_2}\right)^2}$$

Substituting for X_1 and X_2,

$$T = \sqrt{T_{01}^2 + \frac{1}{V_1^2}\left(\frac{XZ_1}{Z_1+Z_2}\right)^2} + \sqrt{T_{02}^2 + \frac{1}{V_2^2}\left(\frac{XZ_2}{Z_1+Z_2}\right)^2}$$

$$= \sqrt{T_{01}^2 + \left[\frac{XT_{01}}{2(Z_1+Z_2)}\right]^2} + \sqrt{T_{02}^2 + \left[\frac{XT_{02}}{2(Z_1+Z_2)}\right]^2}$$

$$= (T_{01} + T_{02})\sqrt{1 + \left[\frac{X}{2(Z_1+Z_2)}\right]^2} \qquad \text{(A-5)}$$

This is the desired result for multiples.

APPENDIX B

DERIVATION OF IMPULSE RESPONSE OF VELOCITY FILTER

Ideally, a velocity filter should have the transfer function shown in Figure 16, i.e., unity response in the hourglass-shaped area and zero response outside there. The impulse response function corresponding to this transfer function will now be derived. If the transfer function is called $G(\omega;k)$, then

$$g(t;x) = \int_{-\infty}^{\infty}\int G(\omega;k)e^{j(\omega t-kx)}\,\frac{d\omega}{2\pi}\,\frac{dk}{2\pi} \qquad \text{(B-1)}$$

where $g(t;x)$ is the Fourier transform (impulse response) of $G(\omega;k)$; Fourier transform pairs like these will be signified by

$$g(t;x) \overset{F}{\Longleftrightarrow} G(\omega;k)$$

Substituting for $G(\omega;k)$ in (B-1), one has

$$g(t;x) = \int_{-\omega_{max}}^{\omega_{max}}\int_{-\frac{|\omega|}{v}}^{\frac{|\omega|}{v}} e^{j(\omega t-kx)}\,\frac{d\omega}{2\pi}\,\frac{dk}{2\pi}$$

$$= \int_{-\omega_{max}}^{\omega_{max}} e^{j\omega t}\cdot\frac{d\omega}{(2\pi)^2}\cdot\left[\frac{e^{-jkx}}{-jx}\right]_{-\frac{|\omega|}{v}}^{\frac{|\omega|}{v}}$$

$$= \frac{1}{2\pi^2 x} \int_{-\omega_{max}}^{\omega_{max}} \sin \frac{|\omega| x}{v} e^{j\omega t} \, d\omega \qquad \text{(B-2)}$$

In order to avoid singularities in the transfer function there is no sample point at the time-space origin. Rather, spatial samples are located at positions given by

$$X_m = (|m| - 0.5) \cdot X \cdot \text{sgn}(m)$$

where m is a non-zero integer and X is the distance between spatial samples. Since in the above Equation (B-2) x-dependence appears as an even function, the sgn(m) factor can be ignored. If one defines

$$m^* = |m| - 0.5$$

then, upon substitution of the sample points $t = nT$ and $x = m^* X$, T being the distance between sample points in time, one has

$$g(n;m^*) = \frac{1}{2\pi^2 m^* X} \int_{-\frac{\pi}{T}}^{\frac{\pi}{T}} \sin\left(\frac{m^* |\omega| X}{v}\right) e^{jn\omega T} \, d\omega$$

where the substitution $\omega_{max} = \pi/T$ has been made. Using $v = X/pT$,

$$g(n;m^*) = \frac{1}{2\pi^2 m^* X} \int_{-\pi/T}^{\pi/T} \sin(pm^* |\omega| T) e^{jn\omega T} \, d\omega$$

$$= C_0 \int_{-\pi/T}^{\pi/T} [\cos(n\omega T)\sin(pm^*|\omega|T) + j\,\sin(n\omega T)\sin(pm^*|\omega|T)]d\omega$$

$$= -C_0 \int_{-\pi/T}^{0} [\cos(n\omega T)\sin(pm^*\omega T) + j\,\sin(n\omega T)\sin(pm^*\omega T)]d\omega$$

$$+C_0 \int_{0}^{\pi/T} [\cos(n\omega T)\sin(pm^*\omega T) + j\,\sin(n\omega T)\sin(pm^*\omega T)]d\omega \qquad \text{(B-3)}$$

Consider the first term of the first integral of this last equation. If one sets $\omega_1 = -\omega$, then

$$-C_0 \int_{-\pi/T}^{0} \cos(n\omega T)\sin(pm^*\omega T)d\omega =$$

$$-C_0 \int_{-\pi/T}^{0} \cos(n\omega_1 T)[-\sin(pm^*\omega_1 T)](-d\omega_1)$$

$$= C_0 \int_{0}^{\pi/T} \cos(n\omega_1 T)\sin(pm^*\omega_1 T)d\omega_1$$

This is the same integral as the first term of the second integral. Using the same substitution, the second terms in each integral of Equation (B-3) cancel one another. Then (B-3) becomes

$$g(n;m^*) = 2C_0 \int_{0}^{\pi/T} \cos(n\omega T)\sin(pm^*\omega T)d\omega$$

Using standard trigonometric substitutions, this becomes

$$g(n;m^*) = C_0 \int_0^{\pi/T} [\sin(n+pm^*)\omega T - \sin(n-pm^*)\omega T]d\omega$$

$$= C_0\left[\frac{-\cos(n+pm^*)\omega T}{(n+pm^*)T}\right]_0^{\pi/T} - C_0\left[\frac{-\cos(n-pm^*)\omega T}{(n-pm^*)T}\right]_0^{\pi/T}$$

$$= C_0\left[\frac{1}{(n+pm^*)T} - \frac{1}{(n-pm^*)T}\right]$$

$$+ C_0\left[\frac{\cos(n-pm^*)\pi}{(n-pm^*)T} - \frac{\cos(n+pm^*)\pi}{(n+pm^*)T}\right]$$

$$= \frac{C_0}{T}\left[\frac{-2pm^*}{n^2-(pm^*)^2}\right]$$

$$+ \frac{C_0}{T}\left[\frac{(n+pm^*)\cos(n-pm^*)\pi - (n-pm^*)\cos(n+pm^*)\pi}{n^2 - (pm^*)^2}\right]$$

(B-4)

Consider for the moment just the numerator of the second term of this equation. Calling it N, one can write

$$N = (n+pm^*)[\cos(n\pi)\cos(pm^*\pi) + \sin(n\pi)\sin(pm^*\pi)]$$

$$- (n-pm^*)[\cos(n\pi)\cos(pm^*\pi) - \sin(n\pi)\sin(pm^*\pi)]$$

Since $\sin(n\pi) = 0$ and $\cos(n\pi) = (-1)^n$, this becomes

$$N = (n+pm^*) \cdot (-1)^n \cdot \cos(pm^*\pi) - (n-pm^*) \cdot (-1)^n \cdot \cos(pm^*\pi)$$

$$= 2pm^* \cdot (-1)^n \cdot \cos(pm^*\pi)$$

Thus Equation (B-4) becomes

$$g(n;m^*) = \frac{C_0}{T} \cdot 2pm^* \cdot \left[\frac{(-1)^n \cos(pm^*\pi) - 1}{n^2 - (pm^*)^2}\right]$$

$$= \frac{p}{\pi^2 XT} \left[\frac{(-1)^n \cos(pm^*\pi) - 1}{n^2 - (pm^*)^2}\right] \qquad \text{(B-5)}$$

This is the desired impulse response function. Observe that if $p = 1.0$, i.e., $V = \omega_{max}/k_{max}$, then this reduces to

$$g(n;m^*) = \frac{1}{\pi^2 XT} \cdot \frac{1}{m^{*2} - n^2}$$

since

$$\cos(m^*\pi) = \pm\cos(\pi/2)$$

$$= 0$$

BIBLIOGRAPHY

1. Dobrin, M. B., 1960, Introduction to geophysical prospecting: New York, McGraw-Hill Book Company, Inc.

2. Fail, J. P., and Grau, G., 1963, Les filtres en eventail: Geophysical Prospecting, v. 11, p. 131.

3. Embree, P., Burg, J. P., and Backus, M. M., 1963, Wide band velocity filtering--The pie slice process: Geophysics, v. 28, p. 948-974.

4. Papoulis, A., 1962, The Fourier integral and its applications: New York, McGraw-Hill Book Company, Inc.

5. Sengbush, R. L., and Foster, M. R., 1968, Optimum multichannel velocity filters: Geophysics, v. 33, p. 11-35.

6. Treitel, S., Shanks, J. L., and Frasier, C. W., 1967, Some aspects of fan filtering: Geophysics, v. 32, p. 789-800.

7. Robinson, E. A., 1967, Statistical communication and detection with special reference to digital data processing of radar and seismic signals: London, Charles Griffin and Company, Ltd.

8. Wiener, N., 1949, The extrapolation, interpolation, and smoothing of stationary time series: New York, John Wiley and Sons, Inc.

9. Robinson, E. A., 1957, Predictive decomposition of seismic traces: Geophysics, v. 22, p. 767-778.

10. Kunetz, G., 1961, Essai d'analyse de traces sismiques: Geophysical Prospecting, v. 9, p. 317.

11. Rice, R. B., 1962, Inverse convolution filters: Geophysics, v. 27, p. 4-18.

12. Foster, M. R., Hicks, W. G., and Nipper, J. T., Optimum inverse filters which shorten the spacing of velocity logs: Geophysics, v. 27, p. 317-326.

13. Clarke, G. K. C., Time-varying deconvolution filters: Geophysics, v. 33, p. 936-944.

14. Jury, E. I., 1964, Theory and application of the z-transform method: New York, John Wiley and Sons, Inc.

15. Mayne, W. H., 1962, Common reflection point horizontal data stacking techniques: Geophysics, v. 27, p. 927-938.

16. Mayne, W. H., 1967, Practical considerations in the use of common reflection point techniques: Geophysics, v. 32, p. 225-229.

17. Meyerhoff, H. J., 1966, Horizontal stacking and multi-channel filtering applied to common depth point seismic data: Geophysical Prospecting, v. 14, p. 441-454.

18. Robinson, J. C., 1968, Noise attenuation on common-depth-point seismic records by a semideterministic approach: Geophysics, v. 33, p. 723-733.

19. Galbraith, J. N., and Wiggins, R. A., Characteristics of optimum multichannel stacking filters: Geophysics, v. 33, p. 36-48.

20. Special June 1967 issue of Geophysics devoted to reports of the Geophysical Analysis Group (GAG).

21. Burg, J. P., 1964, Three-dimensional filtering with an array of seismometers: Geophysics, v. 29, p. 693-713.

22. Backus, M. M., Burg, J. P., Baldwin, D., and Bryan, E., 1964, Wide-band extraction of mantle P waves from ambient noise: Geophysics, v. 29, p. 672-692.

23. Schneider, W. A., Larner, K. L., Burg, J. P., and Backus, M. M., 1964, A new data-processing technique for the elimination of ghost arrivals on reflection seismograms: Geophysics, v. 29, p. 783-805.

24. Schneider, W. A., Prince, E. R., and Files, B. F., 1965, A new data-processing technique for multiple attenuation exploiting differential normal moveout: Geophysics, v. 30, p. 348-362.

25. Zadeh, L. A., 1950, Frequency analysis of variable networks: Proceedings of the IRE, v. 38, p. 291-299.

26. Kailath, T., 1959, Sampling models for linear time-variant filters: M.I.T. Research Laboratory of Electronics Technical Report No. 352.

27. Schneider, W. A., and Backus, M. M., 1968, Dynamic correlation analysis: Geophysics, v. 33, p. 105-126.

28. Blackman, R. B., and Tukey, J. W., 1958, The measurement of power spectra: New York, Dover Publications.

29. Bruce, J. D., 1968, Discrete Fourier transforms, linear filters, and spectrum weighting: IEEE Transactions on Audio and Electroacoustics, v. AU-16, p. 495-499.

30. Ricker, N., 1940, The form and nature of seismic waves and the structure of seismograms: Geophysics, v. 5, p. 348-366.

31. Van Trees, H. L., 1968, Detection, estimation, and modulation theory, part I: New York, John Wiley and Sons, Inc.

VITA

Winsor Letton, III was born in Montgomery, Alabama, on July 10, 1943. After attending public school there, he entered Vanderbilt University in 1961 and was graduated in 1965 with a B. E. in electrical engineering. He completed the requirements for the M. S. in electrical engineering there in September, 1966, at which time he entered the Ph.D. program in electrical engineering at the Georgia Institute of Technology.

He was married on September 2, 1965, to the former Martha Ann Finch of Tulsa, Oklahoma.